2007

Mechanistic modeling of an underbalanced drilling operation utilizing supercritical carbon dioxide

Faisal Abdullah ALAdwani
Louisiana State University and Agricultural and Mechanical College

MECHANISTIC MODELING OF AN UNDERBALANCED DRILLING OPERATION UTILIZING SUPERCRITICAL CARBON DIOXIDE

A Dissertation

Submitted to the Graduate Faculty of the
Louisiana State University and
Agricultural and Mechanical College
in partial fulfillment of the
Requirements for the degree of
Doctor of Philosophy

in

The Department of Petroleum Engineering

by
Faisal Abdullah ALAdwani
B.S., Kuwait University, 1998
M.S., Louisiana State University, 2003
August, 2007

ACKNOWLEDGMENTS

I would like to express my deepest gratitude to my advisor Prof. Julius P. Langlinais for supervising this work and his valuable guidance and genuine interest in completing this study. In addition I am greatly indebted to my country, Kuwait, for supporting my education through the scholarship from Kuwait University. Extended appreciation goes to committee members Dr. Dandina Rao, Dr. Stephen Sears, Dr. Richard Hughes, and Dr. Kenneth J. Schafer for their valuable time and supervision on this work. Special thank goes to Dr. Andrew Wojtanowicz, and Dr. John Smith for their valuable help and genuine advice. I am grateful to Dr. Roland Span from "Universität Paderborn" and Eric W. Lemmon from the National Institute of Standards and Technology (NIST) for providing the required programs in order to complete this work.

TABLE OF CONTENTS

LIST OF TABLES

LIST OF FIGURES

ABSTRACT

Mechanistic modeling of an underbalanced drilling operation using carbon dioxide has been developed in this research. The use of carbon dioxide in an underbalanced drilling operation eliminates some of the operational difficulties that arises with gaseous drilling fluids, such as generating enough torque to run a downhole motor. The unique properties of CO_2, both inside the drill pipe and in the annulus are shown in terms of optimizing the drilling operation by achieving a low bottomhole pressure window. Typically CO_2 becomes supercritical inside the drill pipe at this high density; it will generate enough torque to run a downhole motor. As the fluid exits the drill bit it will vaporize and become a gas, hence achieving the required low density that may be required for underbalanced drilling.

The latest CO_2 equation of state to calculate the required thermodynamic fluid properties is used. In addition, a heat transfer model taking into account varying properties of both pressure and temperature has been developed. A marching algorithm procedure is developed to calculate the circulating fluid pressure and temperature, taking into account the varying parameters. Both single phase CO_2 and a mixture of CO_2 and water have been studied to show the effect of produced water on corrosion rates. The model also is capable of handling different drill pipe and annular geometries.

CHAPTER 1. INTRODUCTION

The recent increase in oil prices during the past years has led to re-investing in reservoirs that were not previously economical to produce. In addition, many reservoirs have been partially depleted and the current industry trend is to infill drill and/or sidetrack abandoned reservoirs; seeking new reserves. The existence of such reservoirs has led to the extensive use of underbalanced drilling (UBD), because it minimizes formation damage. UBD is the best available technology for low pressure and/or depleted reservoirs. An UBD operation is considered a success when it achieves the required underbalanced pressure. Different UBD techniques may not achieve the required wellbore pressures. For example two-phase drilling fluids have been used extensively, but tend to generate high bottomhole pressure. In many situations, the high pressure is not the best solution for UBD. In cases such as deep wells with low bottomhole pressure, the use of these fluids will not achieve the required minimum circulating downhole pressure. The use of gases as drilling fluids may achieve the required circulating pressure but generate other problems. One such problem is the circulating gas density in the drill pipe is not able to operate down-hole motors. Recently, supercritical carbon dioxide (SC-CO_2) has been used in a few select applications. The unique features of SC-CO_2 make it a potential candidate for an UBD drilling fluid, since at higher pressure and temperature it will become supercritical, which gives it both gaseous and liquids properties. Recent authors have shown the potential of using SC-CO_2 in drilling operations[1,2]. This work will investigate the possible use of CO_2 as a drilling fluid by modeling the fluid hydraulics in such an UBD operation. Proper hydraulic modeling will optimize the drilling operation in terms of optimum pressure control and project design. In addition, developing a complete hydraulic model, which

takes into account a detailed study of the thermodynamic properties of CO_2, is needed, since the operation is very sensitive to temperature and pressure.

1.1 Underbalanced Drilling

Underbalanced Drilling (UBD) is the drilling process in which the circulating fluid bottomhole pressure is maintained below the formation flowing pressure. Many benefits are gained from using UBD operations, such as:

- Increase rate of penetration and bit life
- Minimization or elimination of differential sticking
- Minimization of lost circulation
- Reduced formation damage
- Increased well productivity

To obtain the best results, accurate design of UBD operations and knowledge of the previous reservoir history is needed for optimal results. In addition, UBD operations have increased in recent years due to the following:

- Depleted reservoirs.
- Awareness of skin damage.
- Elimination of lost circulation.
- Cost of differential sticking.
- Environmental benefits.

As in any operation, UBD has some limitations and is not used in:

- Geo-pressured shale.
- Thick salt formations.
- Unconsolidated sands.

UBD techniques can be categorized into two major categories based on the fluid used, which are:

- Gaseous drilling fluid.
- Gasified liquid and liquid drilling fluids.

Figure 1.1 shows density ranges for common UBD fluids; the most common fluid used is diesel aerated by injecting nitrogen into the liquid stream. This will achieve a reasonable UBD pressure window, hence achieving its goal. In addition to gasified liquids, gaseous fluids are used as an UBD fluid where low pressures can be achieved; common fluids are air, nitrogen, natural gas, and exhaust gas. The use of gaseous fluids is limited to dry formations where there are no hydrocarbons or water influxes.

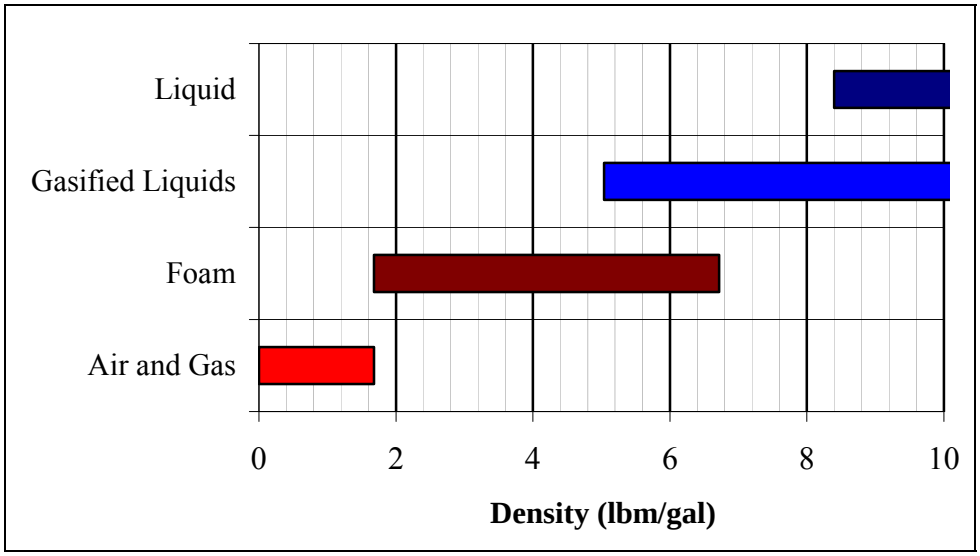

Figure 1.1 UBD Fluid Density Ranges

In addition, some of the limitations of using gaseous fluids can be:

- Water inflows
- Downhole fires
- Hole Instability
- Volume Requirement
- Compression Requirement

- Insufficient torque to run a downhole motor

The proper selection of the drilling fluid will increase the success of drilling in Underbalanced conditions by increasing the overall drilling rate, drilling unstable formation, and finally prevent formation damage due to lost circulation. For water inflow zone and high pressure zone it is preferred to use liquid of gasified liquid drilling fluids over gaseous drilling fluids. Figure 1.2 shows an aid for selecting the best UBD fluid[3].

Drilling Fluid	Improved ROP	Drill in Lost Circulation Zone	Water Inflow Zone	Sloughing Zone	Hard Rock Formation	High Pressure Zone	Borehole Collapse
Air and Gas Foam Gasified Liquids Liquid	⇧	⇧	⇩	⇩	⇧	⇩	⇩
Potential use	Increasing	Increasing	Increasing	Increasing	Increasing	Increasing	Increasing

Figure 1.2 Candidate UBD Fluids Based on Different Drilling Situations

1.2 Air and Gaseous Drilling Fluids

As discussed in the previous section, low circulating fluid pressures can be achieved with gaseous drilling fluids. The use of air as a circulating fluid was introduced in the early 1950's. A significant increase in rate of penetration and longer bit life were the major advantages from drilling with air, in addition to achieving low circulating pressures. The generated cuttings at the bit are lifted by the drag force exerted by the flowing air, opposing gravity. If the drag force is larger that the gravitational force then cuttings will travel up in the hole. On the other hand, cuttings will fall back where drag forces are lower than gravitational forces. There is a minimum threshold air velocity for cuttings transport. The criteria for minimum air injection required to lift the particles has been studied extensively in the literature by several authors[4,5,6,7,8]. The two criteria for minimum air or gas volume requirement are[3]:

- Minimum Kinetic Energy
- Minimum Velocity

Both criteria shown above will be discussed later in the model development. As in any operation, additional equipment is needed for air or gas drilling operations. The primary equipment needed is an air compressor capable of handling the gas volume required. Also, a rotating blowout preventor is recommended when drilling underbalanced. In some cases a closed circulating system is recommended[9]. In addition to air, nitrogen is also used in UBD operations as a drilling fluid, where as an inert gas will prevent downhole fires. Additionally it can be generated onsite (using membrane units). Identical to air drilling, gas volume requirements must be accurately predicted to optimize the process, in terms of cuttings lift capacity, compression requirements, and gas volumes.

1.3 Statement of Problem

In this work, the UBD operation hydraulics will be modeled to determine possible limitations and identify areas remaining further investigation. Since the thermodynamic properties of CO_2 are critical to this calculation, an accurate modeling of the wellbore temperature and pressure is needed. Also, an accurate equation of state describing the properties of CO_2 is needed. To this end, predicting the temperature at any point in the wellbore requires a heat transfer modeling of the wellbore. This means calculating heat flow gained or lost by the fluid both inside the drill pipe (CO_2) and the annulus (CO_2 or CO_2–water mixture) and by the earth. This calculation requires an iterative procedure. Simultaneously, this heat transfer model along with the equation of state is coupled with the fluid hydraulics to predict pressure at any point in the well. This calculation procedure requires a fairly large program code which is the primary result of this work.

Key assumptions made in the calculations are:

- Energy associated with a phase change of CO_2 (liquid to supercritical and supercritical to vapor) is ignored.
- Pressure drop across the bit is modeled with a simple choke equation for gases. This work merely requires a pressure drop across the bit, and exactly how that pressure is predicted or affected is left for future investigation.
- The annulus fluid is modeled as a single phase CO_2 gas or a mixture of formation water and CO_2. Cuttings in an UBD operation are assumed to be minimal and have minimal effect on the annular fluid. This is supported by the fact that UBD typically involves small diameter bits, controlled rate of penetration, and short intervals. However, minimum gas velocities to lift cuttings to the surface are calculated to assure hole cleaning.

Additionally, CO_2, when mixed with water is a known corrosive acid. This work will estimate corrosion rates as a function of temperature and pressure using an industry accepted procedure formulated by the Norwegian petroleum industry (NORSOK Standard).

CHAPTER 2. PROBLEM DESCRIPTION

In some ultra deep reservoirs (typically gas reservoirs), the need is to develop an UBD fluid which will achieve UBD conditions while optimizing operational costs. Some fluids have the unique ability to achieve such requirements. Carbon dioxide (CO_2) has been used in recent years as a jetting fluid where it's unique features above critical conditions makes it a best candidate to be used as an UBD fluid. Figure 2.1 shows the phase diagram of CO_2.

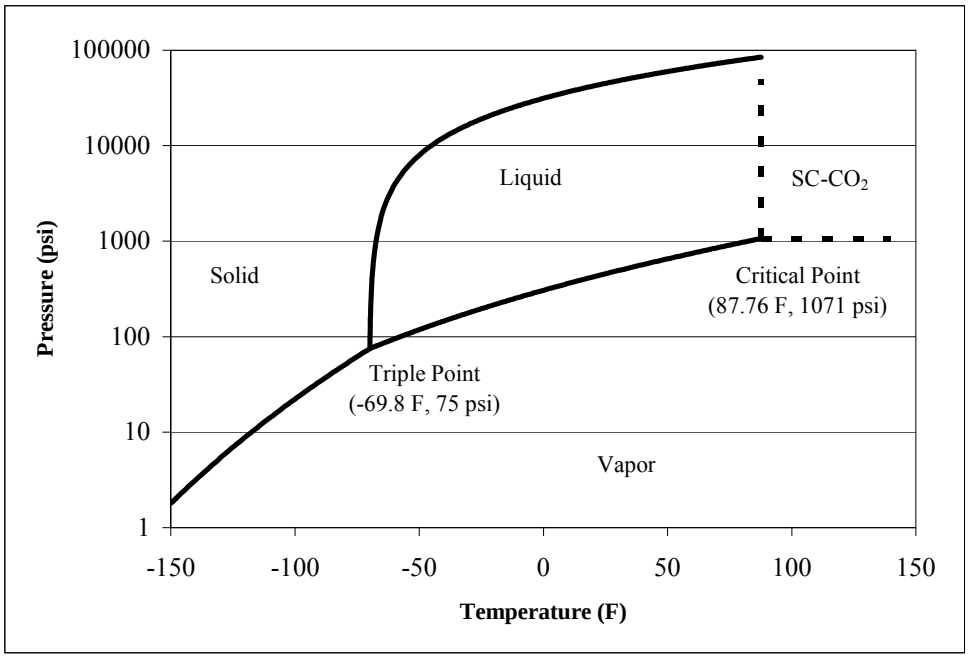

Figure 2.1 CO_2 Phase Diagram

As shown in the above figure, CO_2 will reach its supercritical condition at lower temperatures and pressures than most gases (T_{crit} = 87.8 °F, P_{crit} = 1071 psi). Supercritical fluids are highly compressed fluids that combine properties of gases and liquids in an intriguing manner; they have both the gaseous property of very low viscosity, and the liquid property high density. Figure 2.2 shows a comparison between CO_2 and nitrogen density over wide ranges of pressures and temperatures and compares the viscosities of both fluids. As seen in both figures, the unique properties of Supercritical CO_2 enables it to be an ideal candidate as a drilling fluid,

where the higher density will generate momentum to run a downhole motor and as soon as it exits the nozzle, the vapor phase will generate the required underbalanced conditions.

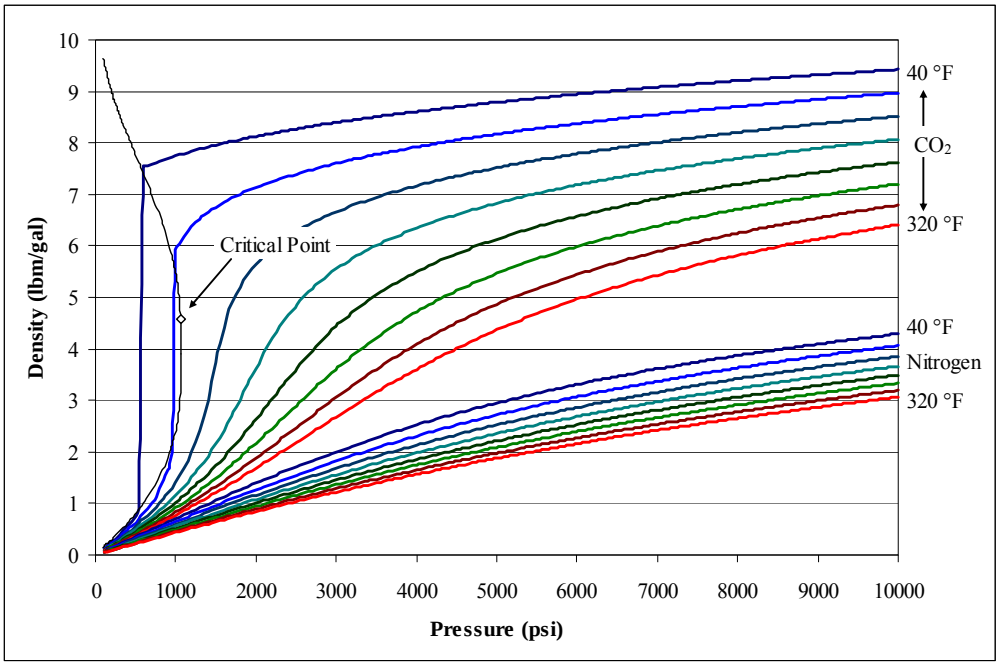

Figure 2.2 Comparison Between CO_2 and Nitrogen Densities at Various Conditions

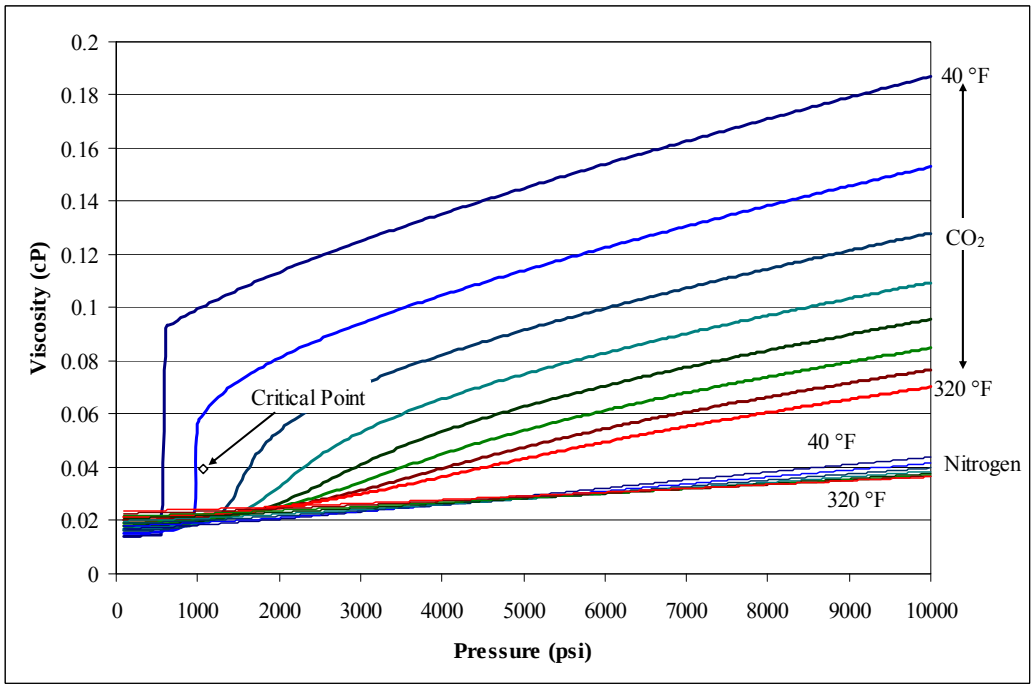

Figure 2.3 Comparison Between CO_2 and Nitrogen Viscosities at Various Conditions

Supercritical CO_2 (SC-CO_2) is used extensively in industrial applications as a solvent and as a cleaning material. The main advantages of using supercritical fluids in a drilling operation are:

- Increased mass transport
- Gases are totally miscible
- Minimal interfacial tension with many materials.
- Excellent for infusion and extraction
- Chemically inert and non-toxic
- Inexpensive fluids
- Environmentally compatible
- Solvent is tunable with pressure

Also, the use of SC-CO_2 as a drilling fluid will increase formation productivity since as an acid it will stimulate the Formation. Further stimulation after drilling would be minimized. Also, when using a closed drilling system, SC-CO_2 can be considered environmentally friendly since the gas will not be released to the atmosphere. The precise modeling of such systems in terms of predicting bottomhole conditions will optimize the use of such drilling fluids, and as shown in previous studies the use of mechanistic models tends to reduce errors in calculating expected pressure and injection parameters.

CHAPTER 3. LITERATURE REVIEW

3.1 Coil Tubing Drilling with SC-CO_2

Using SC-CO_2 as a jetting fluid for UBD operation has been investigated by Kolle[2,10], where a study of coiled-tubing with SC-CO_2 was investigated. High penetration rates were achieved as stated in the reference, as well as to productivity enhancements after drilling (no need to stimulate). Recently, Gupta et al.[1] investigated the use of SC-CO_2 coiled-tubing drilling for drilling deep reservoirs where common UBD fluids did not achieved the required UBD pressure windows. In addition, he observed that a gaseous drilling fluid could not generate sufficient torque for a downhole motor to rotate the bit.

These investigations have used the most common equation of state (Peng-Robinson) to describe the physical properties of CO_2. The use of this equation may give inaccurate results, since it is shown in the literature that equations of state will give inaccurate results near critical conditions[11].

3.2 Fluid Properties Model

Span and Wagner[12] have developed an equation of state designed for CO_2 which covers a wide range of pressure and temperature. They have used the free Helmholtz energy concept to model fluid properties in term of temperature and density. Pressures can be calculated using an iterative technique. In addition, they have developed their model using a regression of experimental measurements of CO_2 properties; this will cause their model to run smoothly through critical points, hence eliminating the irregular behavior around the critical conditions. This irregular behavior can be seen when using ordinary equation of states (PR, SRK and others)[13].

3.2 Heat Transfer Model

The use of a geothermal temperature gradient may not predict the correct bottomhole temperature, since at such conditions the fluid injection may alter bottomhole temperatures. Several authors have stated that the bottomhole temperature is changing for either production or injection. The temperature will increase for oil production due to the large heat capacity of oil, while gas will reduce the bottomhole temperature with the Joule-Thompson effect. The change of temperature is due to the exchange of heat between the wellbore fluid and its surroundings[14]. Several authors[15,16,17,18] have developed circulating temperature models, assuming steady state heat transfer in both conduits and formations[14]. Hasan and Kabir[18] have developed an un-steady state model for predicting bottomhole temperature for both forward and reverse circulations. In their model the specific heat capacity is fixed over the length of the wellbore.

3.3 Gas Volume Requirements

Several authors[4,5,6,7,8] have developed minimum gas volume requirements using the minimum kinetic energy criterion, which is based on the minimum annular velocity for effective lifting of the cuttings under standard conditions, assumed to be 50 ft/sec (3000 ft/min), which is usually referred as Angel's Method. To check whether we have an effective cuttings transport capacity, the cuttings transport ratio should be positive and larger than 0.7 for effective cutting transport in vertical wells and larger than 0.9 in horizontal wells[19].

3.4 Circulation Model

3.4.1 Single Phase Gas Flow

The models developed by Giffin et al[20] and Guo[21] are typically used to predict bottomhole pressure in UBD utilizing air or gas. In the case of drilling with SC-CO_2, a phase

change will occur in both the drill pipe and the annulus, hence the need for a more accurate prediction of bottomhole pressure. This prediction method must take into account the sensitivity of the phase state as a function of temperature and depth. The methods available for calculating the flowing bottomhole pressure, used in production operations, can be applied to simulate conditions during UBD operations. The method developed by Cullender and Smith[22] for gas flow makes no simplifying assumptions for the variation of temperature and compressibility factor. The Cullender and Smith technique calculates flowing bottomhole pressure by dividing the wellbore into multiple segments and using a marching algorithm to enhance the accuracy of the calculations.

3.4.2 Two Phase Flow

Several models exist for multiphase flow, divided into three main categories

- Homogenous approach.
- Empirical correlations approach.
- Mechanistic approach.

The homogenous approach was first used by Guo et al[23]. Their model calculated the required air rate for both maximum rate of penetration and cutting transport in foam drilling operations. They assumed that the foam can be treated as a two phase fluid in the bubbly region, in spite of the fact that they expected other flow regimes (bubble, slug, churn, and annular).

Empirical correlations are formulated by establishing a mathematical relationship based on experimental data. Application of empirical models is limited to the data range used to generate the model. Liu et al[24] developed a computer algorithm which analyzed the behavior of foam in UBD operations, modeling it as a two phase mixture. They calculated the frictional pressure drop using the mechanical energy equation coupled with a foam rheology model using

an equation of state. In addition, they united their model with the Beggs and Brill[25] method for calculating bottomhole pressure and developed a computer program called MUDLITE[26,27]. The current version of MUDLITE includes two phase flow correlations in addition to Beggs and Brill such as Orkiszewski[28], Hagedorn-Brown[29], and others. Those correlations also give reasonable results under certain flow conditions (such as stable flow in an oil well), but do not give reasonable results under other conditions. Tian[30,31] developed a commercial computer program named Hydraulic Underbalanced Simulator (HUBS), which was used to assist engineers in designing UBD operations, especially for the process of optimizing circulation rate and obtaining sufficient hole cleaning. HUBS uses empirical correlations for the UBD hydraulic calculations.

Mechanistic models were developed in recent years, making significant improvements in these types of calculations. These models are based on a phenomenological approach that takes into account basic principles (conservation of mass and energy). Recently ALAdwani[32] has developed a mechanistic multiphase steady state model to estimate the correct bottomhole pressure and temperature for flow in a vertical pipe. In addition, the two-phase flow model developed can handle different pipe and annular geometries, as well as deviated wellbores.

CHAPTER 4. METHODOLOGY

In order to better estimate circulating pressure, both inside both the drill pipe and the annulus, an accurate calculation scheme must take into account temperature and hole size / tubing geometries. The circulation model is divided into three main sub-models.

- Fluid Properties Model.
- Heat Transfer Model.
- Circulation Model.

All the above models are coupled together to estimate the circulating fluid pressure and temperature at different depth intervals. The equation of state by Span Wagner[12] will be used for the fluid properties model since it was designed specifically for CO_2. It is more accurate than the typically used Peng-Robinson equation of state. The accurate prediction of fluid properties requires accurate temperature and pressure prediction. The temperature inside the drill pipe and the annulus will not be equal to the geothermal gradient; a heat transfer model is used to calculate temperature distributions inside both the drill pipe and the annulus taking into account the variations of heat capacities and properties of the drilling fluid as a function of depth. The circulation model couples the two models above to estimate bottom hole pressure and temperature for either single phase CO_2 in the annulus or two phase flow of water and CO_2 in the annulus.

Figure 4.1 shows the logic flow of the calculations. In a calculation increment (ΔL), fluid properties (e.g. density, specific heat capacity and compressibility factor) are determined from the equation of state. Results from the heat transfer model are used by the circulation model to iteratively determine pressure and temperature.

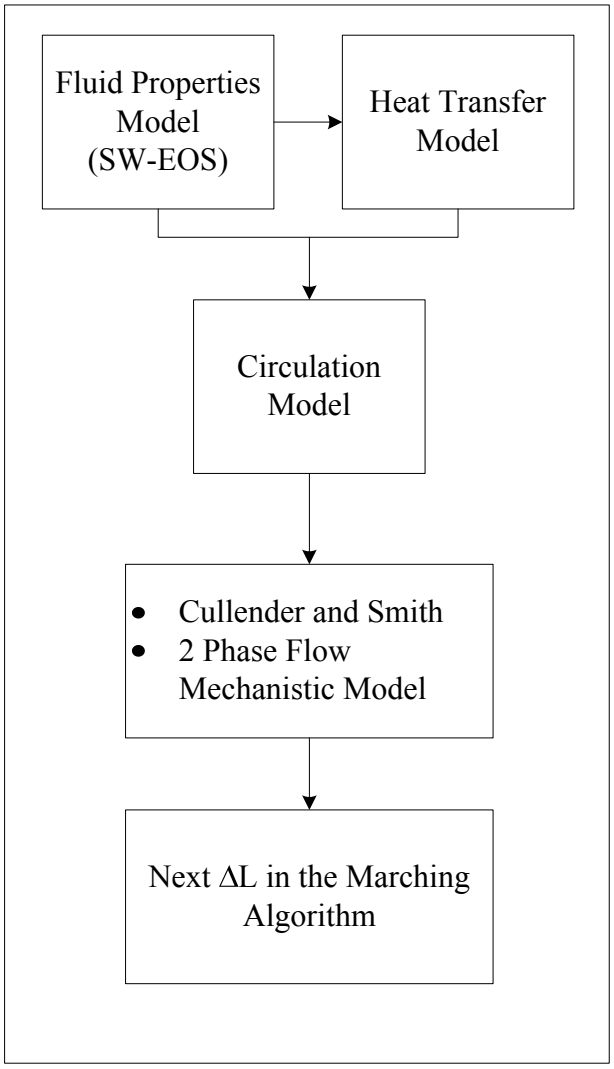

Figure 4.1 Flow Chart of Calculation Algorithm

CHAPTER 5. FLUID PROPERTIES MODEL

Accurate fluid property predictions have to account for varying pressures and temperatures. The use of the Peng-Robinson equation of state is feasible in the range of low pressure and temperature. Recently, Span and Wagner[12] developed a new equation of state for CO_2, and take into account varying temperature and pressure profiles. The model was developed using the basic form of the dimensionless Helmholtz energy (Φ),

$$\Phi = HE(\rho_r, T_r)/(RT) \tag{5.1}$$

where $HE(\rho_r, T_r)$ is the Helmholtz energy with reduced density and reduced temperature ($\rho_r=\rho_c/\rho$ and $T_r=T/T_c$). The dimensionless Helmholtz energy is divided into an ideal part (ϕ^o) and a residual part (ϕ^r) and is written as

$$\Phi(\rho_r, T_r) = \Phi^o(\rho_r, T_r) + \Phi^r(\rho_r, T_r) \tag{5.2}$$

From (5.2) other thermodynamics properties can be obtained from both the ideal and residual parts of the dimensionless Helmholtz energy as follow:

$$P(T,\rho) = -\left(\frac{\partial HE}{\partial \upsilon}\right)_T \tag{5.3}$$

$$z = \frac{P(\rho_r, T_r)}{\rho RT} = 1 + \rho_r \Phi^r_{\rho_r} \tag{5.4}$$

Other important parameters which are needed is the specific isobaric heat capacity (Cp) where

$$Cp(T,P) = \left(\frac{\partial h}{\partial T}\right)_P \tag{5.5}$$

(h) is the specific enthalpy and it is expressed as follows:

$$h(T,P) = HE - T\left(\frac{\partial HE}{\partial T}\right)_\upsilon - \upsilon\left(\frac{\partial HE}{\partial \upsilon}\right)_T \tag{5.6}$$

Or in terms of reduced Helmholtz energy and its derivative

$$h(\rho_r, T_r) = \left[1 + T_r\left(\Phi^o_{T_r} + \Phi^r_{T_r}\right) + \rho_r \Phi^r_{\rho_r}\right](RT) \tag{5.7}$$

Then (5.5) can be written as:

$$Cp(\rho_r, T_r) = \left[-T_r^2\left(\Phi^o_{T_r^2} + \Phi^r_{T_r^2}\right) + \frac{\left(1 + \rho_r \Phi^r_{\rho_r} - \rho_r T_r \Phi^r_{\rho_r T_r}\right)^2}{1 + 2\rho_r \Phi^r_{\rho_r} + \rho_r^2 \Phi^r_{\rho_r^2}}\right](R) \tag{5.8}$$

where the derivatives of both Ideal and residual Helmholtz terms are computed as follows:

$$\Phi_{\rho_r} = \left(\frac{\partial \Phi}{\partial \rho_r}\right)_{T_r} \tag{5.9}$$

$$\Phi_{T_r} = \left(\frac{\partial \Phi}{\partial T_r}\right)_{\rho_r} \tag{5.10}$$

$$\Phi_{\rho_r^2} = \left(\frac{\partial^2 \Phi}{\partial \rho_r^2}\right)_{T_r} \tag{5.11}$$

$$\Phi_{T_r^2} = \left(\frac{\partial^2 \Phi}{\partial T_r^2}\right)_{\rho_r} \tag{5.12}$$

$$\Phi_{\rho_r T_r} = \left(\frac{\partial^2 \Phi}{\partial \rho_r \partial T_r}\right) \tag{5.13}$$

Span and Wagner[12] have developed a regression model which calculates both the ideal and residual Helmholtz energy terms. The regression model takes the following form:

$$\Phi^o(\rho_r, T_r) = \ln(\rho_r) + a_1^o + a_2^o T_r + a_3^o \ln(T_r) + \sum_{i=4}^{8} a_i^o \ln\left(1 - e^{(-T_r \theta^o_{i-3})}\right) \tag{5.14}$$

And

$$\Phi^r(\rho_r, T_r) = \sum_{i=1}^{7} n_i \rho_r^{d_i} T_r^{t_i} + \sum_{i=8}^{34} n_i \rho_r^{d_i} T_r^{t_i} e^{\rho_r^{c_i}} + \sum_{i=35}^{39} n_i \rho_r^{d_i} T_r^{t_i} e^{\left[-\alpha_i(\rho_r-\varepsilon_i)^2-\beta_i(T_r-\gamma_i)^2\right]} + \sum_{i=40}^{42} n_i \Delta^{b_i} \rho_r e^{\left[-C_i(\rho_r-1)^2-D_i(T_r-1)^2\right]} \quad 5.15$$

where

$$\Delta = \left[1 - T_r + A_i\left((\rho_r - 1)^2\right)^{1/(2\beta_i)}\right]^2 + B_i\left((\rho_r - 1)^2\right)^{a_i} \quad 5.16$$

All the parameters in 5.14 and 5.15, except for the reduced density and temperature, are tabulated and are computed from the regression computed from Span and Wagner[12]. The estimated uncertainty in density ranges from 0.03% to 0.05%, as reported by the authors.

Typical fluid properties in circulation models are computed in terms of pressure and temperature, where the equations developed above are in terms of density and temperature. A modified bisection procedure is developed in order to compute the density and other parameters, using the original equation developed by Span and Wagner. From Eq (5.4)

$$P(\rho_r, T_r) = \left(1 + \rho_r \Phi^r_{\rho_r}\right)(\rho RT) \quad 5.17$$

Equation 5.17 can be minimized to find the required density (ρ) in terms of pressure and temperature, where the objective function is calculated at a given pressure (P) and temperature (T).

Viscosity is calculated using the Vesovic, et al.[33] correlation, the uncertainty in viscosity ranges from 0.3% in a dilute gas near room temperature to 5% at the highest pressures, as reported by the authors. Figure 5.1 shows the effect of temperature and pressure on density for both Peng-Robinson EOS and Span-Wagner EOS. As shown in the figure below, for the higher pressure ranges expected in the drill pipe, the PR-EOS over-estimates the density for the full temperature range, and at the lower pressure ranges (expected in the annulus) the two equations

of state are nearly equal. The density disparity between the two equations of state will tend to overestimate the calculated pressure in the drill pipe. In addition, other parameters calculated from the PR-EOS will suffer the same effect. Figure 5.2 shows a plot of viscosity variations for different pressure and temperature values. For higher pressure and temperatures (supercritical conditions) the viscosity of CO_2 is low, and has a density approaching that of water. In addition, Figure 5.3 shows the effect of pressure and temperature on the compressibility factor (z).

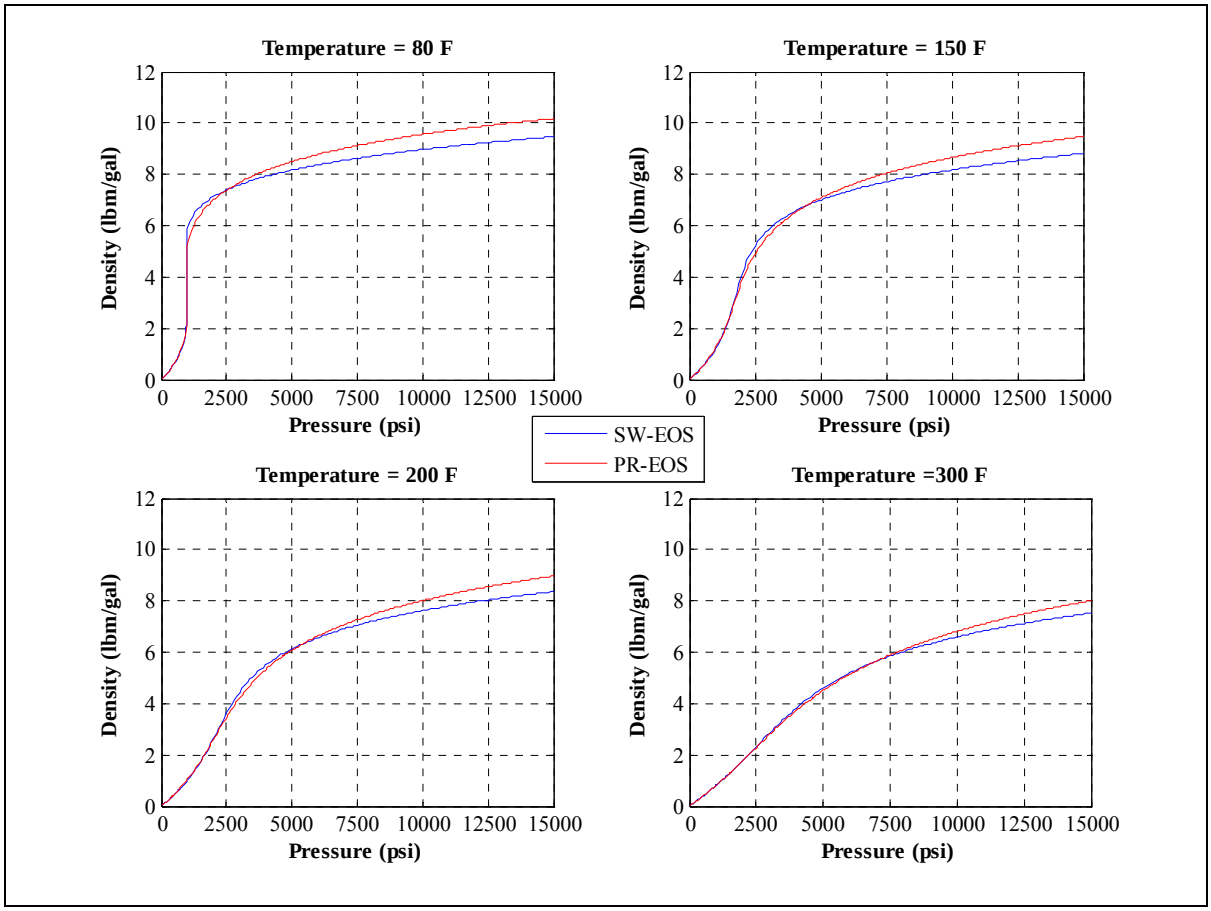

Figure 5.1 Density Comparison between PR-EOS and SW-EOS at Various Pressures and Temperatures

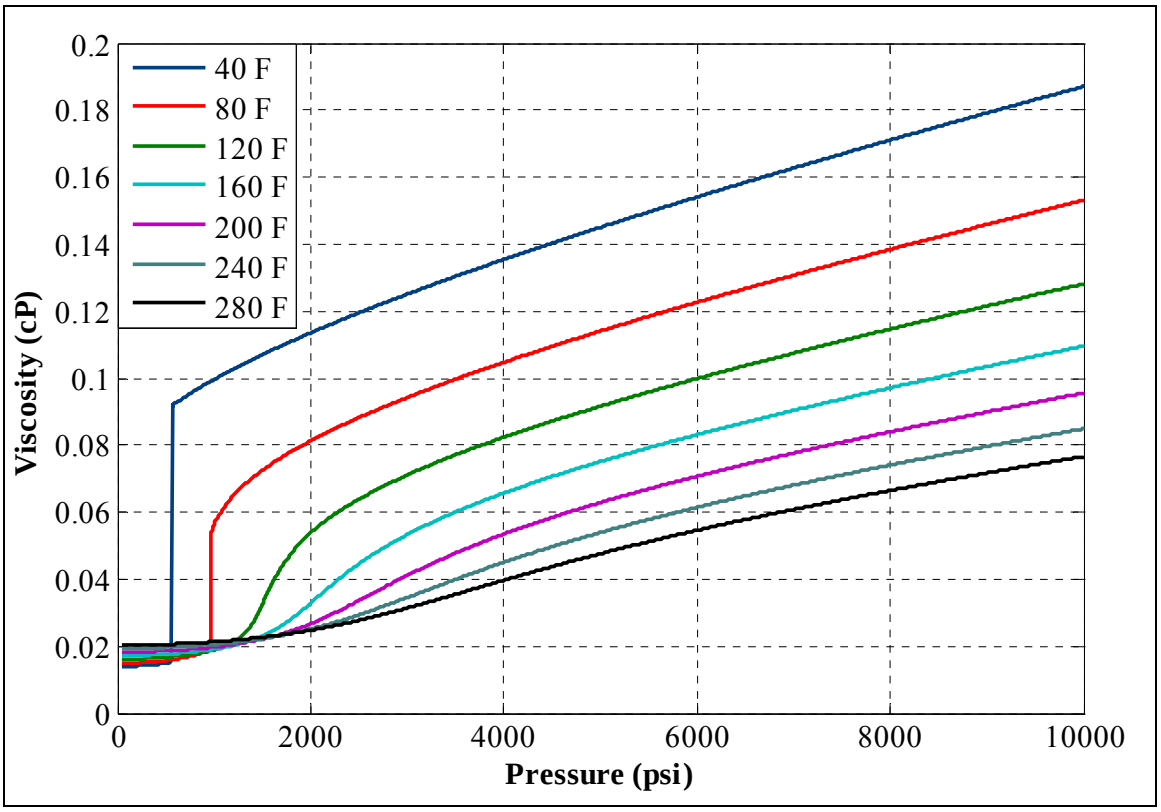

Figure 5.2 Viscosity of CO_2 vs. Pressure at Various Temperatures

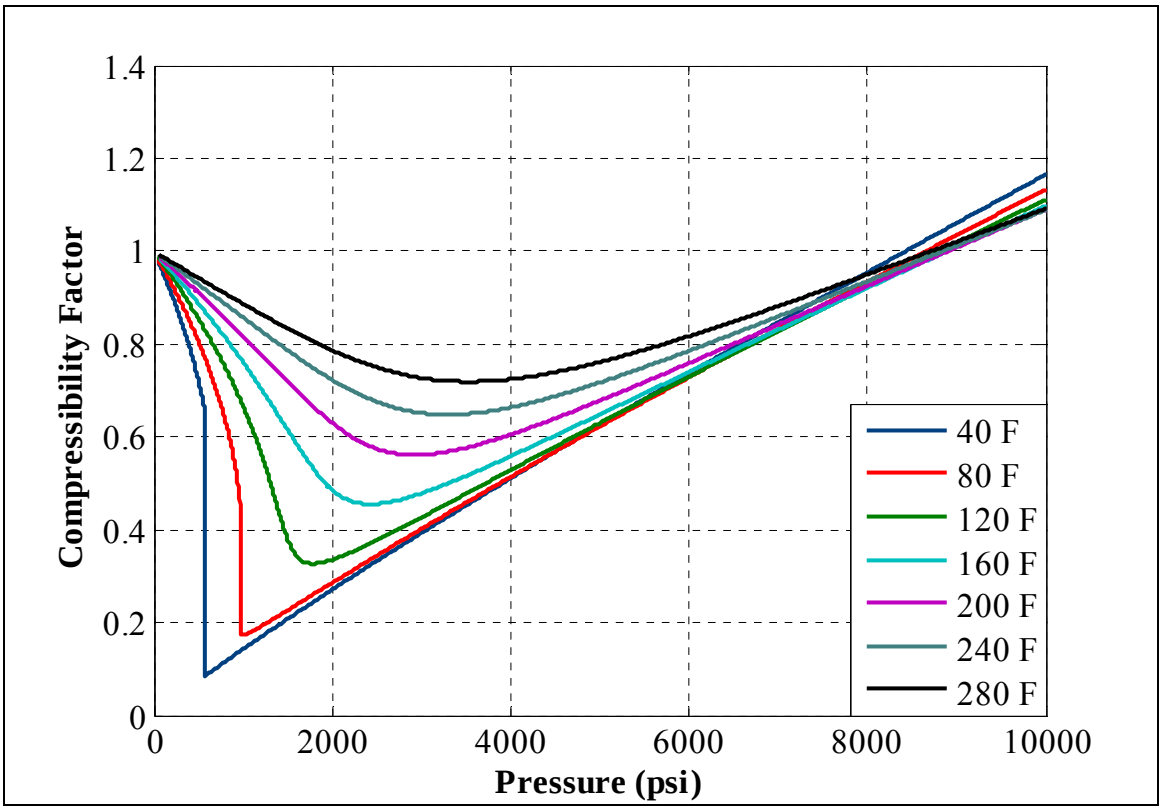

Figure 5.3 Compressibility Factor of CO_2 vs. Pressure at Various Temperatures

CHAPTER 6. HEAT TRANSFER MODEL

The knowledge of wellbore temperature during circulation has a direct effect on the computation of several fluid properties and the calculation of bottom hole pressure. The calculations of circulating temperature as a function of both depth and elapsed circulation time will enable one to control the circulation rate and consequently control bottom hole pressure.

6.1 Development of Heat Transfer Model for Single Phase Flow

Kabir, et al., have developed a circulating fluid temperature model to predict fluid circulation temperatures as a function of both depth and circulation time[18]. Using Kabir et al. as a starting point, this work improves the calculations by allowing density and specific heat capacity to vary with pressure along the length of the wellbore, rather than using fixed values. Figure 6.1 shows a schematic illustration of the heat transfer model.

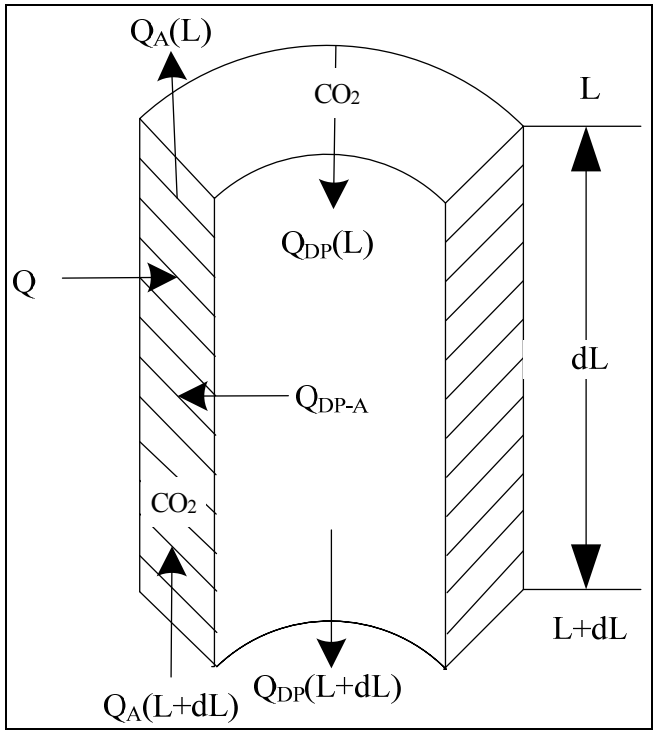

Figure 6.1 A Schematic Illustration of the Heat Transfer Model – Single Phase

In the above figure, Q, is the heat flow from the formation to the wellbore per unit length of the well per unit mass of the fluid (drilling mud) and is defined as

$$Q = \frac{2\pi k_e}{\dot{m} T_D}\left(T_{ei} - T_{wb}\right)dL \qquad 6.1$$

where:

k_e : Formation conductivity (BTU/(ft °F hr))

T_{ei} : Formation Initial Temperature (°F)

T_{wb} : Wellbore/formation interface temperature (°F)

$\dot{m}$: Mass flow rate (lbm/hr)

T_D : Dimensionless heat transfer time parameter (hr/ft^2)

In addition (Q_A), the convective heat flow in the annulus, is defined as

$$Q_A(L) = Cp_f\, T_A\, (L) \qquad 6.2$$

where

$Q_A(L)$: Convective heat flow in the annulus at length L (Btu/hr)

Cp_f : Drilling fluid specific isobaric heat capacity (Btu/(lbm °F))

T_A : Temperature inside the annulus (°F)

The convective heat flow in the drill pipe is given below as

$$Q_{DP}(L) = Cp_f\, T_{DP}\, (L) \qquad 6.3$$

where

$Q_{DP}(L)$: Convective heat flow in the drill pipe at length L (Btu/hr)

T_{DP} : Temperature inside drill pipe (°F)

The heat transfer from the fluid in the drill pipe to the annulus fluid is given by

$$Q_{DP-A} = \frac{Cp_f}{\beta}(T_{DP} - T_A)dL \quad 6.4$$

where β is defined as

$$\beta = \frac{Cp_f \dot{m}}{2\pi d_{DP} U_{DP}} \quad 6.5$$

where

U_{DP} : Drill pipe heat transfer coefficient (Btu/(hr °F ft^2))

d_{ODP} : Drill pipe outer diameter (ft)

The energy balance for the above model accounts for a downward flow through the drill pipe and then upward flow through the annulus. The convective energy associated with the mud entering a differential element is $Q_A(L+\Delta L)$, and leaves the element with $Q_A(L)$. In addition, heat enters this element by conduction (Q) from the formation. Therefore

$$Q_A(L+\Delta L)-Q_A(L)=Q_{DP-A}-Q \quad 6.6$$

$$Cp_f\left[T_A(L+\Delta L) - T_A(L)\right] = Q_{DP-A} - Q \quad 6.7$$

The dimensionless temperature (T_D) is estimated[34] from the dimensionless circulation time (t_D) as follow:

$$t_D = \left(\frac{k_e}{c_e \rho_e}\right) t_{circ} / r_{wb}^2 \quad 6.8$$

where

k_e : Earth conductivity (BTU/hr-ft-°F)

c_e : Earth heat capacity (BTU/lbm-°F)

ρ_e : Earth density (lbm/ft^3)

t_{circ} : Drilling fluid circulating time (hr)

r_{wb} : Wellbore radius (ft)

$$T_D = \left(1.1281\sqrt{t_D}\right)\left(1-0.3\sqrt{t_D}\right), \quad 10^{-10} \le t_D \le 1.5 \tag{6.9}$$

$$T_D = \left(0.4063+0.5\ln(t_D)\right)\left(1+0.6/\sqrt{t_D}\right), \quad t_D \ge 1.5 \tag{6.10}$$

The overall heat transfer coefficient for the annulus system relates the wellbore/formation interface temperature to the annular fluid temperature (T_A) as follows:

$$Q_F = \frac{2\pi d_{IC} U_a}{\dot{m}}\left(T_{wb} - T_A\right)dL \tag{6.11}$$

Equating 6.1 to 6.11 for the heat flow from the annulus to the formation, to eliminate (T_{wb}), we obtain the following expression:

$$Q = \frac{Cp_f}{\alpha_t}\left(T_{ei} - T_A\right)dL \tag{6.12}$$

where (α) is the time parameter as defined by Ramey[35], which accounts for the overall heat transfer coefficient for the wellbore/formation system and it is defined as follows:

$$\alpha = \frac{Cp_f\ \dot{m}}{2\pi}\left[\frac{k_e + d_{IC} U_a T_D}{d_c U_a k_e}\right] \tag{6.13}$$

where

d_{IC} : Casing Inner diameter (ft)

U_A : Annulus heat transfer coefficient (Btu/(hr °F ft^2))

From 6.12 and 6.4 equation 6.7 is written as

$$\alpha\frac{dT_A}{dL} = (T_A - T_{DP})\frac{\alpha}{\beta} - (T_{ei} - T_A) \tag{6.14}$$

In 6.14 the two unknowns are the annular fluid temperature (T_A) and the drill pipe fluid temperature (T_{DP}). The energy balance for the drill pipe leads to the following expression

$$Q_{DP}(L+dL) - Q_{DP}(L) = Q_{DP-A} \tag{6.15}$$

This means that

$$T_A = T_{DP} + \beta \frac{dT_{DP}}{dL} \quad 6.16$$

Combining 6.4 and 6.16 we get the following second-order linear differential equation:

$$\alpha\beta \frac{d^2T_{DP}}{dL^2} - \beta \frac{dT_{DP}}{dz} - T_{DP} + T_{ei} = 0 \quad 6.17$$

Formation temperature (T_{ei}) can be assumed to increase linearly with depth by the temperature geothermal gradient (G) at any depth (L) with initial surface temperature (T_{is}) as follows:

$$T_{ei} = T_{is} + G * L \quad 6.18$$

Thus equation 6.17 can be written as:

$$\alpha\beta \frac{d^2T_{DP}}{dL^2} - \beta \frac{dT_{DP}}{dz} - T_{DP} + T_{is} + Gg * L = 0 \quad 6.19$$

The following boundary conditions are needed to solve equation 6.19:

- $T_{DP} = T_{Inj}$, L = 0, i.e. at the surface the drill pipe fluid temperature equals fluid injection inlet temperature (T_{Inj}).
- dT_{DP}/dL, at total depth is zero. This means that there is no heat exchange between the annulus and wellbore fluid.

The solution of equation 6.19 yields a temperature distribution in both the drill pipe and the annulus in terms of depth and circulation time (a detailed solution is provided in Appendix B). For gaseous drilling fluids the accurate calculation of specific heat capacity is required, because of its low value. In addition, since pressure and temperature changes with depth, then an iteration scheme is needed to predict the temperature distribution in both the drill pipe and the annulus as follow:

1. Guess an initial temperature. A good estimate is the initial formation temperature at any given depth (L) where $T_{DP1} = T_{is}+G * L$.

2. Calculate specific heat capacity of the drilling fluid (Cp_{f1}) at T_{DP1}.
3. Calculate the temperature in drill pipe T_{DP2}.
4. Calculate new value for the specific heat capacity (Cp_{f2})
5. Check whether [Abs(Cp_{f1}- Cp_{f2}) < 1E-6].
    a. If True finish calculations.
    b. Else $T_{DP1} = T_{DP2}$, Goto step 2.

Table 6.1 Input Required for Heat Transfer Model

Well Total Depth	Drilling Fluid Specific Heat
Drill pipe Outer Diameter	Formation Geothermal Gradient
Drill bit size	Formation Specific Heat
Drilling Fluid Injection Rate	Formation Density
Drilling Fluid Density	Surface Temperature

6.2 Development of Heat Transfer Model with Formation Water Influxes

The model developed above assumes the same mass flow rate in both the drill pipe and the annulus, i.e., only single phase CO_2 exists in both the drill pipe and the annulus. In the case of drilling with CO_2, the high pressure inside the drill pipe causes the injected CO_2 to exist as the supercritical phase. After exiting through the nozzle it may encounter formation water influx, hence a modification to the above model is required to estimate the correct temperature distribution. Water, with its high specific heat, will have an effect on the heat transfer model (Kabir, et al.[36]) as well as the bottomhole pressure. Figure 6.2 indicates the CO_2 flow path and heat flow. The energy balance for the element shown is the same as the previous case (eq 6.6), with a different formulation of the heat transfer from the formation to the two phase mixture of water and CO_2, where a mean heat capacity of the mixture[37] ($Cp_{2\phi}$) is given as

$$Q_{2\phi} = \frac{Cp_{2\phi}}{\alpha}\left(T_{ei} - T_A\right)dL \qquad 6.20$$

The heat transfer from the injected gas inside the drill pipe to the annulus mixture is given by (Q_{DP-A}) as follow:

$$Q_{DP-A} = \frac{Cp_f}{\beta_A}(T_{DP} - T_A)dL \qquad 6.21$$

where

$$\beta_A = \frac{\dot{m}_A Cp_{2\phi}}{2\pi d_{DP} U_{DP}} \qquad 6.22$$

From (6.16) we have the annulus temperature - drill pipe temperature relationship as

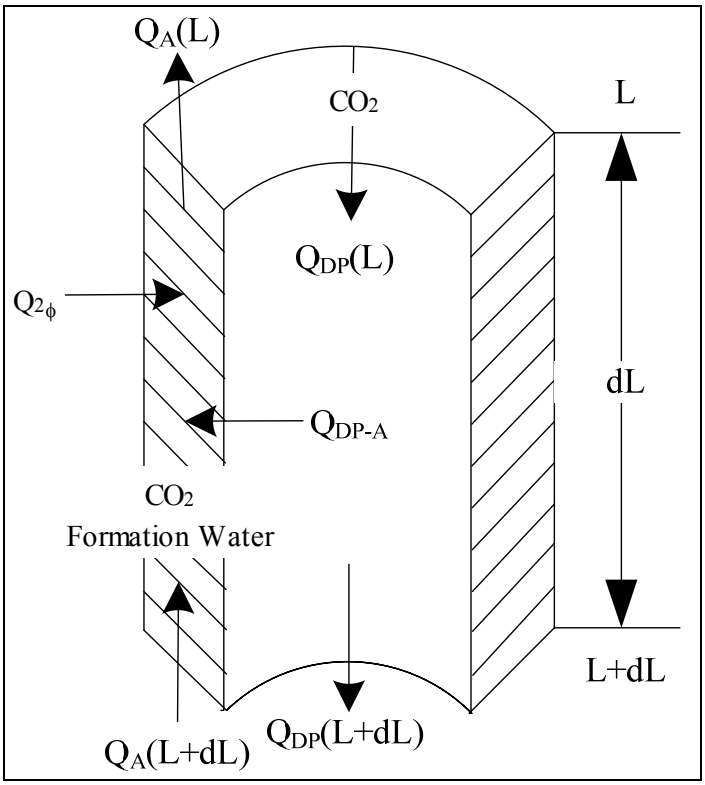

Figure 6.2 Schematic Illustration of the Heat Transfer Model-Two Phase Flow

$$T_A = T_{DP} + \beta_{DP}\frac{dT_{DP}}{dL} \qquad 6.23$$

$$\beta_{DP} = \frac{\dot{m}_{DP} Cp_{DP}}{2\pi d_{DP} U_{DP}} \qquad 6.24$$

Substituting the above expression in the general energy balance expression we have

$$Cp_{2\phi}\frac{dT_A}{dL}=\frac{Cp_{2\phi}}{\beta_A}(T_A-T_{DP})-\frac{Cp_{2\phi}}{\alpha}(T_{ei}-T_A) \quad 6.25$$

Rearranging we have the following equation

$$Cp_{2\phi}\frac{dT_A}{dL}-\frac{Cp_{2\phi}}{\beta_A}(T_A-T_{DP})+\frac{Cp_{2\phi}}{\alpha}(T_{ei}-T_A)=0 \quad 6.26$$

The above equation has three terms as follow:

$$Cp_{2\phi}\frac{dT_A}{dL}=Cp_{2\phi}\frac{dT_{DP}}{dL}+Cp_{2\phi}\beta_{DP}\frac{d^2T_{DP}}{dL^2} \quad 6.27$$

$$\frac{Cp_{2\phi}}{\beta_A}(T_A-T_{DP})=Cp_{2\phi}\frac{\beta_{DP}}{\beta_A}\frac{dT_{DP}}{dL} \quad 6.28$$

$$\frac{Cp_{2\phi}}{\alpha}(T_{ei}-T_A)=\frac{Cp_{2\phi}}{\alpha}\left(T_{is}+GL-T_{DP}(L)-\beta_{DP}\frac{dT_{DP}}{dL}\right) \quad 6.29$$

Substituting in 6.26 and rearranging we have:

$$\zeta_1\frac{d^2T_{DP}}{dL^2}+\zeta_2\frac{dT_{DP}}{dL}-T_{DP}(L)+T_{is}+GgL=0 \quad 6.30$$

With

$$\zeta_1=\alpha\beta_{DP} \quad 6.31$$

$$\zeta_2=\alpha-\alpha\frac{\beta_{DP}}{\beta_A}-\beta_{DP} \quad 6.32$$

Equation 6.30 is a second order differential equation with the following boundary conditions:

- $T_{DP}(0)=T_{DPi}$, drill pipe fluid temperature equals injection temperature at the surface.
- $T_A=T_{is}+(G)(WTD)$, annulus temperature at the bottom of the hole is the initial earth temperature and (WTD) is the well total depth.

Equation 6.30 is a general equation for predicting circulating fluid temperature in the drill pipe and the annulus, given conditions such as single phase flow in both the drill pipe and the annulus or two phase flow in the annulus. Equation 6.19 can be derived from the general differential equation, where, for single phase flow in both the drill pipe and annulus, we have $\beta_{DP}=\beta_A=\beta$, hence $\zeta_1=\alpha\beta$, $\zeta_2=-\beta$.

Thus equation 6.30 reduces to the following form

$$\alpha\beta\frac{d^2T_{DP}}{dL^2}-\beta\frac{dT_{DP}}{dL}-T_{DP}(L)+T_{is}+GgL=0$$

This is same as the differential equation derived for single phase flow in both the drill pipe and the annulus.

6.3 Sample Calculations

6.3.1 Single Phase Flow Heat Transfer Model

In the following section, some numerical calculations are performed to evaluate results obtained from the developed models, assuming that thermal properties are constant, i.e., don't change with depth. Validation of this model against physical data is presented in Chapter 8.

Table 6.2 Heat Transfer Example Input Data

Well Total Depth	7000	ft
Drill pipe Outer Diameter	1.75	in
Drill bit size	4.5	in
Injection Rate	3000	SCFM
Formation Specific Heat	0.2	BTU/(lbm-F)
Formation Density	165	lbm/ft3
Surface Temperature	60	F
Geothermal Gradient	0.01494	F/ft
Circulation Time	10	hrs

Two fluids (CO_2 and Air) were used as examples to predict the circulating fluid temperature in both the drill pipe and the annulus, as shown in Figure 6.3. As expected, air did not have a significant effect on the temperature distribution, due to its low heat capacity relative to other drilling muds[38]. CO_2 has a higher heat capacity, and hence the injected CO_2 will gain more heat than using air as a drilling medium. This is also shown in Figure 6.4 and Figure 6.5. As can be seen from Figures 6.6 and 6.7, lower injection rates tend to reduce heat storage, (which will not resist formation heat), for the air drilling scenario, at the lower rates, the temperature distribution is essentially the same as the geothermal gradient temperature, this compares to the CO_2 case where the temperature is lower at the lower injection rate.

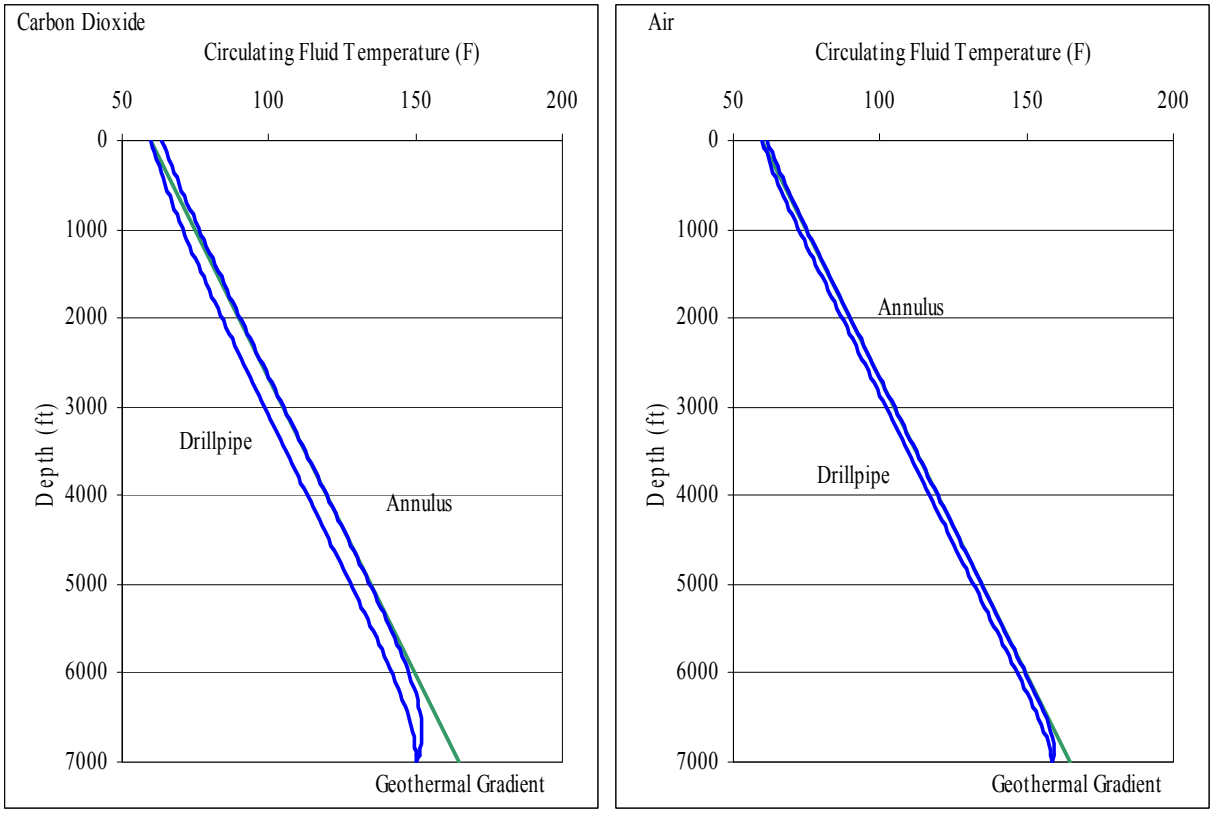

Figure 6.3 Comparison Between CO_2 and Air Temperature Distribution

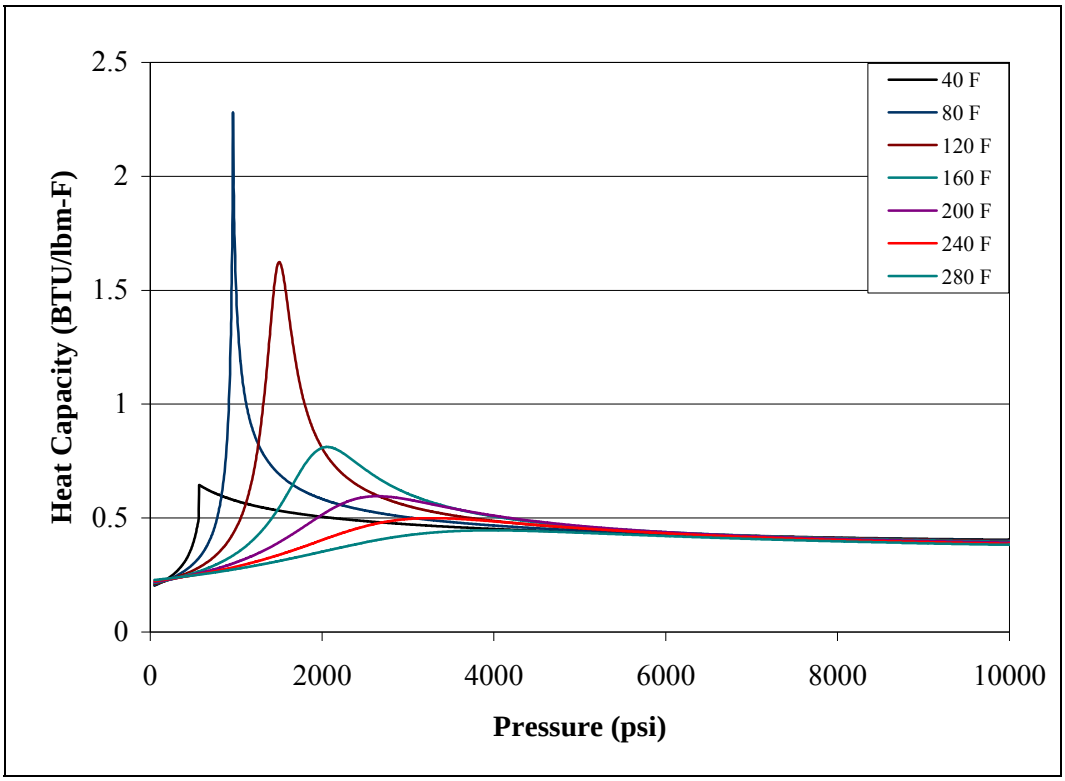

Figure 6.4 CO_2 Heat Capacity at Various Pressures and Temperatures

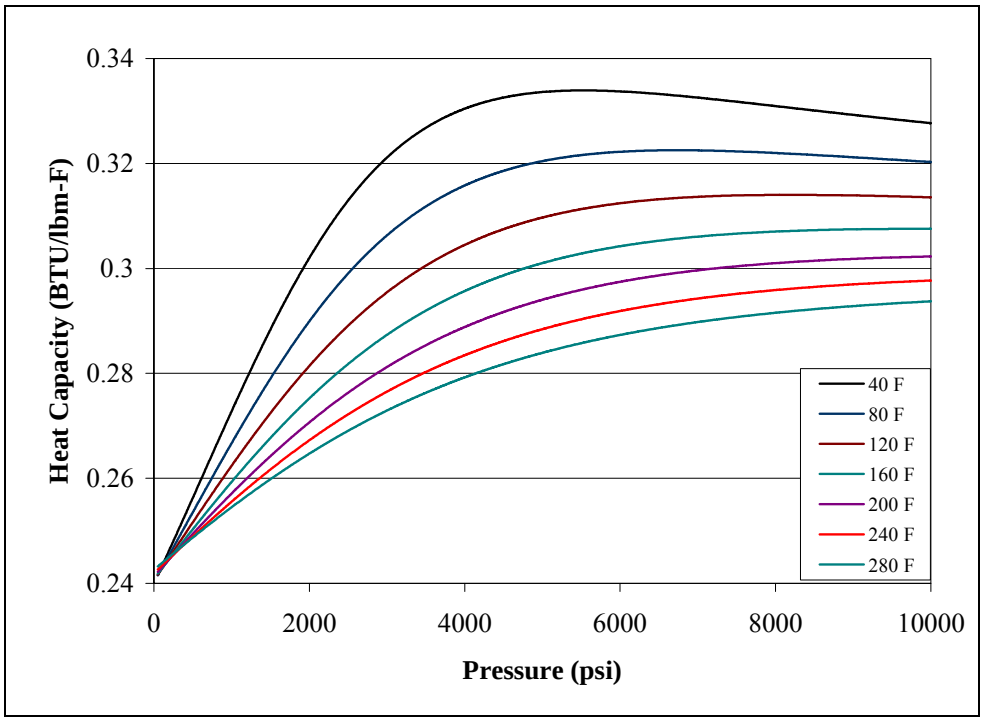

Figure 6.5 Air Heat Capacity vs. Pressure at Various Temperatures

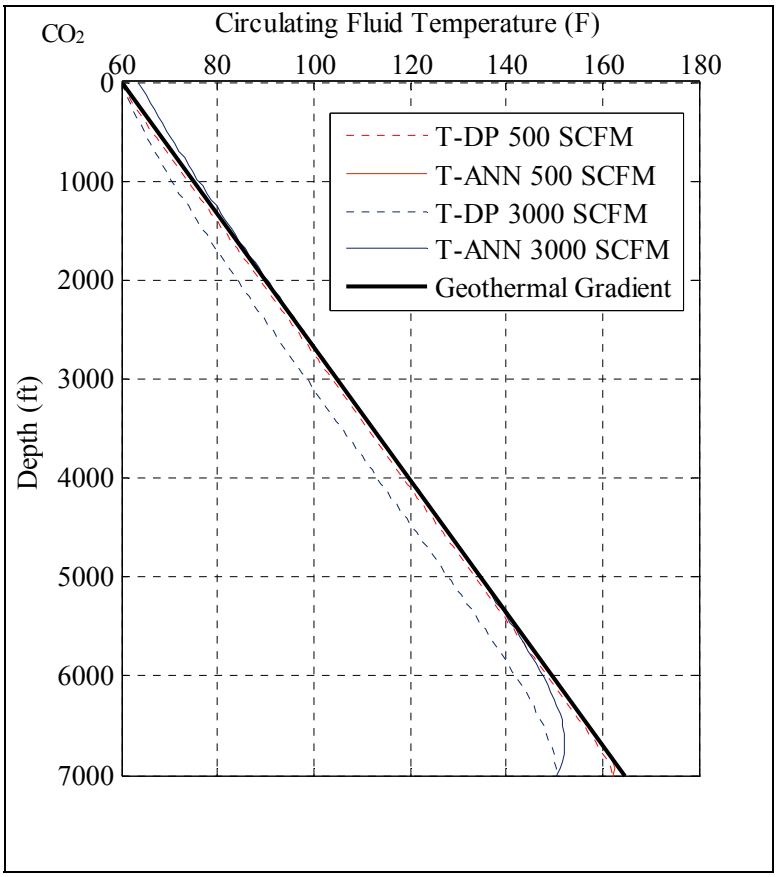

Figure 6.6 Effect of Injection Rate on CO_2 Circulating Temperature

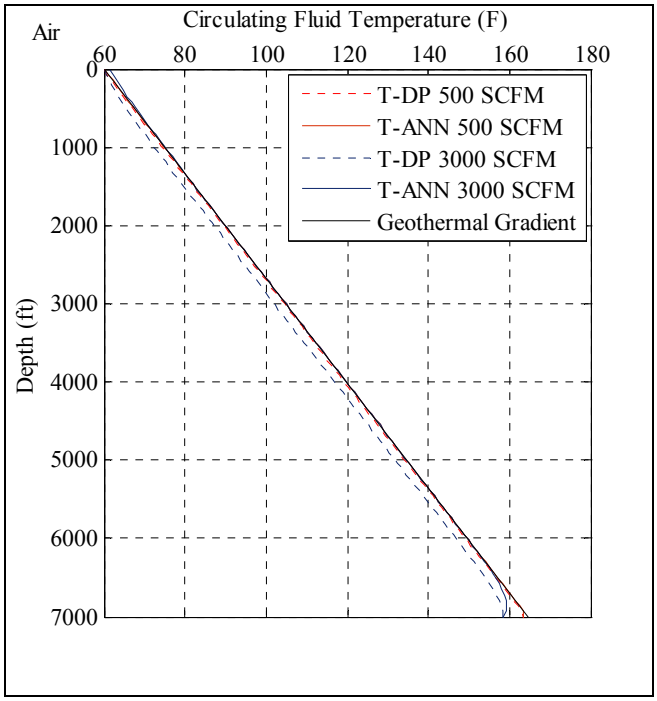

Figure 6.7 Effect of Injection Rate on Air Circulating Temperature

In addition, Figure 6.8 shows the temperature sensitivity of the circulating fluid temperature to the CO_2 injection rate. For higher mass rates injected at the drill pipe, the overall heat capacity will be reduced due to the low heat capacity of CO_2. As for the annulus, its temperature is higher than the drill pipe temperature because it is able to exchange heat with the surrounding formation at a rate faster than the drill pipe. This is shown with the increased temperature inside the annulus while at the same depth it is simultaneously decreased in the drill pipe.

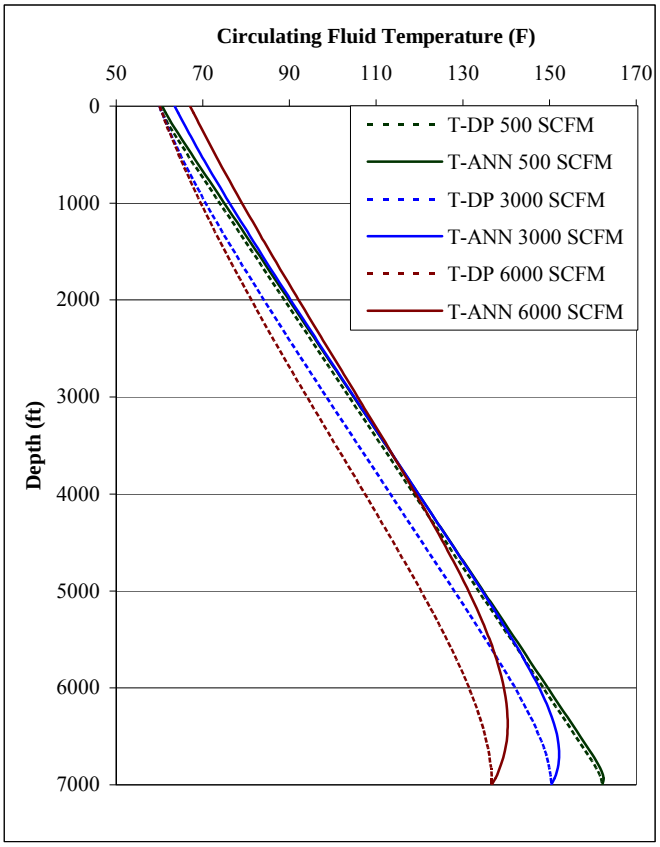

Figure 6.8 Effect of Increasing CO_2 Injection Rate on Circulating Temperature Distribution

6.3.2 Two Phase Flow Heat Transfer Model

The following examples show temperature distributions inside the drill pipe and annulus with formation water influx during air or gas drilling. A sensitivity study of the developed model will show how the models behave for different operational parameters as follows:

- Gas Type (CO_2 or nitrogen)

- Gas Injection Rate (500 SCFM, 3000 SCFM, 6000 SCFM)
- Water Production Rate (10 STB/D, 100 STB/D, 1000 STB/D)

Figure 6.9 shows how the bottomhole exit fluid temperature is affected by the gas type in addition to the various injection / influx rates. The reference line shows the earth initial bottomhole temperature. The bottomhole temperature increases with both increasing gas injection and water production rates. In addition, because of the lower heat capacity of the injected gas, a lower temperature at the exit is expected, due to the reduction of the total overall heat transfer coefficient.

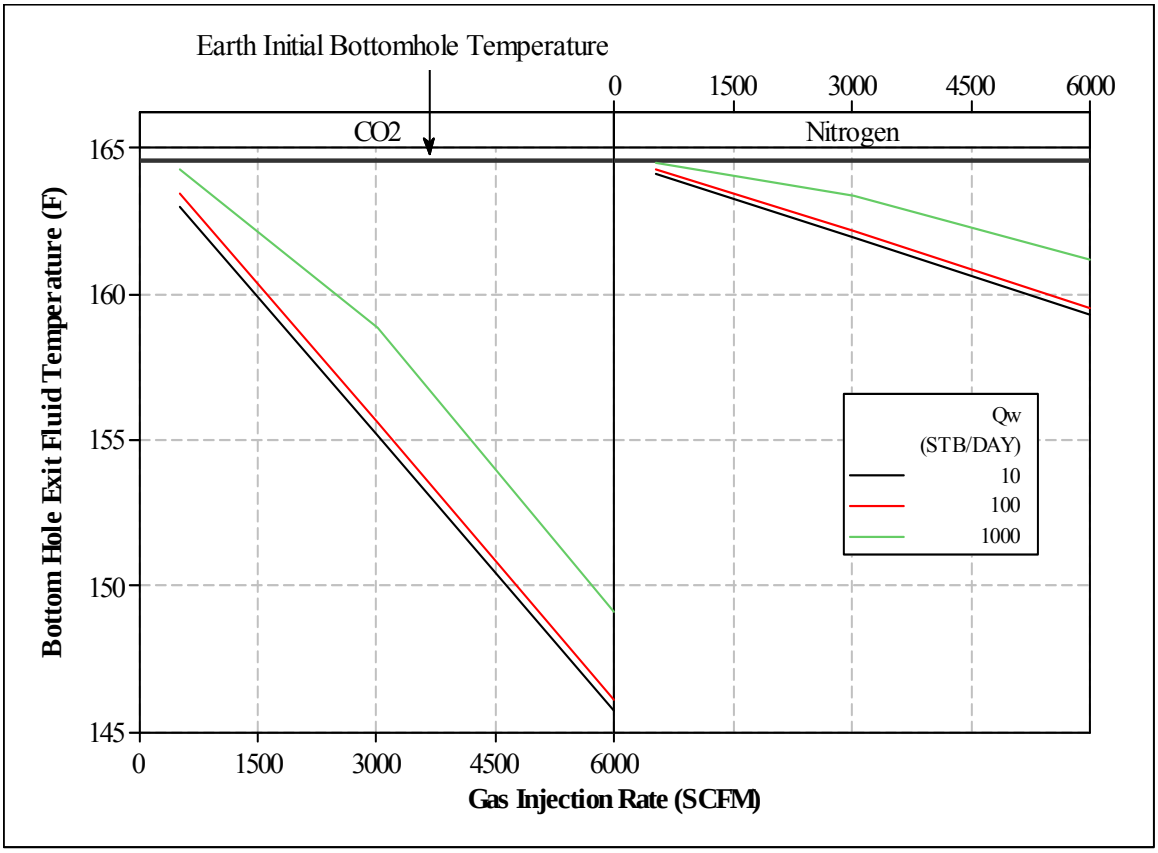

Figure 6.9 Bottomhole Exit Fluid Temperature Sensitivity

Figure 6.10 shows the sensitivity of the surface exit fluid temperature at the choke. The exit temperature increases with both increases in gas injection rate and water production rates. The

increase in temperature is due to the effect of the produced water on temperature, where a higher surface temperature is achieved with high gas injection rates due to the higher mass rate associated with it. In addition the same surface temperature is achieved with lower water production and gas injection rates.

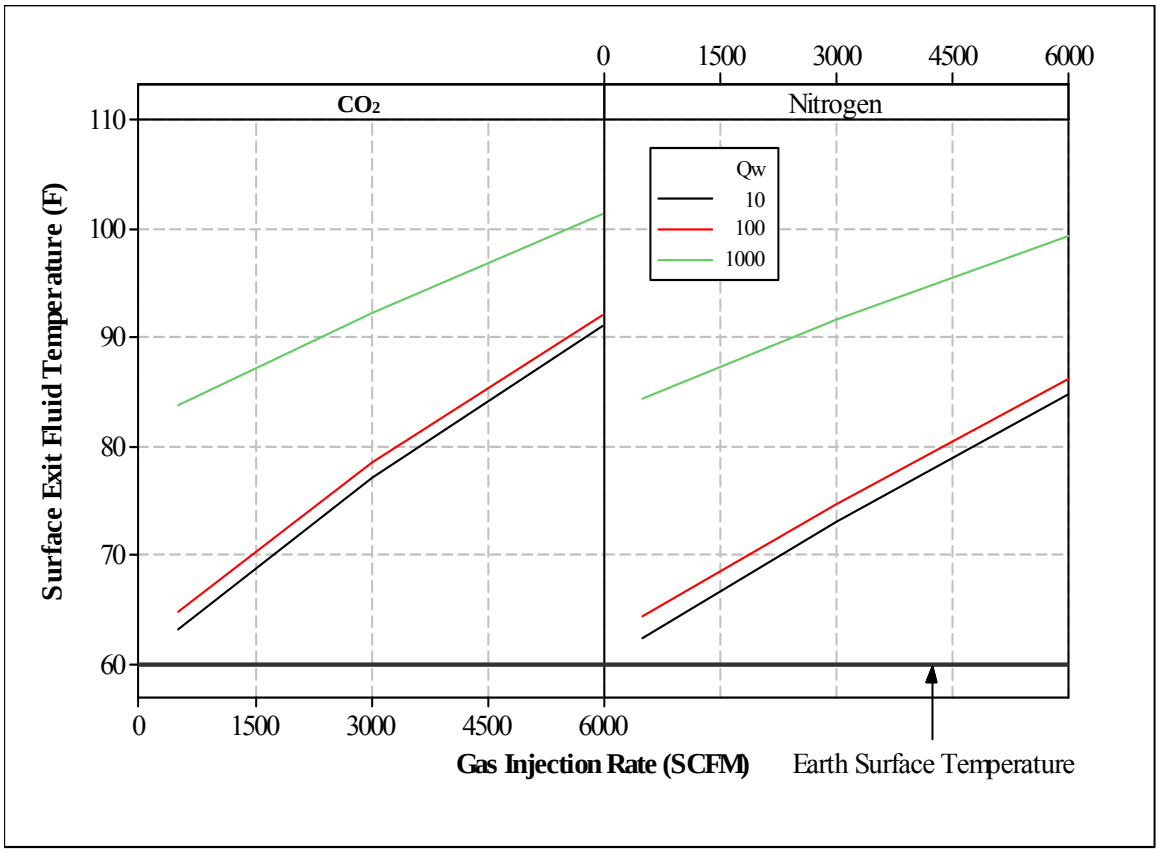

Figure 6.10 Surface Exit Fluid Temperature Sensitivity

CHAPTER 7. CIRCULATION MODEL

7.1 Model Assumptions

Both the PVT and heat transfer models were used for predicting the circulation pressure and the temperature inside the drill pipe and the annulus, with the following assumptions:

- For supercritical CO_2 the fluid is considered highly compressible, hence the Cullender and Smith[22] method is recommended for calculating flowing bottomhole pressure for the drilling fluid inside drill pipe, using the marching algorithm as shown above.
- In the annulus, the model is designed to account for formation water influxes, with CO_2 solubility in the formation water.
- For the case of only CO_2 in the annulus, the model will use the Cullender and Smith[22] method. For formation water influx, a two-phase mechanistic model[32] will be used to handle mixture of these fluids, to estimate the correct bottomhole pressure and temperature. In addition, the two-phase flow model can handle different pipe and annular geometries in deviated wellbores.
- The corrosion calculations were conducted as defined by NORSOK[41] (Appendix C). This NORSOK standard model is developed with broad petroleum industry participation by interested parties in the Norwegian petroleum industry and is owned by the Norwegian petroleum industry represented by The Norwegian Oil Industry Association (OLF) and Federation of Norwegian Manufacturing Industries (TBL)[41].
- Water properties were modeled according to the IAPWS IF97 standard formulation[42].

The computer program is divided into the following subroutines to facilitate the necessary calculations:

- Heat Transfer Subroutine: For calculating temperature distributions in the drill pipe and the annulus.
- PVT Subroutine: Subroutine for calculating the required fluid and thermal properties. In this case, using the multi-parameter equation of state by Span and Wagner[12] (the equation of state was used in a version programmed by the "Lehrstuhl feur Thermodynamik, Ruhr-Universitaet Bochum").
- Circulation Model Subroutine:
    - Downward flow inside the drill pipe for single phase CO_2.
    - Upward flow in the annulus
        - Single Phase CO_2.
        - Two-Phase CO_2 and formation water influx.

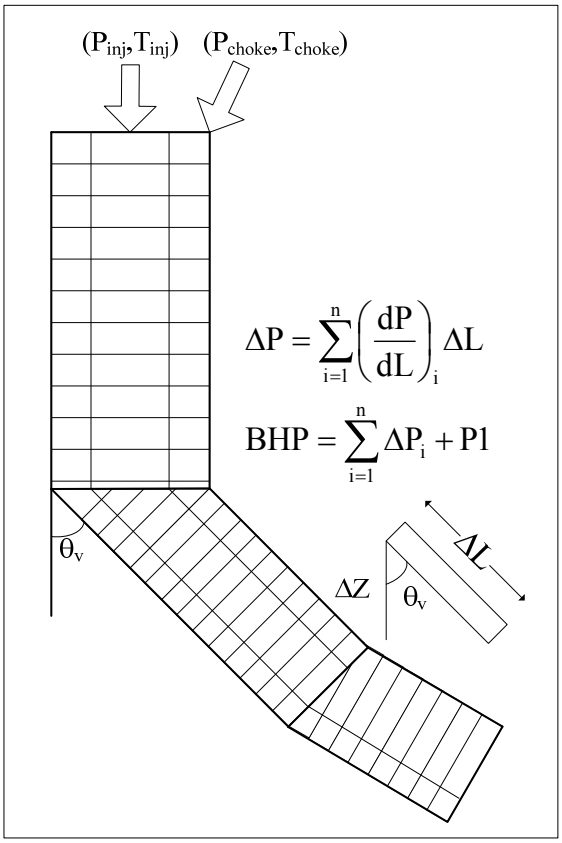

Figure 7.1 Wellbore Calculations Path in Deviated Wells

Length intervals (ΔL's) as shown in Figure 7.1, are identical in the annulus and the drill pipe and therefore identical along side one another. That length may change if a pipe diameter change is encountered, where (ΔL's) of different values are used. However this new length is used inside the drill pipe and the annulus along side each other. After this encounter ΔL is reset to its original value. The above subroutines are coupled in order to perform the calculation for bottomhole pressure as shown below in the calculation procedure.

7.2 Calculation Procedure

For typical UBD, the operation is controlled by manipulating the exit choke pressure to achieve the required underbalanced window. As shown above, the calculations begin from a known point, which is the surface choke pressure and temperature and the calculations march incrementally along the length ΔL with an angle θ_V. At each step the differential pressure is calculated, until the bottom of the hole is reached. At the bit nozzle, the pressure drop across the nozzle is calculated and the calculations continue up the drill pipe until the injection point is reached. The calculation direction is opposite to the flow direction because the assumed known starting point is the surface choke pressure and temperature. In the case for gaseous drilling fluids, the exit mass flow rate across the nozzle is needed to calculate the temperature distribution inside the annulus. Hence the following procedure is used to calculate the expected bottomhole pressure and temperature:

1. From the drill pipe, assume different injection pressures and calculate the pressure and temperature above the bit nozzle (P_1, T_1) using the downward flow of CO_2 with the Cullender and Smith[39] method.
2. (P_1, T_1) and the mass flow rate will be used as an input for the annulus heat transfer model.

3. From the annulus, start the calculations from the surface choke pressure and temperature and calculate the bottomhole pressure and temperature (P_2, T_2) using either single phase CO_2 or two-phase CO_2 and formation water influx.
4. Calculate the pressure drop across the bit nozzles assuming the supercritical CO_2 will exit the nozzle at sonic velocity. Add this pressure drop P_2 to get the nodal pressure, as shown in Figure 7.2.
5. The nodal point now has two pressure values, one from the drill pipe and one from the annulus.
6. A unique solution exists where the required injection pressure will match both pressure points.
7. Once the required injection pressure is determined then the bottomhole pressure and temperature are calculated at the specified injection pressure.

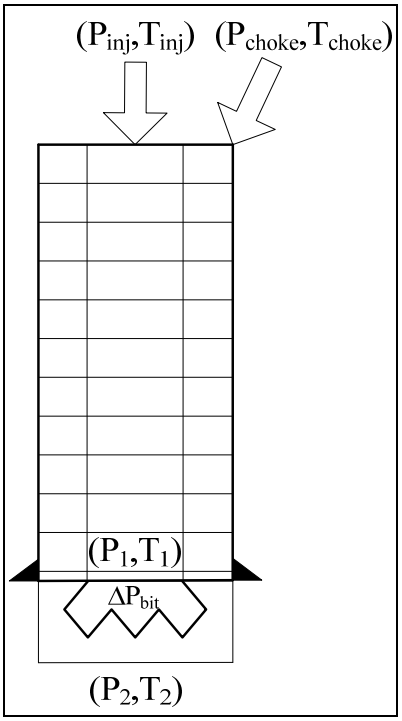

Figure 7.2 Schematic Illustration of the Proposed Solution

7.3 Single Phase Gas Flow Model Development

From the basic mechanical energy equation, with no shaft work or kinetic energy, we have[43]

$$\frac{144}{\rho_G}dP + \frac{g}{g_c}dz + \frac{f v_G^2}{2 g_c d'}dL = 0 \qquad 7.1$$

where

ρ_G: Gas density (lbm/ft^3)

f: Friction factor term

v_G: Gas velocity (ft/sec)

z: Compressibility factor

g: Acceleration of gravity (ft/sec^2)

g_c: Dimensional constant (ft-lbm/lbf-sec^2)

d': Pipe diameter (ft)

Using real gas law we have the following:

$$\rho_G = \frac{PM_G}{zRT} = \frac{P\gamma_G M_{air}}{zRT} \qquad 7.2$$

In addition the velocity can be expressed as follows:

$$v_G = \frac{5.17 Q_G}{d^5}\frac{zT}{P} \qquad 7.3$$

where

Q_G: Gas injection rate at standard conditions (SCF/min)

d: Diameter of the flow path (in)

Inside the drill pipe (d) is the inner pipe diameter whereas in the annulus, d is the hydraulic diameter (d_h), where

$$d_h = d_{IC} - d_{ODP} \tag{7.4}$$

The friction factor term is calculated based on Reynold's number (N_{RE}) as follows:

$$N_{RE} = \frac{13.88\gamma_G Q_G}{\mu_G d} \tag{7.5}$$

where

d_{IC}: Casing inner diameter (in)

d_{ODP}; Drill pipe outer diameter (in)

The friction factor is calculated as follows[43]:

$$f:\begin{cases} f = \dfrac{64}{N_{RE}}, & N_{RE} \le 2000 \\ \dfrac{1}{\sqrt{f}} = 1.74 - 2\log\left(\dfrac{2\varepsilon}{d} + \dfrac{18.7}{N_{RE}\sqrt{f}}\right) & 2000 < N_{RE} \le 4000 \\ \dfrac{1}{\sqrt{f}} = 1.74 - 2\log\left(\dfrac{2\varepsilon}{d}\right) & N_{RE} > 4000 \end{cases} \tag{7.6}$$

For a deviated wellbore with an angle θ_V from the vertical (Figure 7.1) we have

$$\Delta Z = \cos(\theta_V)\Delta L \tag{7.7}$$

Combining (7.2-7.7) with equation 7.1 we have the following

$$\frac{53.34}{\gamma_G}\left(\frac{Tz}{P}\right)dP + \cos(\theta)dL + \frac{0.0346 f Q_G^2}{d^5}\left(\frac{Tz}{P}\right)^2 dL = 0 \tag{7.8}$$

Cullender and Smith[22] solved the above equation as a function of both temperature and (z).

Separating variables we have:

$$\frac{\left(\dfrac{Tz}{P}\right)}{\cos(\theta) + \dfrac{0.0346 f Q_G^2}{d^5}\left(\dfrac{Tz}{P}\right)^2} dP = -\frac{\gamma_G}{53.34} dL \tag{7.9}$$

Rearranging we have

$$\frac{\left(\frac{P}{Tz}\right)}{\left(\frac{P}{Tz}\right)^2 \cos(\theta) + \frac{0.0346 f\, Q_G^2}{d^5}} dP = -\frac{\gamma_G}{53.34} dL \qquad 7.10$$

Integrating and reversing the limits of integration to solve for the bottomhole pressure, we have

$$\int_{P_s}^{P_{bh}} \frac{\left(\frac{P}{Tz}\right)}{\left(\frac{P}{Tz}\right)^2 \cos(\theta) + \frac{0.0346 f\, Q_G^2}{d^5}} dP = \frac{\gamma_G}{53.34} L \qquad 7.11$$

Using numerical integration the right hand side integral can be solved as follow[43]:

$$P_{bh} = P_S + \frac{6\alpha_{CS}}{I_{bh} + I_{mp} + I_S} \qquad 7.12$$

with

$$\alpha_{CS} = 0.01875 \gamma_G L$$

$$I = \frac{(P/Tz)}{(P/Tz)^2 \cos(\theta) + \Omega}$$

$$\Omega = \frac{0.0346 f\, Q_G^2}{d^5}$$

The subscripts (bh), (mp) and (s) refer to bottomhole, mid-point and surface.

The following procedure is used to perform Cullender and Smith type calculations to solve for bottomhole pressure at the top of an interval assuming pressure at the top of the interval is known:

1. Calculate α_{CS} and Ω
2. Calculate (I_s) at the top of the interval from known values
3. Calculate mid-point pressure (P_{mp}) :
    a. Assume $I_{mp}=I_s$

b. $P_{mp1} = P_s + \frac{\alpha_{CS}}{I_s + I_{mp}}$

c. Calculate I_{mp}, from pressure and temperature at step (b)

d. $P_{mp} = P_s + \frac{\alpha_{CS}}{I_s + I_{mp}}$

e. Iterate with the new mid-point pressure until it converges

4. Calculate pressure at the bottom of the interval (P_{bh}) :

a. Assume $I_{bh}=I_{mp}$

b. $P_{bh1} = P_{mp} + \frac{\alpha_{CS}}{I_{mp} + I_{bh}}$

c. Calculate I_{bh}, from pressure and temperature at step (b)

d. $P_{bh} = P_{mp} + \frac{\alpha_{CS}}{I_{mp} + I_{bh}}$

e. Iterate with the new mid-point pressure until it converges

Using Simpson's rule the final bottomhole pressure is calculated as follows:

$$P_{bh} = P_S + \frac{6\alpha_{CS}}{I_S + I_{mp} + I_{bh}}$$

In the above procedure specific gas gravity is used. The specific gravity of CO_2 is larger than 1 relative to air. This will generate errors in the calculation procedure. Kelly[44] proposed changing the equation appropriately, and using the specific gravity relative to water.

The above procedure is used to calculate the bottomhole pressure for positive upward flow, as is the case calculating the bottomhole pressure inside the annulus. For calculating the bottomhole injection pressure inside the drill pipe we need to account for the negative downward

flow of the fluid. In order to perform the calculation for a downward flow of CO_2 the integration factor (I) need to be changed as follows[39]:

$$I = \frac{(P/Tz)}{(P/Tz)^2 \cos(\theta) - \Omega}$$

The calculations are then performed as described above to calculate bottomhole injection pressure.

In the following section, a multiphase flow model is developed in order to calculate bottomhole pressure and pressure distributions when produced water is encountered while drilling underbalanced. In addition, a fluid properties model and a heat transfer model are coupled in order to calculate the parameters needed.

7.4 Multiphase Flow Mechanistic Model Development

A mechanistic model of multiphase flow (in this case, CO_2 and water) was previously developed and written[32]. Since the literature suggested mechanistic models are superior to empirical correlations models, the mechanistic model was selected to model the annular flow mixture. Additionally, empirical models were developed for natural gas and liquid (water or oil), which questions its ability to model CO_2 and water. Particularly, gas density differences raise questions. Mechanistic modeling is not affected in this way.

7.4.1 Model Assumptions

Mechanistic modeling is well defined and explained in the literature[45], all the assumptions inherent in the development of those models are also assumed here.

- Mixture velocity and viscosity will be used, as opposed to the usual mud cleaning rheology models, because of the high friction gradients which results from multiphase flow.

- Effects of cuttings transport are neglected.

7.4.2 Multiphase Flow Parameters

During the simultaneous flow of gas and liquid, the most distinguishing aspect of such flow is the inconsistency of the distribution of both phases in the wellbore. The term flow pattern is used to distinguish such a distribution, which depend on the relative magnitude of forces acting on the fluids[45]. The following terms are defined in order to assist in the multiphase flow calculations.

Liquid Holdup

Liquid holdup (H_L) is defined as the fraction of a pipe cross-section or volume increment that is occupied by the liquid phase[46]. The value of H_L ranges from 0 (total gas) to 1 (total liquid). The liquid holdup is defined by

$$H_L = \frac{A_L}{A_P} \tag{7.13}$$

where A_L is the pipe area of the liquid occupied by the liquid phase and A_P is pipe cross-sectional area.

The term void fraction or gas holdup is defined as the volume fraction occupied by the gas where

$$H_G = 1 - H_L \tag{7.14}$$

When the two fluids travel at different velocities then the flow is referred to as a slip flow. No slip flow occurs when the two fluids travels at the same velocity. Hence, the term no slip liquid holdup can be defined as the ratio of the volume of liquid in a pipe element that would exist if the gas and liquid traveled at the same velocity divided by the volume of the pipe element[46]. The no-slip holdup (λ_L) is defined as follows:

$$\lambda_L = \frac{q_L}{q_L + q_G} \tag{7.15}$$

where q_L is the in-situ liquid flow rate and q_G is the in-situ gas flow rate.

Superficial Velocity

Superficial velocity is the velocity of a phase if it flowed through the total cross sectional area available for flow[46]. Thus, the liquid and gas superficial velocities are defined by:

$$v_{SL} = \frac{q_L}{A_P} \tag{7.16}$$

and

$$v_{SG} = \frac{q_G}{A_P} \tag{7.17}$$

The mixture velocity can be defined as the velocity of the two phases together, as follows:

$$v_M = \frac{q_L + q_G}{A_P} = v_{SL} + v_{SG} \tag{7.18}$$

The in-situ velocity is the actual velocity of the phase when the two phases travel together. They can be defined as follows:

$$v_L = \frac{v_{SL}}{H_L} \tag{7.19}$$

And

$$v_G = \frac{v_{SG}}{H_G} = \frac{v_{SG}}{1 - H_L} \tag{7.20}$$

7.4.3 Two Phase Flow Patterns

The variation in the physical distribution of the phases in the flow medium creates several flow patterns. Multiphase flow patterns depend on flow rates, wellbore geometry, and the fluid

properties of the phases. In addition, flow patterns can change with variations in wellbore pressure and temperature. The major flow patterns that exist in multiphase flow are dispersed bubble, bubble, slug, churn and annular. These are accepted patterns[45] that exists in two phase vertical flow geometries. As these are the accepted regimes, this work assumes any flow will fall into one of these five categories. Figure 7.3 shows different flow patterns exists in a pipe.

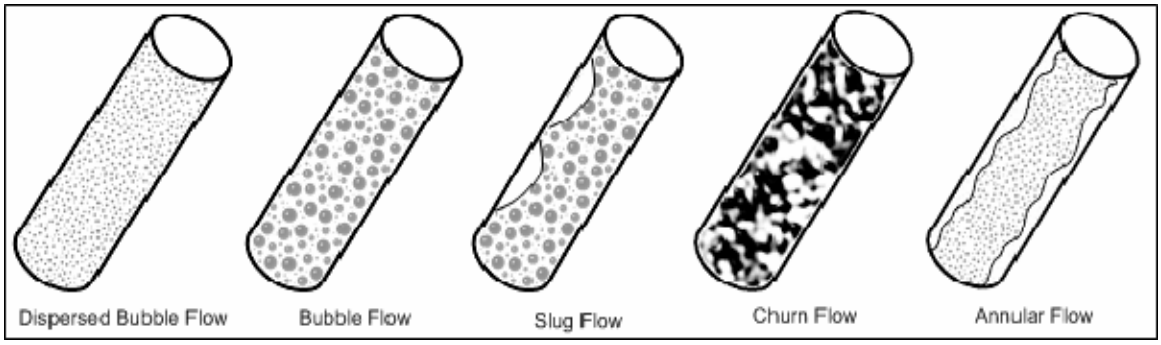

Figure 7.3 Different Flow Patterns in Two Phase Flow

- **Dispersed Bubble Flow:** This flow is characterized by gas being distributed in small spherically shaped bubbles in a continuous liquid phase. Dispersed bubble flow occurs at low gas flow rates and high liquid rates. In dispersed bubble flow, both phases flow at nearly the same velocity. No slip is seen between the phases and the flow is essentially homogenous.
- **Bubble flow:** This flow characterized by a discontinuous gas phase, which is distributed as discrete bubbles in a continuous liquid phase. The discrete gas bubbles tend to deviate from spherical shape and exhibit slippage through the liquid phase due to buoyancy forces. This pattern occurs at low to medium superficial velocities.
- **Slug Flow:** This flow is characterized by a series of slug units. Each unit is composed of alternating gas pockets and plugs of liquid called slugs. In vertical flow the gas pocket is commonly referred to as a Taylor Bubble. A film of liquid exists around the pocket

flowing downward relative to the gas bubble. The liquid slug, carrying distributed small gas bubbles, bridges the conduit and separates two consecutive gas bubbles.

- **Churn Flow:** This flow pattern exists in upward flow only and is very chaotic in nature. The shape of the Taylor bubble and the liquid slug are irregular and seemingly random. Churn flow can be considered to be a transition between bubbly flow and fully developed slug flow.
- **Annular Flow:** This flow pattern is characterized by the axial continuity of a gas phase in a central core, with the liquid flowing upward, both as a thin film along the pipe wall and as dispersed droplets in the core. A small amount of liquid is entrained in the light velocity core region. Annular flow occurs at high gas superficial velocities with relatively little liquid present.

Transition boundaries between the various flow patterns can be plotted on a flow pattern map. Flow pattern maps have been determined experimentally from a wide range of conditions. Figure 7.4 shows the flow pattern map used in the annulus, which was developed by Caetano et al.[47,48]. A flow pattern map was not developed for specifically CO_2 and water, but theory strongly suggests that the generic flow map of Figure 7.4 will apply to CO_2 and water. This work makes that assumption and Figure 7.4 is used in these calculations.

7.4.4 UBD Flow Patterns

In a typical UBD operation with water influx and gas injection rates, certain flow patterns exist in the annulus. Perez-Tellez et al.[49] show that in the annulus, very high superficial velocities would be observed when the flow is at atmospheric pressure. Also any small increase in the choke pressure would be enough to significantly decrease those superficial velocities and thus shift the flow pattern from annular to either slug or churn. This phenomenon is shown

graphically in Figure 7.5, where it shows typical superficial velocities for typical injection gas and flow rates for UBD conditions[49]. Those velocities reflect the actual conditions near the surface in terms of flow pattern in a typical UBD operation.

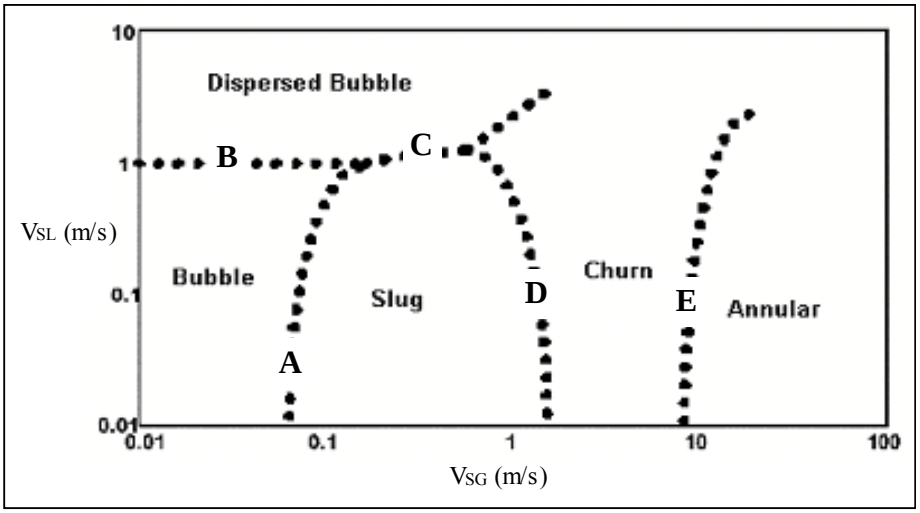

Figure 7.4 Flow Pattern Map for Upward Two Phase Flow in Annulus (Caetano et al[73,74])

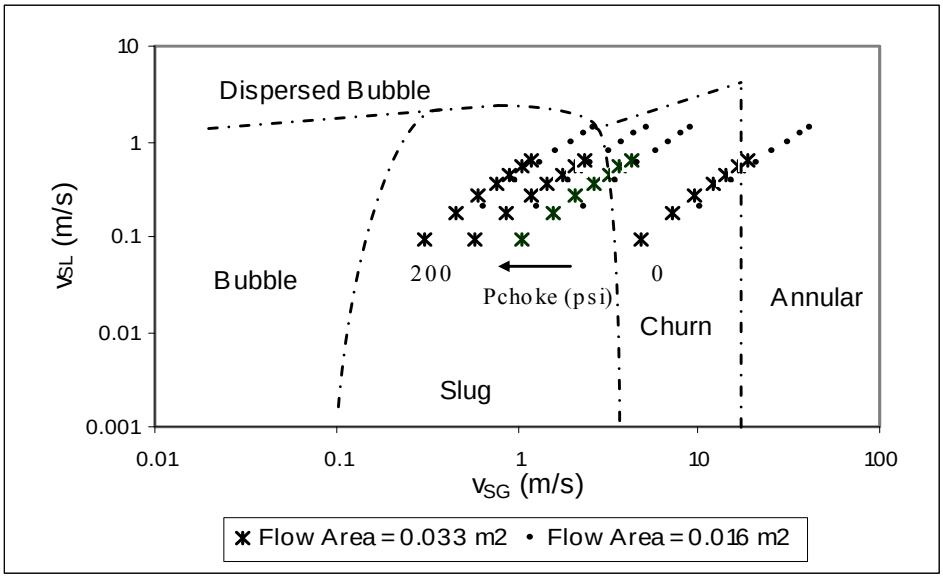

Figure 7.5 Near Surface Annular Flow Pattern in UBD Operations (Perez-Tellez et al.[75])

7.4.5 Flow Pattern Prediction Models

The following flow pattern models can be applied to an upward flow in the annulus with an inclination angle θ_H from horizontal. Several authors[47,48,53,50] agree that using the method

proposed by Taitel et al[51] for predicting flow pattern, in addition to his model and coupling it with the bubble swarm effect and the velocity swarm coefficient is valid. The flow patterns used are shown in Figure 7.4, where the transition boundaries are calculated based on different flow geometry. In each length interval the superficial liquid and gas velocity are calculated and compared to the transition as follow:

Bubble to Slug Transition

During bubble flow, discrete bubbles rise with the occasional appearance of a Taylor bubble. The discrete bubble rise velocity has been defined and is calculated by the Harmathy[52] correlation for upward flow in vertical and inclined channels as follows:

$$v_\infty = 1.53\left[\frac{(\rho_L - \rho_G)g\sigma}{\rho_L^2}\right]^{0.25} \qquad 7.21$$

Hasan and Kabir[53] stated that the presence of an inner tube tends to make the nose of the Taylor bubble sharper, causing an increase in the Taylor bubble rise velocity. As a result, Hasan and Kabir[54] developed an equation where the diameter of the outer tube should be used with the diameter ratio (d_{ODP}/d_{IC}) to obtain the Taylor bubble rise velocity in inclined annulus which will be used later in the calculation for the slug flow prediction model.

$$v_{TB} = (0.345 + 0.1*(d_{ODP}/d_{IC}))\sqrt{\sin\theta_H}(1+\cos\theta_H)^{1.2}\sqrt{gd_{IC}\frac{\rho_L - \rho_G}{\rho_L}} \qquad 7.22$$

Hasan and Kabir[53] stated that the presence of an inner tube does not appear to influence the bubble concentration profile (C_O) and thus the following expression could be used to define transition (A) as shown in Figure 7.4:

$$v_{SL} = \frac{(4 - C_O)v_{SG}}{\sin\theta_H} - v_\infty \qquad 7.23$$

Bubble or Slug to Dispersed Bubble Transition

Equation 7.24 is used to define the transition from bubble or slug to dispersed bubble flow to define transition (B) as follow:

$$v_M^{1.2}\left(\frac{2f_F^{0.4}}{d_h}\right)^{0.4}\left[\frac{1.6\sigma}{(\rho_L-\rho_G)g}\right]^{0.5}\left(\frac{\rho_L}{\sigma}\right)^{0.6}=0.725+4.15\left(\frac{v_{SG}}{v_M}\right)^{0.5} \qquad 7.24$$

An iterative procedure is required to calculate the transition velocities. In the above expression in order to calculate the homogenous fanning friction factor, and since the rise velocity for the dispersed bubble flow is very small compared to the local velocities, the no-slip holdup (λ_L) is used to calculate f_F (Fanning friction factor) . A good starting point for the iterations is to assume a mixture velocity of 1 and obtain a solution for the transition (B) using the Newton method.

Dispersed Bubble to Slug Flow Transition

Taitel et al.[51] determined that the maximum allowable gas void fraction under bubble flow condition is 0.52. Higher values will convert the flow to slug, hence the transition boundary (C) could be defined as follows:

$$v_{SL}=0.923v_{SG} \qquad 7.25$$

Slug to churn transition

Tengesdal et al.[55] developed a transition from slug to churn flow in an annulus. They stated that the slug structure will be completely destroyed and churn flow will occur if the gas void fraction equals 0.78. Thus churn flow will occur. The transition from slug flow to churn flow can thus be represented by:

$$v_{SL}=0.0684v_{sg}-0.292\sqrt{g(d_{IC}+d_{ODP})} \qquad 7.26$$

And it is shown as transition (D) in Figure 4.7.

Churn to Annular Transition

Taitel et al.[51] proposed the following transition which was supported by Hasan and Kabir[53] :

$$v_{SG} = 3.1\left[\frac{(\rho_L - \rho_G)g\sigma}{\rho_G^2}\right]^{0.25} \quad 7.27$$

which is shown as transition (E) in Figure 4.7.

7.4.6 Flow Behavior Prediction Models

After determining the correct flow pattern, the followed behavior prediction models are applied in order to calculate the pressure gradient and phases fractions. The total pressure gradient is calculated as follows:

$$\left(\frac{dP}{dL}\right)_{total} = \left(\frac{dP}{dL}\right)_{el} + \left(\frac{dP}{dL}\right)_{fr} + \left(\frac{dP}{dL}\right)_{acc} \quad 7.28$$

where the following are the component of the total pressure gradient

$\left(\frac{dP}{dL}\right)_{el}$: The elevation change component

$\left(\frac{dP}{dL}\right)_{fr}$: The friction component

$\left(\frac{dP}{dL}\right)_{acc}$: The acceleration component

where

$$\left(\frac{dP}{dL}\right)_{el} = \rho_M g \sin\theta \quad 7.29$$

$$\left(\frac{dP}{dL}\right)_{fr} = \frac{f_M \rho_M v_M^2}{2d_h} \quad 7.30$$

$$\left(\frac{dP}{dL}\right)_{acc} = \frac{\rho_M v_M v_{SG}}{p}\frac{dP}{dL} \tag{7.31}$$

The acceleration term (E_k) is defined as follows:

$$E_k = \frac{\rho_M v_M v_{SG}}{p} \tag{7.32}$$

Then the total pressure drop is calculated by:

$$\left(\frac{dP}{dL}\right)_{total} = \frac{\left(\frac{dP}{dL}\right)_{el} - \left(\frac{dP}{dL}\right)_{f}}{1 - E_k} \tag{7.33}$$

Bubble Flow Model for Annular Geometries

For a bubbly flow the holdup is calculated as reported by Hasan and Kabir[53] as follows:

$$H_L = 1 - \frac{v_{SG}}{v_\infty - C_O v_M} \tag{7.34}$$

The velocity profile coefficient (C_O) has been defined by Zuber and Findlay[56], which results from the effect of non-uniform flow and concentration distribution across the pipe and the effect of local relative velocity between the two phases. Table 7.1 shows the values for the velocity profile coefficients for different inclination angles (for vertical wells Co is 1.25) as given by Alves[57]

Table 7.1 Flow Coefficients for Different Inclination Angle Ranges (After Alves[57])

θ_H (Degrees)	Co
10-50	1.05
50-60	1.15
60-90	1.25

Mixture density and viscosity are calculated below as:

$$\rho_M = \rho_L H_L + \rho_G (1 - H_L) \tag{7.35}$$

$$\mu_M = \mu_L H_L + \mu_G (1 - H_L) \tag{7.36}$$

The elevation pressure gradient is calculated using equation 7.29. The frictional pressure loss is calculated from equation 7.20. Caetano[47,48] suggested the use of the calculation developed by Gunn and Darling[83] for a turbulent flow as follows

$$\left[f_F \left(\frac{F_P}{F_{CA}} \right)^{0.45 \exp\left[-(N_{RE}-3000)/10^6 \right]} \right]^{-0.5} = 4 \log \left[N_{Re} \left(f_F \left(\frac{F_P}{F_{CA}} \right)^{0.45 \exp\left[-(N_{RE}-3000)/10^6 \right]} \right)^{0.5} \right] - 0.4 \qquad 7.37$$

where f_F is the Fanning friction factor.

Equation 7.37 has the following parameters:

F_P and F_{CA} are geometry parameters defined by the following equations

$$F_P = 16/N_{RE} \qquad 7.38$$

$$F_{CA} = \frac{16(1-K)^2}{\left[\frac{1-K^4}{1-K^2} - \frac{1-K^2}{\ln(1/K)} \right]} \qquad 7.39$$

K: diameter ratio, and defined as

$$K = d_{ODP}/d_{IC} \qquad 7.40$$

where OD is the pipe outer diameter and ID is the inner casing diameter.

The mixture Reynolds number is calculated as follow:

$$N_{RE,M} = \frac{\rho_M v_M d_h}{\mu_M} \qquad 7.41$$

The acceleration component is calculated using Beggs and Brill[58] (7.30-7.33)

Dispersed Bubble Flow Model

The dispersed bubble holdup is assumed equal to the no-slip holdup (λ_L). The same equations as in the bubble flow are used to calculate the total pressure gradient.

Slug Flow Model

The model used by Perez-Tellez[59] for calculating the slug parameter is shown below.

$$N_{RE,M} = \frac{\rho_{M_{LS}} v_M d_h}{\mu_L H_{L_{LS}} + \mu_G (1 - H_{L_{LS}})} \tag{7.42}$$

In addition, the acceleration component can be calculated by

$$\left(\frac{dP}{dL}\right)_{acc} = \frac{H_{L_{LS}} \rho_L}{L_{SU}} \left(v_{L_{LS}} + \left|v_{L_{TB}}\right|\right)\left(v_{TB} - v_{L_{LS}}\right) \tag{7.43}$$

Finally the average holdup over the entire slug unit $H_{L_{SU}}$, for either developed of fully developing Taylor bubble can be calculated by[49]

$$H_{L_{SU}} = 1 - \frac{v_{SG} + \left(1 - H_{L_{LS}}\right)\left(v_{TB} - v_{G_{LS}}\right)}{v_{TB}} \tag{7.44}$$

where the remaining variables are defined the nomenclature.

Annular Flow Model

Perez-Tellez[59] suggested using the model developed by Taitel and Barnea[60], where he stated that the use of this model will avoid convergence problems within the computations. Taitel and Barnea[60] stated that the total pressure drop in an annular flow can be calculated as follows:

$$\left(\frac{dP}{dL}\right)_{total} = \frac{r\tau_i}{D_e - 2\delta} + [\rho_L H_L + \rho_G (1 - H_L)] g \, Sin\theta_H \tag{7.45}$$

The annular film thickness can be defined as follows:

$$\delta = 0.115 \left(\frac{\mu_L^2}{g(\rho_L - \rho_G)\rho_L}\right)^{1/3} \left(\frac{\rho_L v_{SL} D_e}{\mu_L}\right)^{0.6} \tag{7.46}$$

D_e is the equivalent pipe diameter and is calculated by

$$D_e = \sqrt{d_{IC}^2 - d_{ODP}^2} \tag{7.47}$$

The interfacial shear stress (τ_i) is defined by

$$\tau_i = \frac{0.5 f_i \rho_G v_{SG}^2}{\left[1 - 2(\delta / D_e)\right]^4} \quad 7.48$$

The interfacial shear friction factor is calculated as suggested by Alves et al[61], as follows:

$$f_i = f_{sc}(\Xi_H \cos^2\theta_H + \Xi_V \sin^2 \theta_H) \quad 7.49$$

where f_{cs} is the superficial core friction factor (gas phase) and is calculated based on the core superficial velocity, density and viscosity. The interfacial correction parameter Ξ is used to take into account the roughness of the interface. The parameter Ξ is an average between the horizontal angle and the vertical angle and is calculated based on an inclination θ_H

The horizontal correction parameter is given by Henstock and Hanratty[62] :

$$\Xi_H = 1 + 800 F_A \quad 7.50$$

where

$$F_A = \frac{\left[(0.707 N_{RE,SL}^2)^{2.5} + (0.0379 N_{RE,SL}^{0.9})^{2.5}\right]^{0.4}}{N_{RE,SG}^{0.9}} \left(\frac{v_L}{v_G}\right)\left(\frac{\rho_L}{\rho_G}\right)^{0.5} \quad 7.51$$

where $N_{RE,SL}$ and $N_{RE,SG}$ are the superficial liquid and gas Reynolds number respectively. Both are calculated below

$$N_{RE,SL} = \frac{\rho_L v_{SL} ID}{\mu_L} \quad 7.52$$

and

$$N_{RE,SG} = \frac{\rho_L v_{SG} ID}{\mu_G} \quad 7.53$$

The vertical correction parameter is given by Wallis[63] as follow

$$\Xi_V = 1 + 300(\delta / D_e) \quad 7.54$$

Finally considering a constant liquid film thickness, the liquid holdup can be calculated by

$$H_L = 4\left[\frac{\delta}{D_e} - \left(\frac{\delta}{D_e}\right)^2\right] \tag{7.55}$$

7.5 Pressure Drop across Bit Nozzles

The pressure drop across a bit nozzle can be calculated using the subsonic flow of gasses through chokes and nozzles as shown below[21]:

$$Q_G = 0.0418 A_n P_{Up} \sqrt{\frac{k}{(k-1)\gamma_G T_{Dn}}\left[\left(\frac{P_{Up}}{P_{Dn}}\right)^{\left(\frac{2}{k}\right)} - \left(\frac{P_{Up}}{P_{Dn}}\right)^{\left(\frac{k+1}{k}\right)}\right]} \tag{7.56}$$

The subscripts "Up" and "Dn" refer to the upstream and downstream pressures at the bit nozzles, (k) is the specific heat ratio, and (A_n) is the total bit nozzles area. The above equation shows that an iterative solution is needed in order to solve for the bit upstream pressure. In addition it depends on the pressure ratio (P_{Up}/P_{Dn}). For sonic flow the pressure ratio is replaced by the critical pressure ratio as

$$\left(\frac{P_{Up}}{P_{Dn}}\right)_C = \left(\frac{2}{k+1}\right)^{\frac{k}{k-1}} \tag{7.57}$$

and the upstream pressure can be calculated using equation (7.56) as

$$P_{Up} = \frac{(8.8542 \text{x} 10^{-6})\gamma_G Q_G}{A_n} \sqrt{\frac{T_{Up}}{\left(\frac{gk\gamma_g}{53.3}\right)\left(\frac{2}{k+1}\right)^{\frac{k+1}{k-1}}}} \tag{7.58}$$

Because of the pressure involved (high pressure at the bottom of a supercritical fluid in the drill pipe and low pressure as desired in the annulus) the pressure drop will be typically sonic (critical). This calculation procedure predicts the pressure drop needed across the bit nozzles, which typically will take the fluid from supercritical to vapor phase. This calculation has an

engineering desired circulating bottomhole pressure in the annulus and a calculated bottomhole pressure in the drill pipe. This defines the pressure drop across the nozzles. The above equations are assumed as an appropriation, but the author recognizes that significant experimental work is required to model exactly the pressure drop across the bit nozzles especially with the fluid being supercritical CO_2.

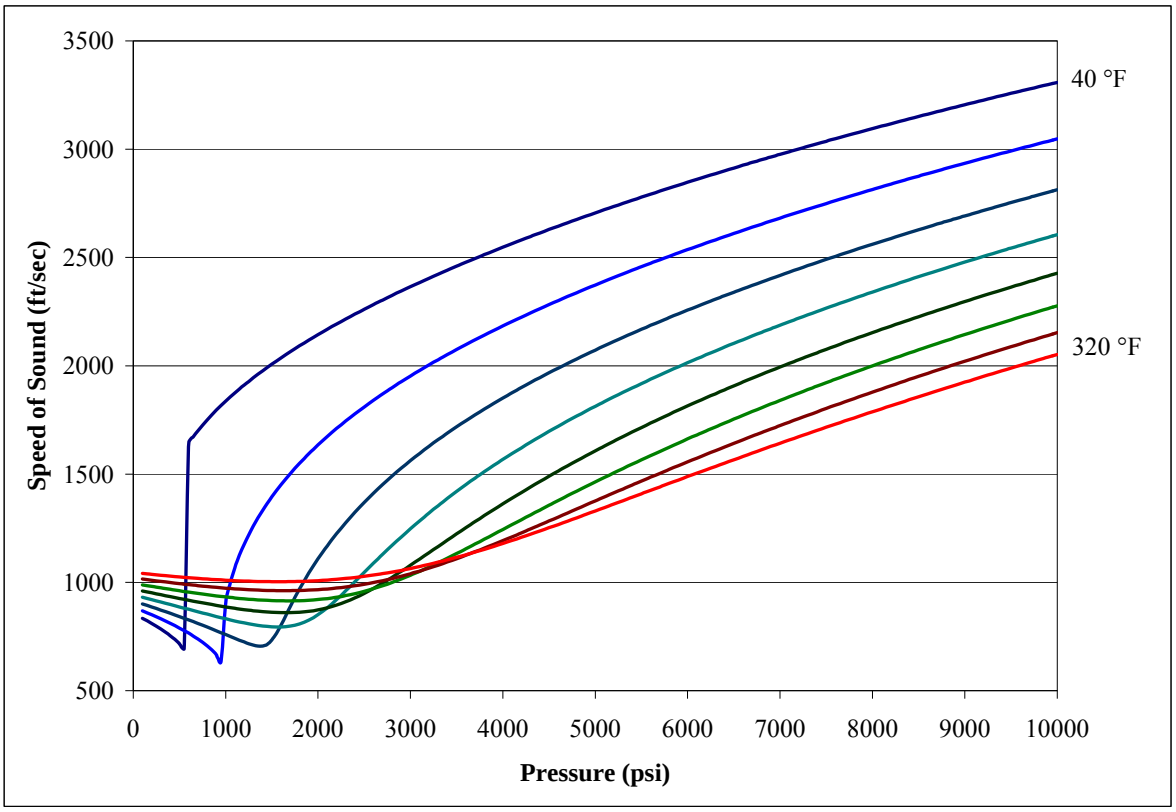

Figure 7.6 Variation of CO_2 Speed of Sound for Different Pressures and Temperatures

7.6 Minimum Gas Volume Requirements

In a typical air drilling operation, a minimum required air volume is calculated to achieve optimum hole cleaning[3,64,]. The main criterion used is the minimum kinetic energy requirements, which is based on experience gained from quarry drilling with air. In this method the minimum velocity to lift cuttings particles is that equivalent to a standard air velocity of 50 ft/sec (3000 ft/min). This velocity is accepted to be high enough to lift drill cuttings and achieve optimum

hole cleaning. Older methods assume a simple relationship between the bottomhole pressure and gas specific gravity, but the deviation of CO_2 from an ideal gas and the rapid change of CO_2 densities with pressure (with low critical conditions) make these methods questionable in this situation.

Another method used to calculate minimum gas volume requirements is based on the minimum gas velocity. In this method, the minimum gas rate required is equal to the sum of the terminal settling particle velocity (v_{sl}) and the required particle transport velocity (v_{tr}). The terminal settling velocity of a particle can be calculated as follows[65]:

$$v_{sl} = \sqrt{\frac{4gd_{DC}(\rho_{DC} - \rho_g)}{3\rho_G \vartheta}} - \frac{\Theta}{1 + d_{DC}/d_h} \qquad 7.59$$

From the above expression, the required velocity depends on the drill cuttings shape and size, in addition to gas density. The drag coefficient (ϑ) depends on particle shape, where flat particles (limestone and shale) have a value of 1.4, and angular to sub-rounded particles (sandstone) have a value of 0.85. The transport velocity accounts for drill cuttings generated by the drill bit during drilling and is defined as[3]:

$$v_{tr} = \frac{\pi d_b}{4C_{DC}A_h}\left(\frac{ROP}{3600}\right) \qquad 7.60$$

In the above expression (C_{DC}) is the drill cuttings concentration in the gas, and (ROP) is the bit rate of penetration. From the above equations the total gas annular velocity at the bottom of the hole should be at least equal to the sum of the two above velocities. The cutting transport ratio (CTR) is defined as the ratio of cutting slip velocity to the average fluid velocity.

$$CTR = 1 - \frac{v_{sl}}{v_G} \qquad 7.61$$

A minimum cutting transport ratio of 0.7 is recommended for vertical sections and a CTR of 0.9 is recommended for horizontal sections.

7.7 Computer Program Description

The models described in the previous chapters were all implemented into a computer program, using EXCEL VBA®. In addition to the heat transfer variables input (Table 6.1), the following parameters are also needed by the program:

- Fluid type and Injection Rates.
- Surface and injection conditions (Pressure and Temperature).
- Wellbore profile (survey).
- Drill pipe, casing and drill bit nozzle size and geometry.
- Rate of penetration.
- Formation properties.
- The fluid properties are calculated using the multi-parameter equation of state (equation of state was used in a version programed by the "Lehrstuhl feur Thermodynamik, Ruhr-Universitaet Bochum").

7.7.1 Algorithm

The following is the calculation steps as performed in the computer program:

- Read the required input data.
- Start Calculations at the top of the drill pipe, with injection pressure and temperature as (P_1,T_1).
    - Select a length increment (ΔL).
    - Calculate the temperature in the drill pipe using the heat transfer model (T_2).

- Calculate the pressure at point 2, using the Cullender-Smith Method (P_2).
- If the calculations do not converge decrease ΔL, and restart calculations.
- Continue calculations with the next length increment (ΔL) until the total depth of the drill pipe is reached (above bit nozzles).

- Start Calculations in the annulus with surface pressure and temperature (P_1,T_1)
  - Calculate the (P_2,T_2) using the model for the drill pipe as follows:
    - Annulus temperature is calculated using the heat transfer model.
    - Bottomhole pressure in the annulus is calculated using either the single phase or the multi-phase mechanistic model.
    - Calculate the pressure drop across bit nozzles.
    - Check if the pressure converges with pressure calculated from the drill pipe model.
      - If convergence is achieved finish calculations.
      - Otherwise increase injection pressure and restart calculations.

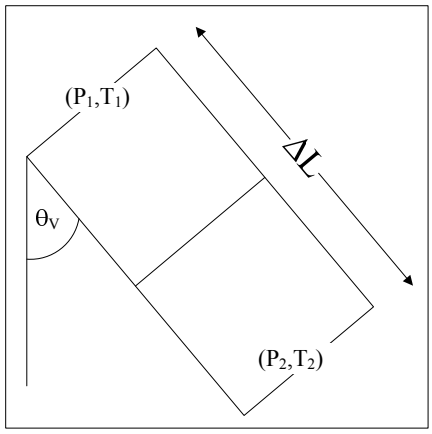

Figure 7.7 Wellbore calculation increment path

The above model requires iterations on the injection pressure, since the model is dynamic and depends on circulating pressure and temperature inside the drill pipe to calculate the circulating

temperature in the annulus. Figure 7.8 shows a flow diagram of the procedure described above. After calculating the required bottomhole pressure, cutting transport ratios are calculated, given the required bottomhole input. In addition Figure 7.9 below shows flow diagram of the mechanistic two phase flow model.

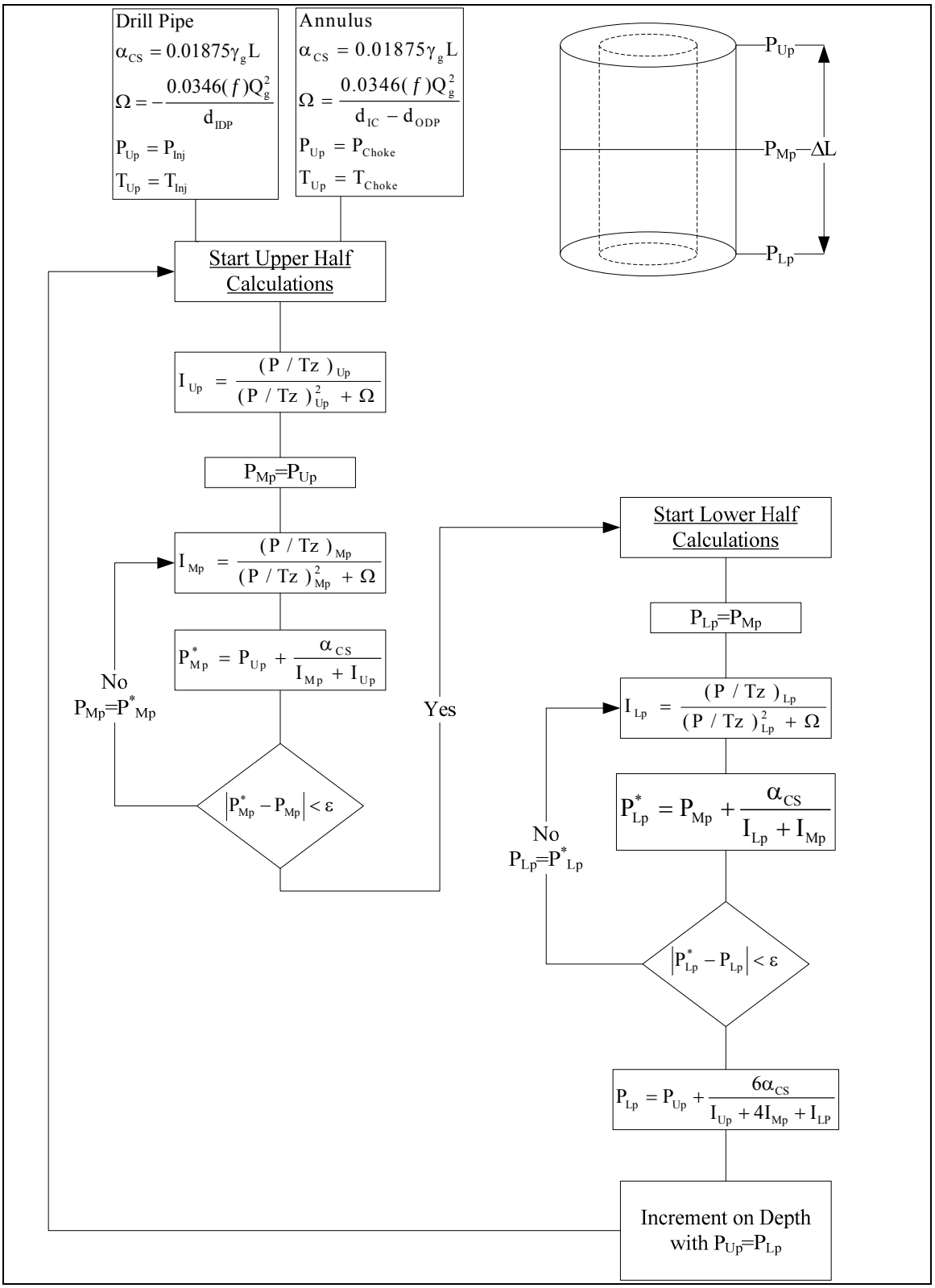

Figure 7.8: Flow Diagram of Cullender and Smith Computer Program

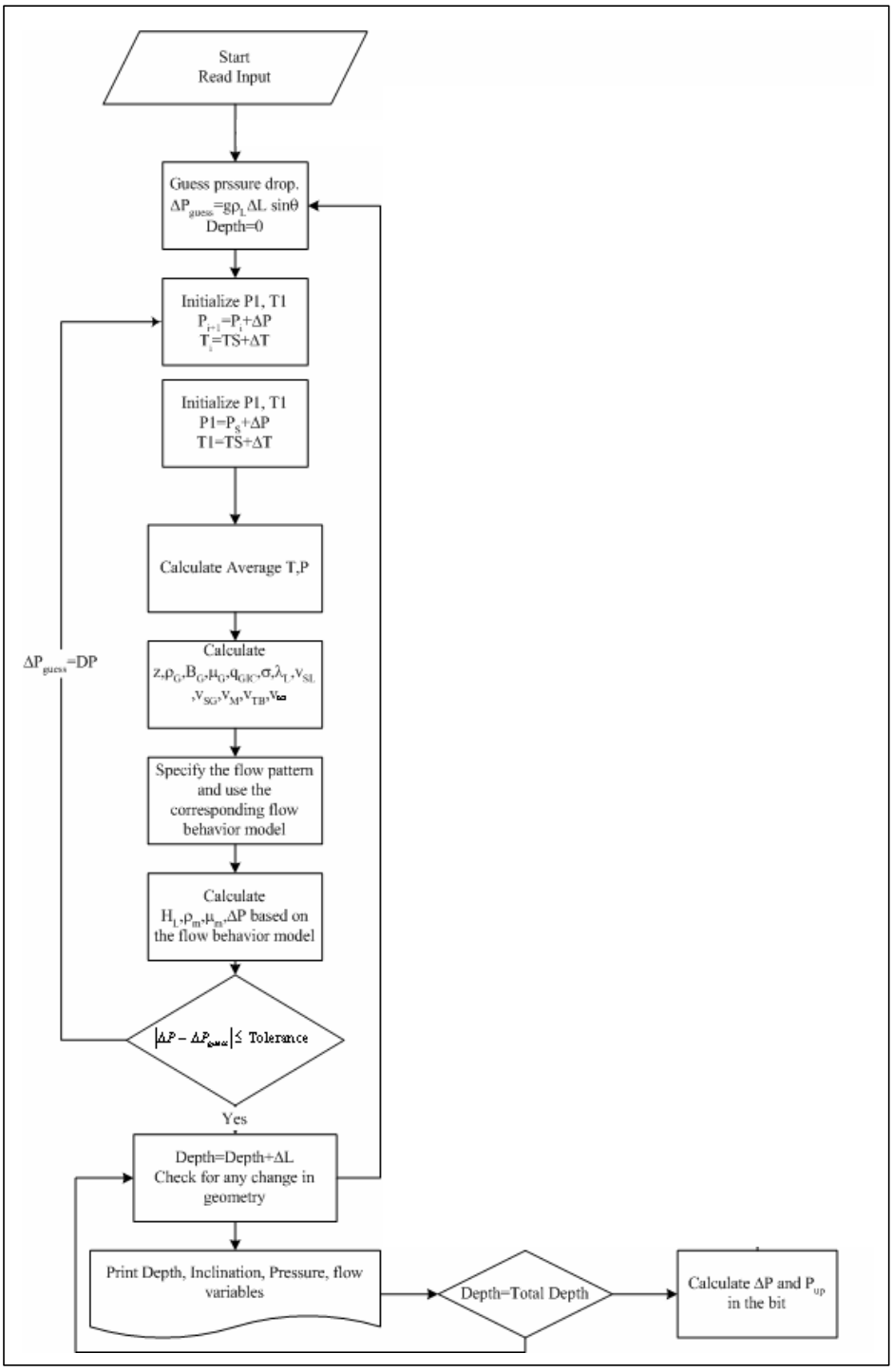

Figure 7.9 Flow Diagram of the Two Phase Flow Computer Program

CHAPTER 8. CALCULATIONS

8.1 Model Validation

The developed model is for an underbalanced drilling operation utilizing SC-CO_2 as drilling fluids; since there are no field operations conducted with CO_2 to date, the developed model will be validated by comparison to gas drilling operations[66]. The developed model can be changed to account for either air or gas drilling, given the appropriate fluid properties model. The NIST "Reference Fluid Thermodynamic and Transport Properties Database (REFPROP)" (Courtesy of Lemmon, E.W.) is used to calculate nitrogen properties[67,68]. Due to the limited data stated in the reference, the model will be validated by comparing bottomhole pressures as reported in the reference. Three case histories will be considered and they are summarized in Table 8.1. The model had an average absolute relative error of less than 10%. Due to the low heat capacity of gases, the temperature distribution is assumed to be the same as the geothermal gradient as discussed earlier in Chapter 6.

Table 8.1 Comparison Between Field Data and Model Calculated[66]

Case	Depth	Gas Injection Rate	BHP[66]	BHP Model	AAE
	ft	SCFM	psi	psi	(%)
1	16610	2300	576	584.0858	1.3844
2	6000	2000	119	113.102	5.2147
3	6000	2500	147	137.5784	6.8482

In the above table the average absolute error (AAE) is defined below as

$$AAE = \left| \frac{BHP_{Actual} - BHP_{Calc}}{BHP_{Actual}} \right| * 100 \qquad 8.1$$

Several cases are provided in the paper by Griffen and Lyons[66], but only three cases have sufficient data for computing and comparing the calculations. Also, some cases involved foam drilling which is not of interest to this work.

8.2 Sample Calculations

8.2.1 Single Phase CO_2 in the Annulus

The sample calculations were taken from Kolle et al.[69]. **Error! Reference source not found.**Table 8.2 and 8.3 shows the input data and the heat transfer model input required for the calculations. Values listed as assumed in the table were not given in the original reference but assumed reasonably.

Table 8.2 Main Model Input

Gas Injection Rate (SCF/Min)	570
Injection Pressure (psi)	10,000
Coiled Tubing Inner Diameter (in)	0.9
Coiled Tubing Outer Diameter (in)	1.25
Drill Bit Size (in)	2
Total Depth (ft)	6560
Choke Pressure (psi)	725

Table 8.3 Heat Transfer Model Input

Mass Injection Rate (lbm/min)	66
Surface Temperature (°F)	60
Injection Temperature (°F)	-4
Geothermal Gradient (°F/ft)	0.0149
Circulation Time (hrs)*	10
Gas Specific Heat (BTU/lbm-°F) (Assumed)	From SW-EOS
Formation Thermal Conductivity (BTU/ft-°F-hr) (Assumed)	1.3
Formation Specific Heat (BTU/lbm-°F) (Assumed)	0.2
Annulus Heat Transfer Coeff. (U_{ANN}) (BTU/(hr-ft^2-°F) (Assumed)	4
Drill Pipe Heat Transfer Coeff. (U_{DP}) (BTU/(hr-ft^2-°F) (Assumed)	10
Formation Density (lbm/cuft) (Assumed)	165

The calculated results were compared to the work performed by Kolle et. al[69]. For the given injection and choke pressures, a bottomhole pressure of 2037 psi was calculated compared with 2750 psi as reported. This is due to the fact that the reported calculations were performed assuming a turbulent Newtonian flow with the Peng-Robinson equation of state, for an assumed vertical well. As shown in Figure 8.1, the model calculated the temperature distribution in both the drill pipe and the annulus. The reduction in annulus pressure is due to the Joule-Thompson cooling. Also, there is no formation influx to increase the circulating bottomhole temperature. Figure 8.2 shows the model calculated pressure distribution. As shown in the figure, the pressure drop across the bit nozzle is calculated as 9945 psi with an injection pressure of 10,000 psi, while the reported calculated value is 8700 psi. In addition, CO_2 would become supercritical at 2240 ft inside drill pipe and at 2360 ft inside the annulus as shown in Figure 8.3.

Table 8.4 Comparison between Calculated Model and Reported Parameters (Kolle et. al.[69])

Parameter	Model	Kolle et. al.[69]
BHP	2037	2750
BHT	136	158
ΔP_{Bit}	9945	8700

Figure 8.4 shows the effect of decreasing and increasing both the drill pipe and annulus heat transfer coefficients. The exit fluid temperature in the drill pipe at the bottom of the hole increases with increases in both coefficients, but the rate of temperature increase decreases with increased drill pipe heat transfer coefficients, as shown in Figure 8.4.

Figure 8.5 and Figure 8.6 show how fluid temperatures inside drill pipe and the annulus change with changing heat transfer coefficients. For a high drill pipe heat transfer coefficient, the exit choke temperature is reduced. This is due to the heat exchanged between the drill pipe and the annulus occurs at a faster rate than for a low drill pipe heat transfer coefficients (Figure 8.5).

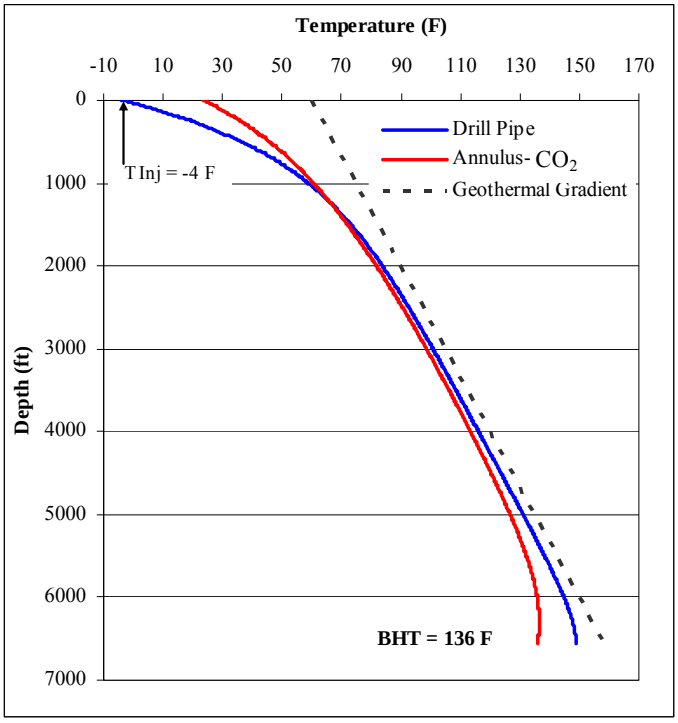

Figure 8.1 Model Temperature Prediction inside Drill pipe and Annulus for Single CO_2

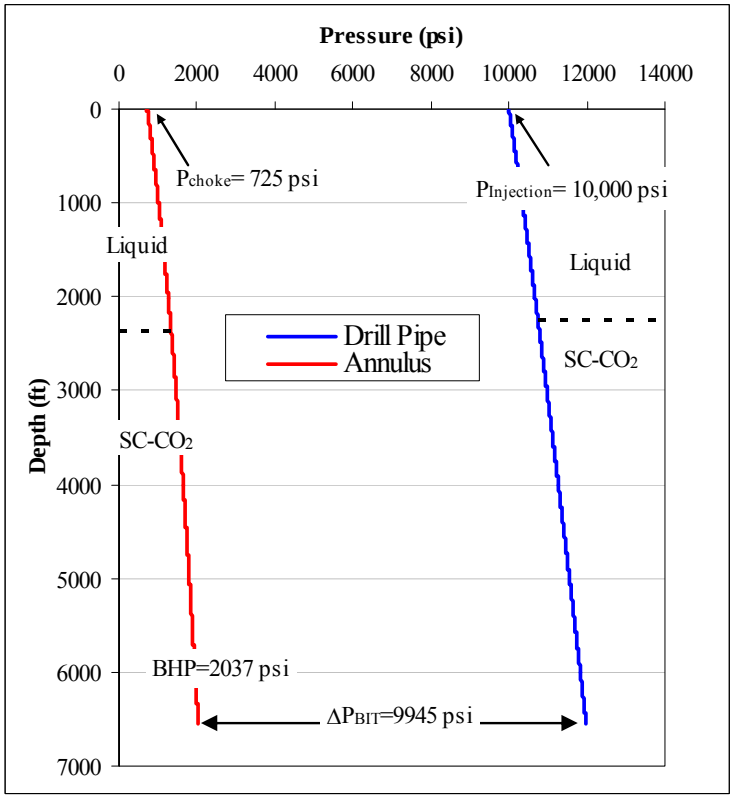

Figure 8.2 Model Pressure Prediction for single CO_2 Flow in the Annulus

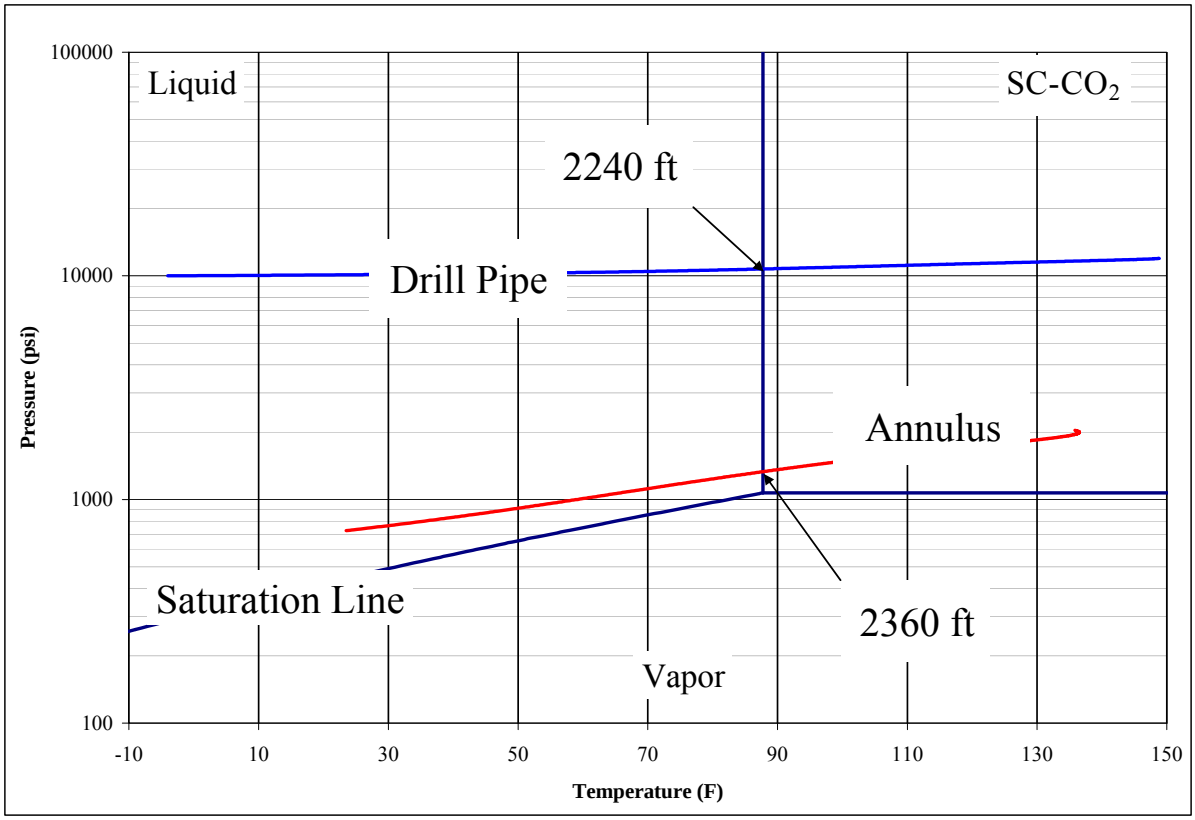

Figure 8.3 Pressure-Temperature Diagram of Circulating Fluid inside Drill Pipe and Annulus

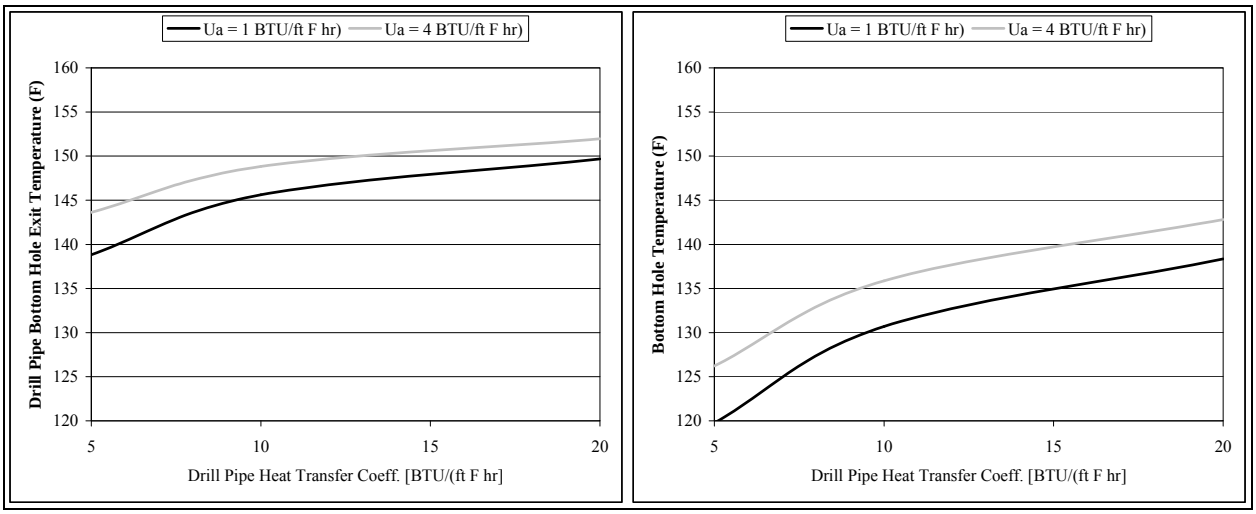

Figure 8.4 Effects of Various Drill Pipe and Annulus Heat Transfer Coefficients

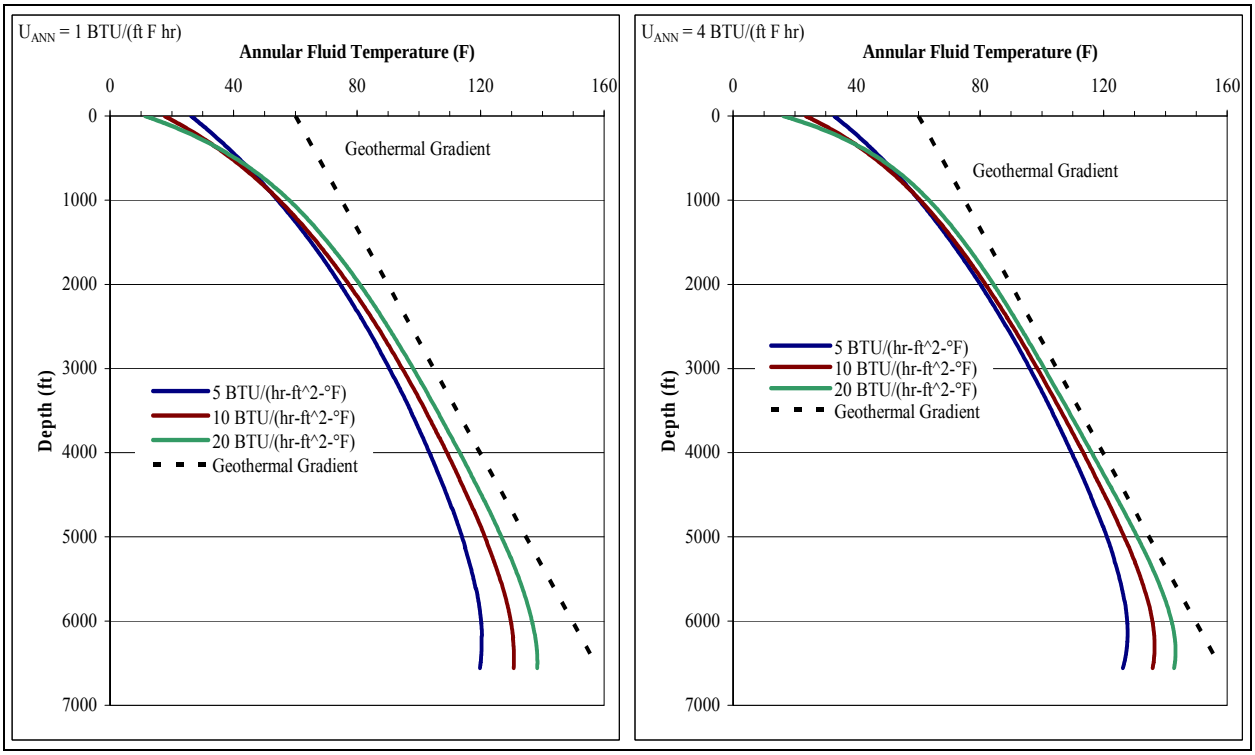

Figure 8.5 Variation of Annular Fluid Temperature for Different Heat Transfer Coefficients

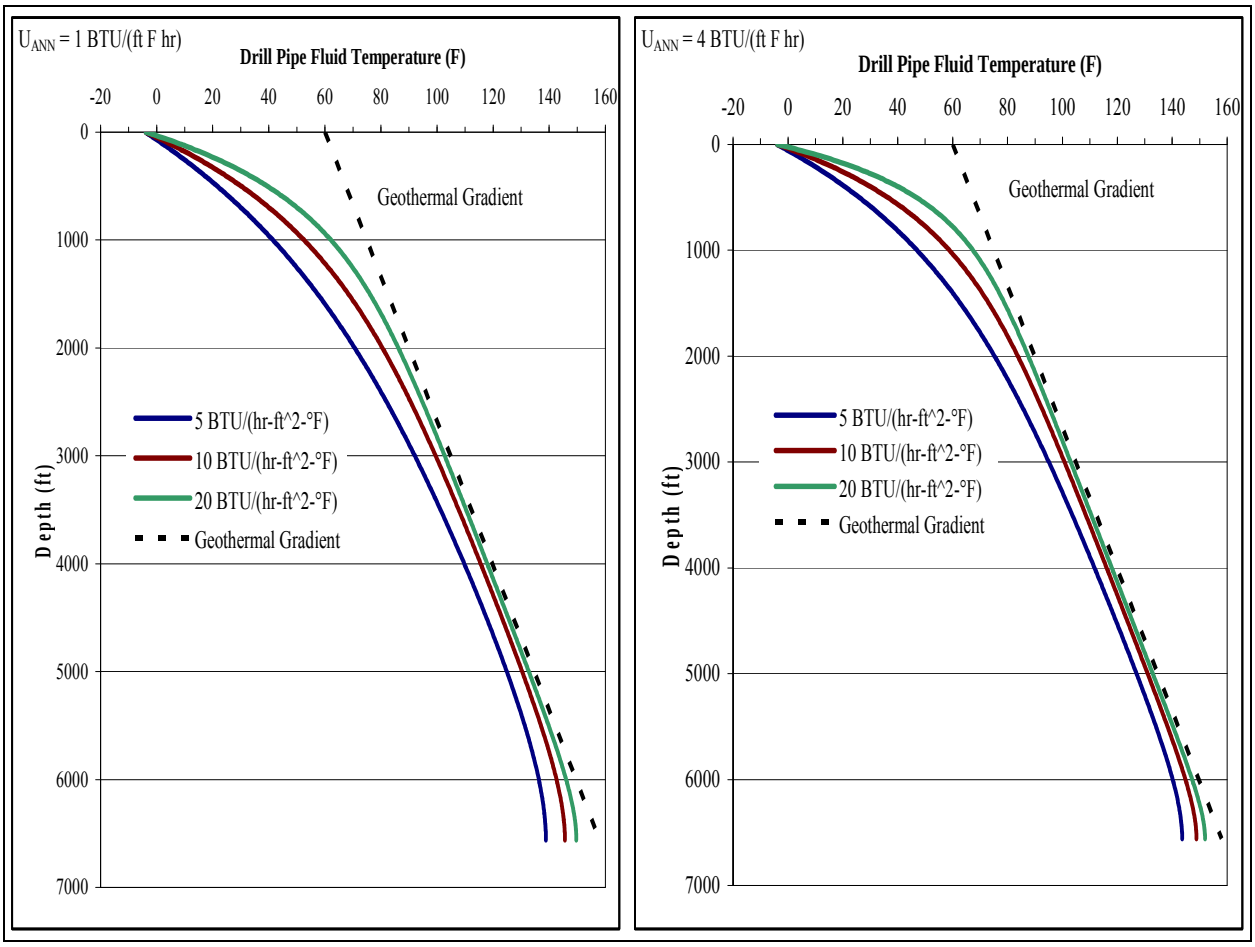

Figure 8.6 Variation of Drill Pipe Fluid Temperature for Different Heat Transfer Coefficients

The pressure drop across the bit varies with nozzle area, which is a function of nozzle size and number of nozzles. Figure 8.7 shows the effect of total nozzle area on pressure drop across the bit. Nozzle sizes (reported in /32 in) were varied from 0.5-14 in as shown in Table 8.5. For a nozzle size less than (1/32 in), the flow of SC-CO_2 is sonic and any change in bottomhole pressure will not be detected from the stand pipe pressure. For a nozzle size of (1/32 in and 1.5/32 in) the flow is subsonic and the SC-CO_2 is vaporized through the bit nozzles. For higher nozzle sizes the pressure drop is insignificant to the phase change of CO_2, hence the pressure drop across bottomhole assembly including MWD (Measure While Drilling) equipment should be large enough.

Table 8.5 Pressure Drop across Bit Nozzle for Different Nozzle Sizes

Nozzle Size	Total Nozzle Area	ΔP_{Bit}	Flow Condition
/32 in	in^2	psi	
0.5	5.7524E-04	31309	Sonic
1	2.3010E-03	3953	Sonic
1.5	5.1772E-03	1031	Subsonic
2	9.2039E-03	360	Subsonic
4	3.6816E-02	23.8966	Subsonic
8	1.4726E-01	1.4997	Subsonic
10	2.3010E-01	0.6140	Subsonic
12	3.3134E-01	0.2963	Subsonic
14	4.5099E-01	0.2038	Subsonic

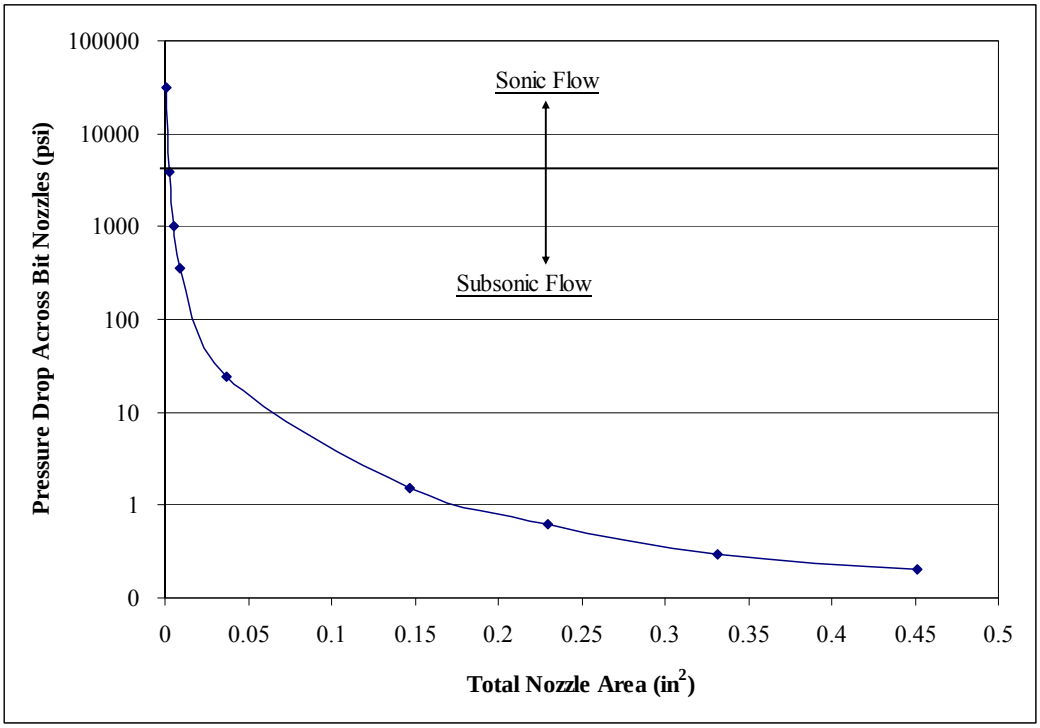

Figure 8.7 Effect of Total Nozzle Area on Pressure Drop across Bit Nozzles

8.2.2 Multiphase Mixture Case - CO_2 and Water in the Annulus

The introduction of produced water while drilling will cause an increase of bottomhole pressure. The mixture of water and CO_2 in the annulus will be addressed here to estimate the

amount of water that can be handled and still achieve the required objective of creating an underbalanced condition. Different water production rates are considered, and the multiphase mechanistic model developed earlier will be used to calculate both bottomhole pressure and temperature. Corrosion rate will also be estimated.

Figure 8.8 shows the pressure distribution in the annulus for a mixture of CO_2 and formation water. As shown, the bottomhole pressure expectedly increases with increased water production rate. In addition, Figure 8.9 shows a plot of water production rate vs. bottomhole pressure. An increase in the water production rate will increase the circulating fluid temperature in the annulus, because of the higher heat capacity of water. The surface choke temperature will also increase with increasing water production rate (Figure 8.11), for the same reason. Figures 8.12-8.14 show plots of various mixture properties (density, liquid holdup and corrosion rate). For low water rates an annular flow pattern is observed in the two phase flow system and this is characterized by a high superficial gas velocity with low superficial liquid velocity. For higher water production rates, the slug/dispersed bubble flow regime will be the dominant pattern as shown in Figure 8.12 and 8.13 where an abrupt slope change occurs as the flow regime changes. The corrosion rate reached a maximum and then decreased, due to the pH effect at different temperature ranges as shown in Figure 8.15.

Table 8.6 Bottomhole Pressure and Choke Temperature at Increasing Water Production Rate

Q_w	BHP	T_{Choke}
STB/D	STB/D	°F
10	1492	69.201
50	2016	78.472
100	2135	87.800
500	2931	122.254
1000	3711	135.937

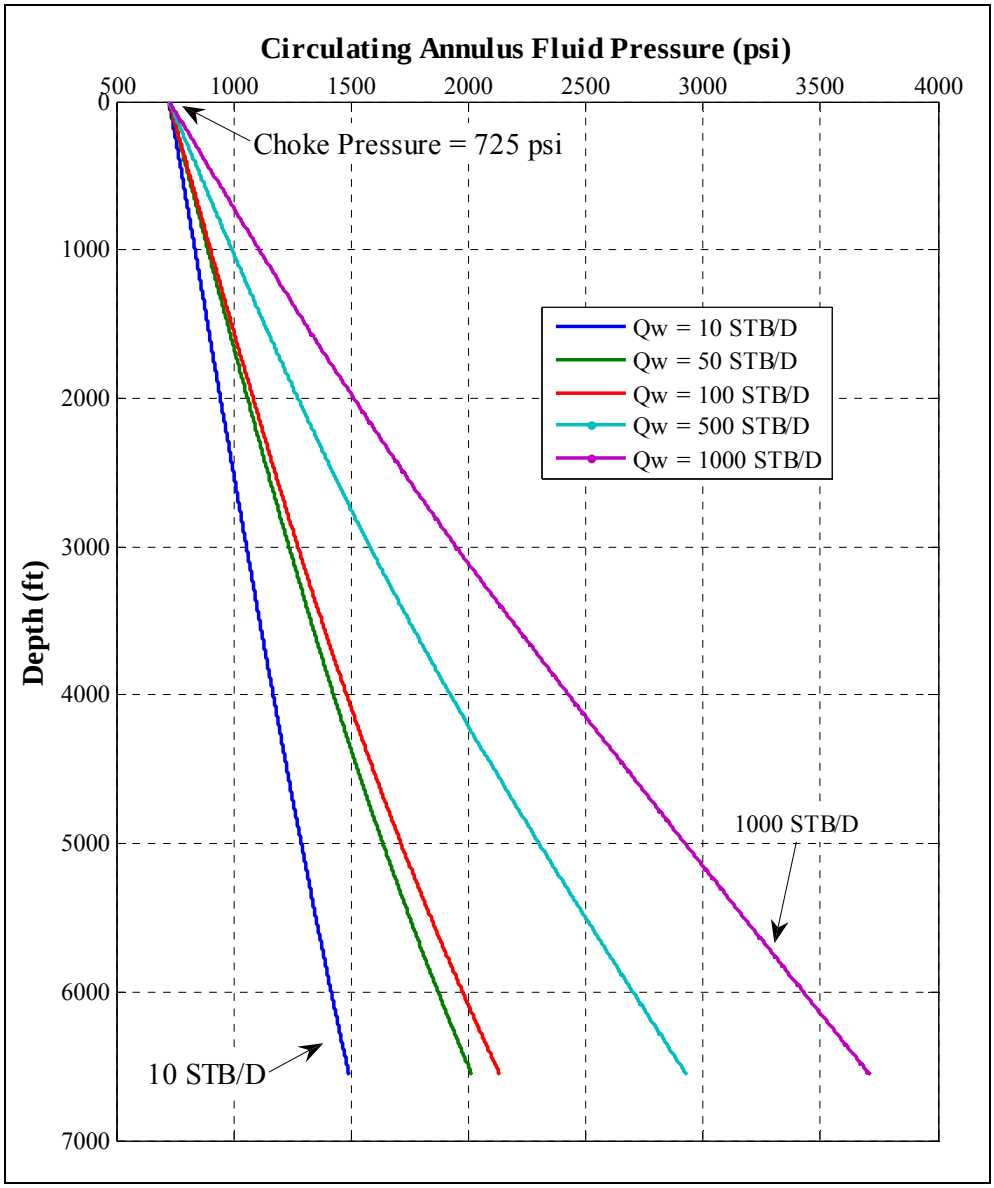

Figure 8.8 Circulating Annulus Fluid Pressure vs. Depth at Various Water Production Rate

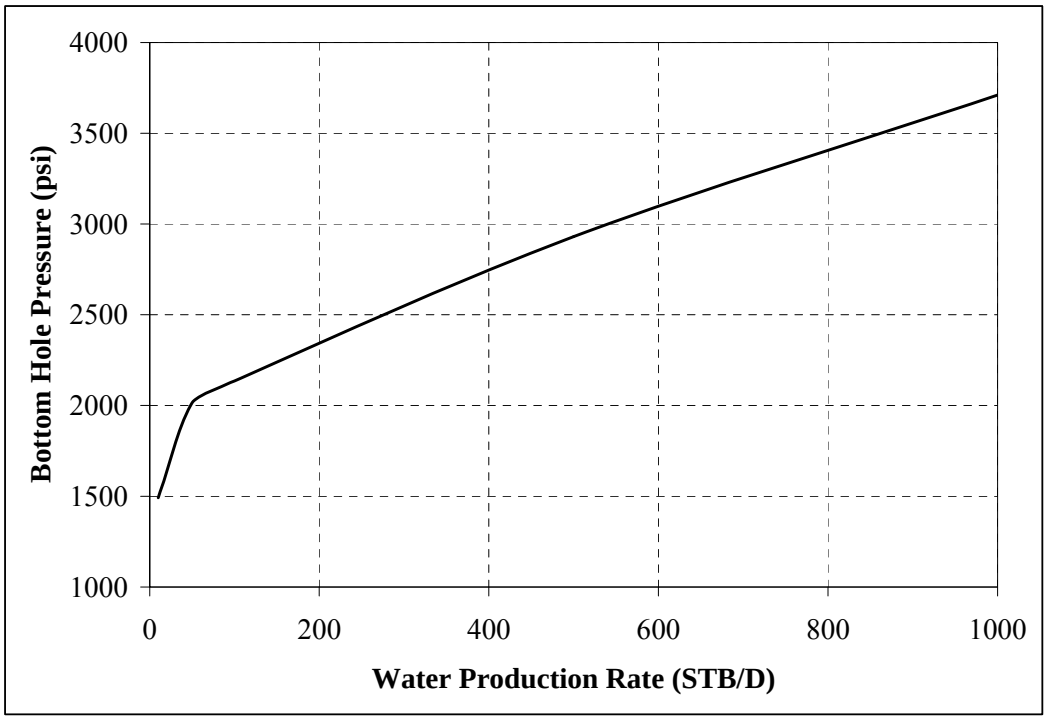

Figure 8.9 Bottomhole Pressure vs. Water Production Rates

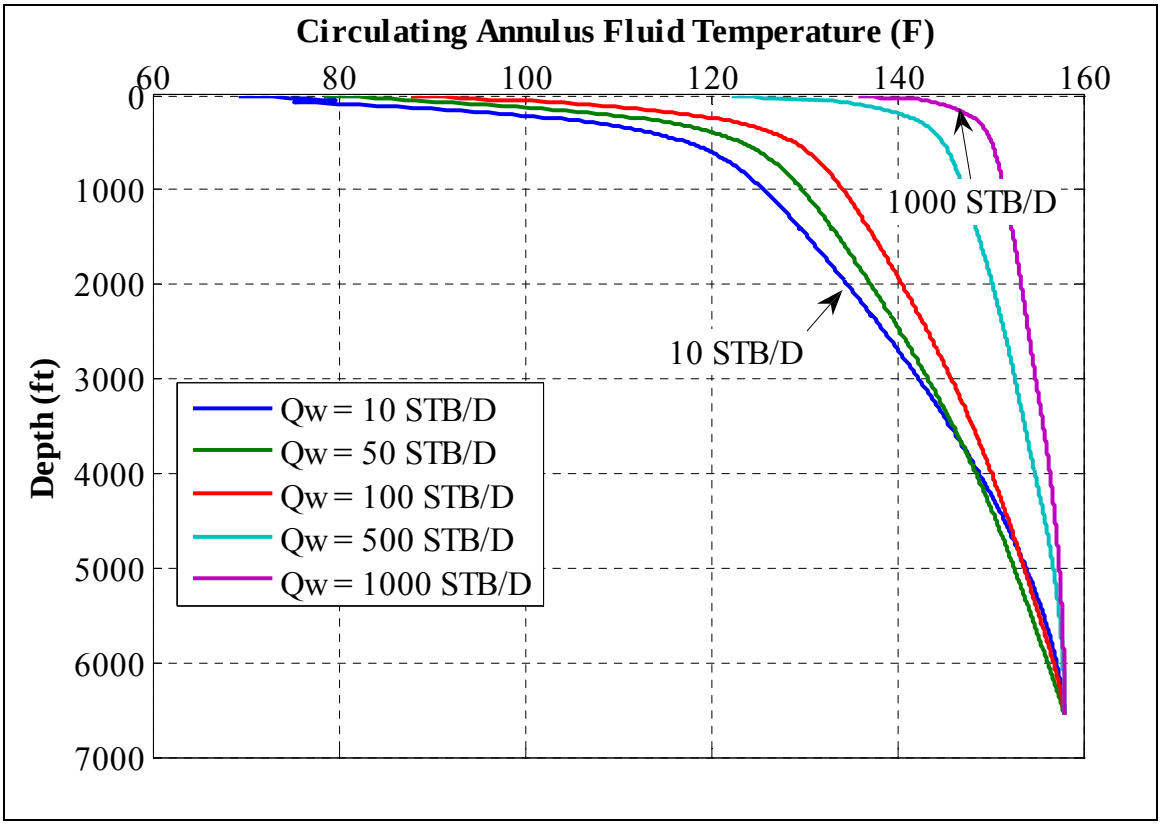

Figure 8.10 Circulating Annulus Fluid Temperature vs. Depth at Various Water Production Rates

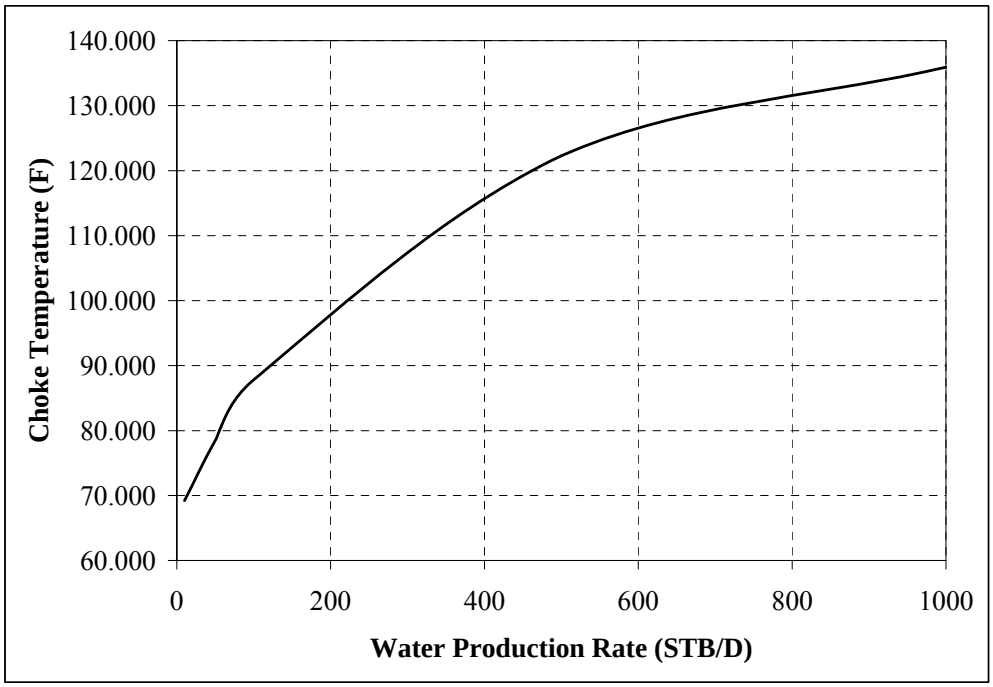

Figure 8.11 Choke Temperature vs. Water Production Rate

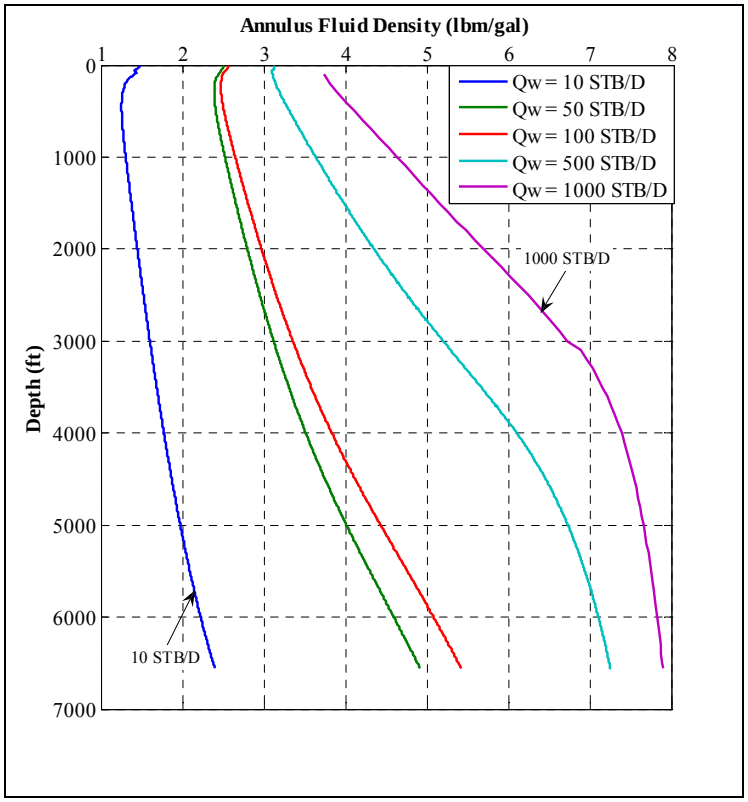

Figure 8.12 Annulus Mixture Density vs. Depth at Various Water Production Rates

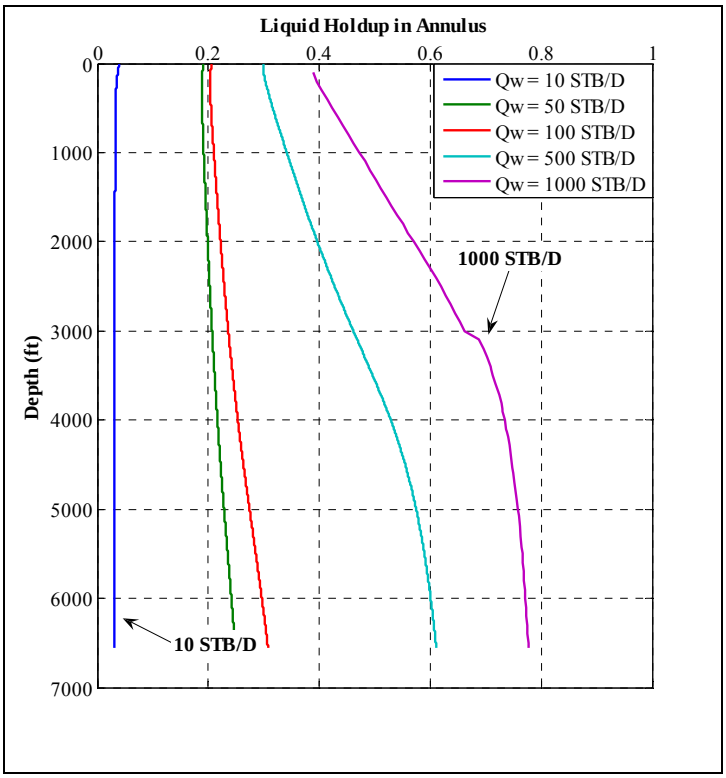

Figure 8.13 Liquid Holdup vs. Depth for Various Water Production Rates

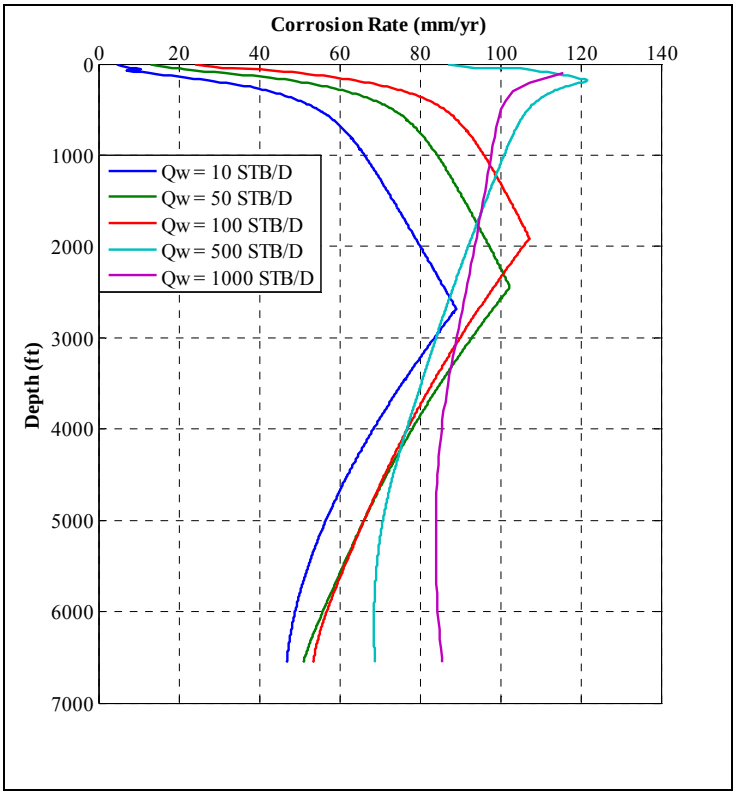

Figure 8.14 Corrosion Rate vs. Depth at Various Water Production Rates

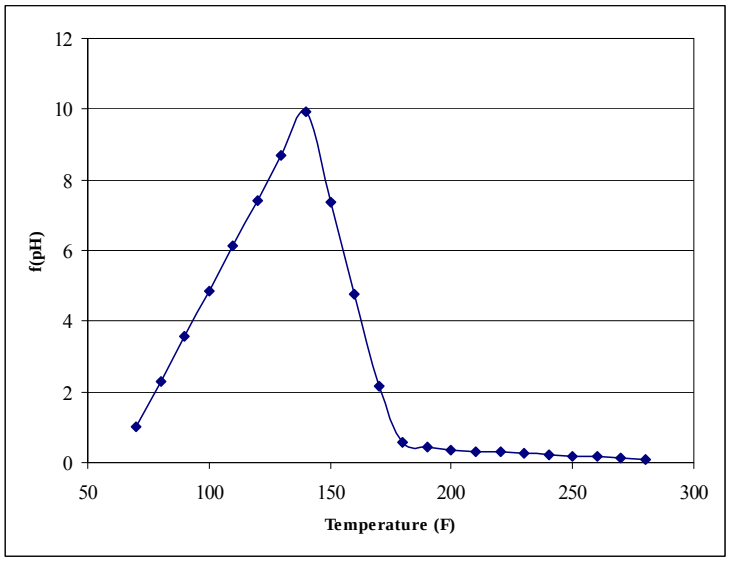

Figure 8.15 Temperature Affect on pH Function

Next, calculations are compared to the work done by Gupta[70]. This case history consists of coiled tubing with a 1.75 in diameter run inside a 4.5 in. casing, (inner diameter of 4 in). to a total depth of 14,364 ft TVD. The same heat transfer model parameters with an injection temperature of -4 °F, will be used in the calculation. In order to achieve a bottomhole pressure of 400 psi the exit choke pressure is set at 100 psi. The model shows that for this choke pressure, the bottomhole pressure is 571 psi with a bottomhole temperature of 276 °F. The figures (8.16-8.20) in the following pages show the sensitivity of the model to different water production rates.

Figure 8.16 shows a diagram which may be used as an aid in selecting the proper choke pressure in order not to have a phase change inside the annulus. At a choke pressure of 800 psi phase change from liquid to supercritical will occur at 2200 ft. Figure 8.17 shows sensitivity to different water production rates, lower bottomhole pressure points are achieved at low water rates (less than 100 STB/D). In addition choke temperature increases with increased water production rate as shown in Figure 8.18. As shown in Figure 8.19 the mixture density changes as the flow pattern changes from annular to slug flow. The corrosion rates for various water

production rates are shown in Figure 8.20 and it shows higher corrosion rates will occur at shallow depths.

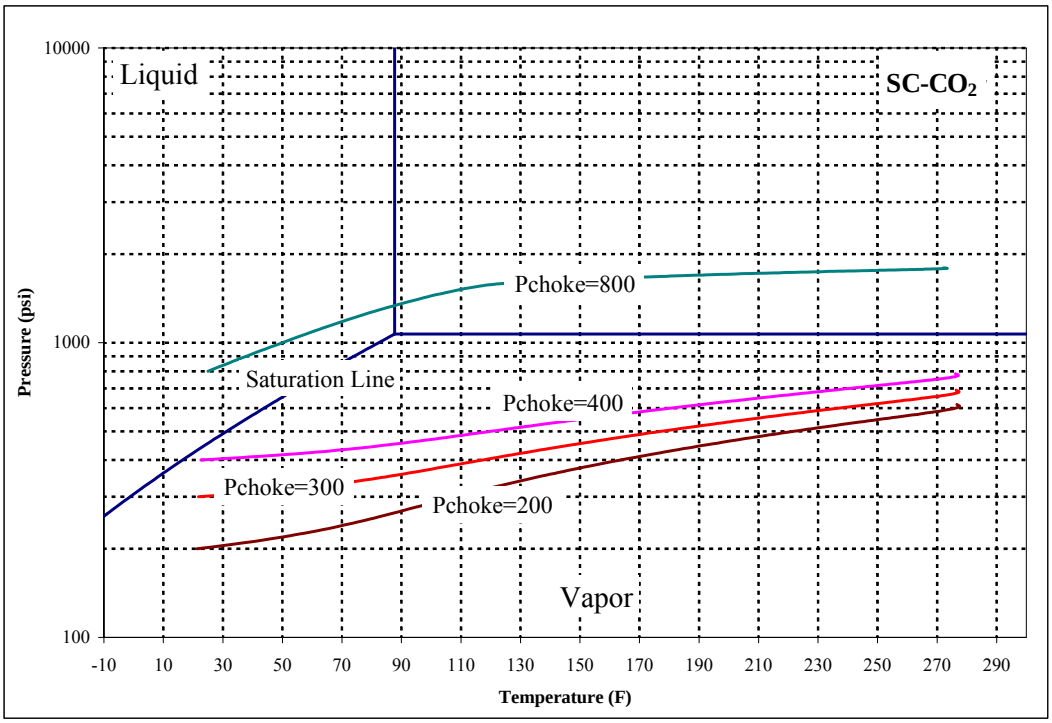

Figure 8.16 Pressure-Temperature Diagram for Increasing Choke Pressure

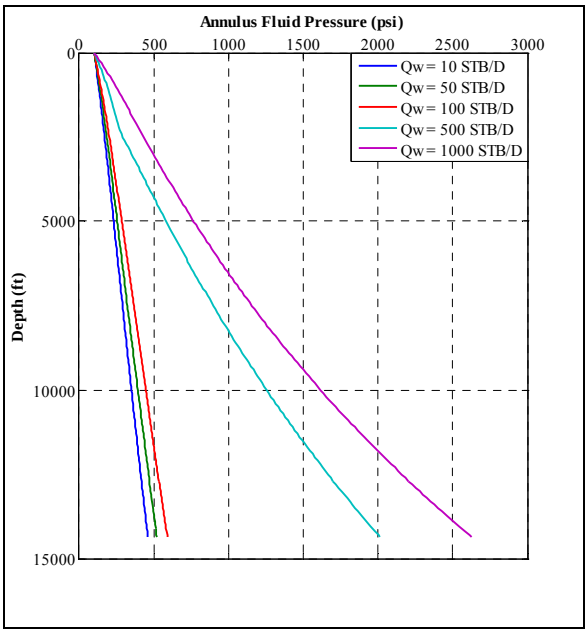

Figure 8.17 Annulus Circulating Pressure vs. Depth

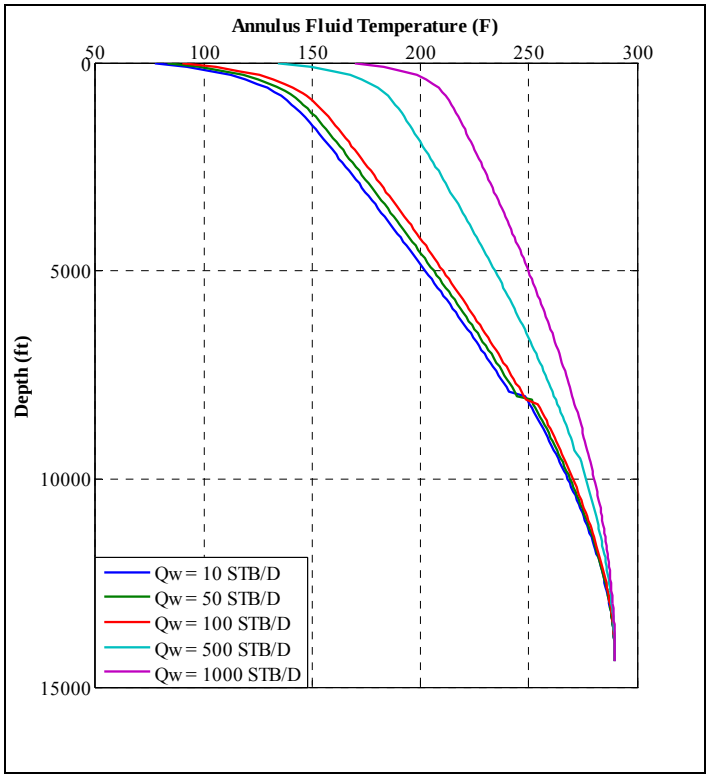

Figure 8.18 Annulus Circulating Temperature vs. Depth

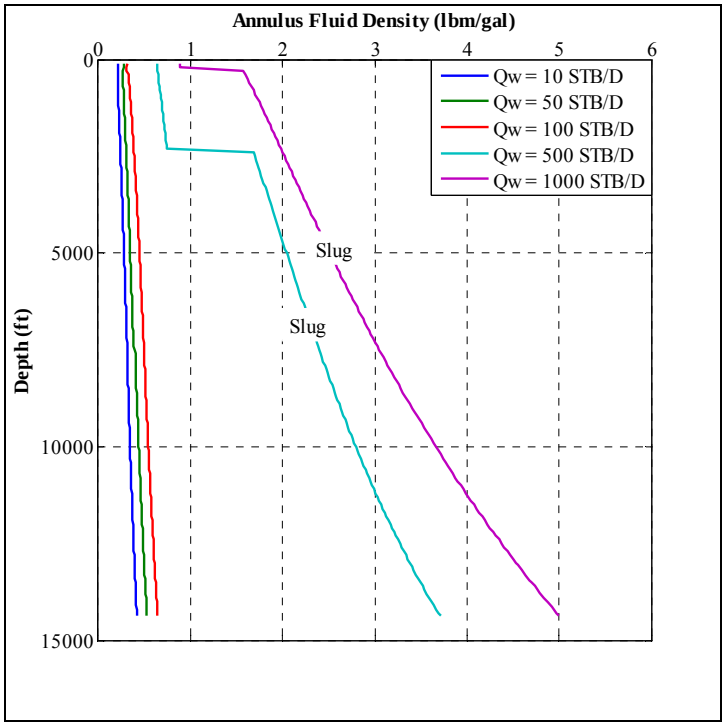

Figure 8.19 Annulus Mixture Density vs. Depth

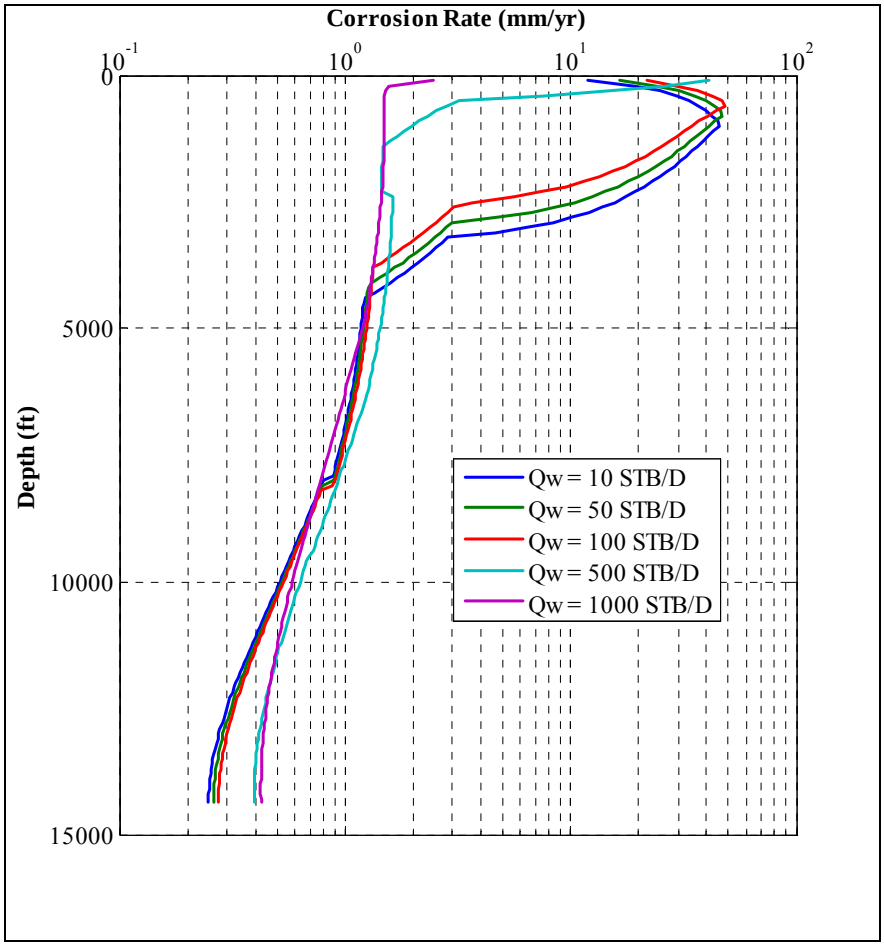

Figure 8.20 Corrosion Rate vs. Depth

CHAPTER 9. CONCLUSIONS AND RECOMMENDATIONS

9.1 Conclusions

- Certain characteristics of CO_2 have suggested its uses in drilling operations.
- Achieving a very low underbalanced pressure window can be accomplished.
- The use of SC-CO_2 as a drilling fluid serves two functions. First as a liquid; SC-CO_2 inside the drill pipe with a high density; and second, will vaporize and exit as a low density gas in the annulus.
- In this work, a mechanistic model for underbalanced drilling operations with SC-CO_2 as the circulating fluid is developed, and indicates SC-CO_2 is a viable UBD fluid
- The use of mechanistic models, based on conservation of energy and mass, has proved to perform better than empirical approaches.
- A two phase heat transfer model was developed, taking into account thermal properties for both fluids and to the surrounding heat losses, with acceptable results.
- A mechanistic two phase flow model was used to simulate small amount of produced water from the formation while drilling underbalanced.
- The model has been validated against available literature data of gas drilling.
- The developed model may be used as a tool to design underbalanced drilling operations in terms of required compression power and gas volumes for generating sufficient velocity to lift drill cuttings.
- The multi-parameter equation of state used in this study predicts CO_2 properties more accurate than Peng-Robinson equation of state, although the latter is a good tool in predicting PVT properties for hydrocarbons and other gases.

9.2 Recommendations

- The model should be validated in future with experimental data, when it becomes available.
- More work is needed to describe SC-CO_2 vaporization through bit nozzles. Sonic flow of such a fluid has not been studied and will be important to the model.
- The development of a mechanistic time dependent model is needed, to upgrade the current model.
- Future development of mechanistic models should improve results by increasing accuracy in liquid holdup and pressure gradient calculations.

REFERENCES

1 Gupta, A.P, Gupta, A, Langlinais J.: "Feasibility of Supercritical Carbon Dioxide as a Drilling Fluid for Deep Underbalanced Drilling Operation," paper SPE 96992-MS, presented at the 2005 SPE ATCE, Dallas, TX October 9-12, 2005.

2 Kolle, J.J: "Coiled-Tubing Drilling with Supercritical Dioxide," paper SPE 65534 presented at SPE/CIM International Conference on Horizontal Well Technology, Canada, Nov 2000.

3 Boyun, G. and Ghalambour, A.: Gas Volume Requirements for Underbalanced Drilling – Deviated Holes, published by the PennWell press, Tulsa, OK, 2002.

4 Martin, D.J.: "Use of Air or Gas as Circulating Fluid in Rotary Drilling-Volume Requirements." *Hughes Engineering Bulletin*, vol. 23, pp. 29, 1952.

5 Martin, D.J.:"Additional Calculations to Determine Volumetric Requirements of Air or Gas as a Circulating Fluid in Rotary Drilling." *Hughes Engineering Bulletin*, vol. 23-A, pp. 22, 1953.

6 Scott, J.O.: "How to Figure How Much Air to Put Down the Hole in Air Drilling." Oil and Gas Journal, pp. 104-107, April-1957.

7 McCray, A.W., and Cole, F.W.: Oil Well Drilling Technology, published University of Oklahoma press, Tulsa, OK, 1959.

8 Angel, R.R.: "Volume Requirements for Air or Gas Drilling." *Trans. AIME*, vol. 210, pp. 325-330, 1957.

9 Jerry, R.A.: "A Closed Circulating System for Air Drilling," paper IADC-SPE 39302 presented at IADC-SPE Drilling Conference, Dallas, TX March 3-6, 1998.

10 Kolle, J.J. and M. Marvin: "Jet-Assisted Coiled Tubing drilling with Supercritical Carbon Dioxide," paper ETCE2000/DRILL-10097, proceedings of ETCE/OMAE 2000 Joint Conference, New Orleans, ASME, New York, Feb 14-17 2000.

11 Whitson, C.H.: "Critical Properties Estimation From an Equation of State," paper SPE/DOE 12634 presented at the SPE/DOE Fourth Symposium on Enhanced Oil Recovery held in Tulsa, OK, April 15-18, 1984.

12 Span, R and Wagner, W.: "A New Equation of State for Carbon Dioxide Covering the Fluid Region from the Triple-Point Temperature to 1100 K at Pressures Up to 800 MPa." J. Phys. Chem. Ref. Data, Vol. 25, No. 6, 1999.

13 Firoozabadi, A.: Thermodynamics of Hydrocarbon Reservoirs, published by McGraw-Hill Professional, 1999.

14 Hasan, A.R. and Kabir C.S.: Fluid Flow and Heat Transfer in Wellbores, published by the Society of Petroleum Engineering, Richardson, TX, 2002.

15 Edwardson, M.J., Girner, H.M., Parkison, H.R., Williams, C.D., Matthews, C.S.: "Calculation of Formation Temperature Disturbances Caused by Mud Circulation," paper SPE 124-PA, JPT, 416-426, Apr 1962.

16 Tragesser, A.F., Crawford, P.B., and Crawford H.R.: "A Method for Calculating Circulating Temperatures," paper SPE 1484-PA, JPT, 1507-1512, Nov 1967.

17 Holmes, C.S. and Swift, S.C; "Calculation of Circulating Mud Temperatures", paper SPE 2318, JPT, 670-674, Jun 1970.

18 Kabir, C.S, Hassan, A.R., Kouba, G.E., Ameen, M.M.:"Determining Circulating Fluid Temperature in Drilling, Workover, and Well-Control Operations." SPE Drilling and Completion. p.75, June (1996).

19 Suryanarayana, P.V., Smith, B., Hasan, ABM, Leslie, C., and, Pruitt, R: "Basis of Design for Coiled tubing Underbalanced Through-Tubing Drilling in Sajaa Field", paper IADC/SPE 87146 presented at IADC/SPE Drilling Conference, Dallas, March 2004.

20 Griffin, D.R., Lyons, W.C.: "Case Histories Design and Implementation of Underbalanced Wells," paper SPE 55606, presented at the Rocky Mountain Regional Meeting held in Gillette, WY, May 15-18 1999.

21 Guo, B.: " Use of Spreadsheet and Analytical Models to Simulate Solid, Water, Oil and Gas Flow in Underbalanced Drilling," paper IADC/SPE 72328, presented at the IAFC/SPE Middle East Drilling Technology held in Bahrain, Oct, 22-24 2001.

22 Cullender, M.H. and Smith, R.V.: " Practical Solution of Gas-Flow Equations for Wells and Pipelines with Large Temperature Gradients," paper SPE 696-G, Published in Petroleum Transactions, AIME, Vol. 207, 1956.

23 Guo, B, Hareland G., and Rajtar, J.: "Computer Simulation Predicts Unfavorable Mud Rate for Aerated Mud Drilling", paper SPE 26892 presented at the 1993 SPE Eastern Regional Conferences held in Pittsburgh, Pa. Nov. 2-4 1993.

24 Liu, G. and Medley, G.H.: "Foam Computer Model Helps in Analysis of Underbalanced Drilling", *Oil and Gas J.* July 1,1996.

25 Beggs, H.D. and Brill, J.P.: "A Study of Two phase Flow in Inclined Pipes", JPT. May 1973. pp. 607-617.

26 Maurer Engineering Inc.: Underbalanced Drilling and Completion Manual, copyrighted 1998, DEA-101, Houston, Texas.

27 Maurer Engineering Inc.: Air/Mist/Foam/ Hydraulics Model, User's Manual, copyrighted 1998, DEA-101, Houston, Texas.

28 Orkiszewski, J.: "Predicting Two-Phase Pressure Drops in Vertical Pipes," *Trans AIME*, vol. 240, pp. 829, 1967.

29 Hagedon, A.R. and Brown, K.E.: "Experimental Study of Pressure Gradients Occurring During Continuous Two-Phase Flow in Small Diameter Vertical Conduits," *Trans AIME*, vol. 234, pp. 475, 1965.

30 Tian, S., Medley G.H. Jr., and Stone, C.R.: "Optimizing Circulation While Drilling Underbalanced", *World Oil*, June 2000, pp 48-55.

31 Tian, S., Medley G.H. Jr.: "Re-evaluating Hole Cleaning in Underbalanced Drilling Applications", paper presented at the IADC Underbalanced Drilling Conference and Exhibitions, Houston, Texas, August 28-29 2000.

32 ALadwani, F.A.: Application Of Mechanistic Models In Predicting Flow Behavior In Deviated Wells Under UBD Conditions, Thesis Louisiana State University, May 2003.

33 Fenghour, A., Wakeham, W.A., Vesovic, V., "The Viscosity of Carbon Dioxide," J. Phys. Chem. Ref. Data, 27:31-44, 1998.

34 Hasan, A.R. and Kabir, C.S.: "Aspects of Wellbore Heat Transfer During Two Phase-Flow," paper SPE 22948-PA, SPEPF Vol. 9, Number 3, Aug 1994.

35 Ramey, H.J., Jr.: "Wellbore Heat Transmission," paper SPE 96-PA, JPT, 427-435, Apr 1962.

36 Hasan, A.R. and Kabir, C.S.: "A Mechanistic Model for Computing Fluid Temperature Profiles in Gas-Lift Well." SPEPF, 179-185, Aug-1996.

37 Hasan, A.R. and Kabir, C.S.: "Aspects of Wellbore Heat Transfer During Two-Phase Flow." SPEPF, 211-216, Aug-1994.

38 Lyons W.C., Guo B. and Seidel F.A., Air and Gas Drilling Manual, 2nd edition, McGraw-Hill, 2001.

39 Cullender, M.H. and Smith, R.V.: "Practical Solution of Gas-Flow Equations for Wells and Pipelines with Large Temperature Gradients," paper SPE 696-G, Published in Petroleum Transactions, AIME, Vol. 207, 1956.

40 ALadwani, F.A.: Application Of Mechanistic Models In Predicting Flow Behavior In Deviated Wells Under UBD Conditions, Thesis, May 2003.

41 NORSOK Standard : "CO2 Corrosion Rate Model", Rev. 2, March. 2005.

42 Wagner, W., J. R. Cooper, et al. (2000). "The IAPWS industrial formulation 1997 for the thermodynamic properties of water and steam." Journal of Engineering for Gas Turbines and Power 122(1): 150-180.

43 Lee, J. and Wattenbarger, R.A.: "Gas Reservoir Engineering." SPE Text Book Series, Vol. 5, 1996.

44 Kelly, T.R.: "Utilizing Compositional Simulation for Material Balance and Bottomhole Pressure Calculations in CO2 WAG Floods," paper SPE 99714 presented at the 2006 SPE/DOE Symposium on Improved Oil Recovery held in Tulsa, Oklahoma, U.S.A., 22-26 April 2006.

45 Brill, J.P. and Mukherjee, H.: Multiphase Flow in Wells, Monograph Volume 17 copyright 1999 by the Society of Petroleum Engineers Inc.

46 Beggs, H.D.: Production Optimization Using Nodal Analysis, OGCI publications, Oil and Gas Consultants International Inc. Tulsa, OK, 1991.

47 Caetano, E.F., Shoham, O., and Brill, J.P.: "Upward Vertical Two phase Flow Through Annulus Part I: Single-Phase Friction Factor, Taylor Bubble Rise Velocity, and Flow Pattern Prediction," *Journal of Energy Resources Technology* (1992) 114, 1.

48 Caetano, E.F., Shoham, O., and Brill, J.P.: "Upward Vertical Two phase Flow Through Annulus Part II: Modeling Bubble, Slug, and Annular Flow," *Journal of Energy Resources Technology* (1992) 114, 14.

49 Perez-Téllez, C., Smith, J.R., and Edwards, J.K.: "A New Comprehensive, Mechanistic Model for Underbalanced Drilling Improves Wellbore Pressure Predictions", paper SPE 74426 presented at the 2002 IPCEM held in Villahermosa, Mexico, February 10-12, 2002.

50 Lage, A.C.V.M and Timer.: "Mechanistic Model for Upward Tow-Phase Flow in Annuli," paper 63127, presented at the 2000 SPE ATCE help in Dallas, Texas, October 1-4, 2000.

51 Taitel, Y., Barnea, D. and Duckler, A.E.: "Modeling Flow Pattern Transitions for Steady Upward Gas-Liquid Flow in Vertical Tubes", *AIChE J.* (1980) 26, pp 345-354.

52 Harmathy, T.Z.: "Velocity of Large Drops and Bubbles in Media of Infinite or Restricted Extent," *AIChE J.* (1960) 6, 281-288.

53 Hasan, A.R. and Kabir, C.S: "Tow-Phase Flow in Vertical and Inclined Annuli," *Intl. J. Multiphase Flow* (1992) 18, 279.

54 Hasan, A.R. and Kabir, C.S.: "Predicting Multiphase Flow Behavior in a Deviated Well," SPEDE (Nov, 1988), 474.

55 Tengesdal, J.O., Kaya, A.S., and Cem Sarica.: "Flow Pattern Transition and Hydrodynamic Modeling of Churn Flow," *SPE J*, No. 4, pp 342-348 December 1999.

56 Zuber, N. and Findlay, J.A.: "Average Volumetric Concentration in Two Phase Flow System", Journal of Heat Transfer, pages 453-468, November 1965.

57 Alves, I. N.: Slug Flow Phenomena in Inclined Pipes, Ph.D. Dissertation, The University of Tulsa, Tulsa, Oklahoma, 1991.

58 Beggs, H.D. and Brill, J.P.: "A Study of Two phase Flow in Inclined Pipes", JPT. May 1973. pp. 607-617.

59 Perez-Tellez, C.: Improved Bottomhole Pressure Control for Underbalanced Drilling Operations, Ph.D Dissertation, Louisiana State University (2002).

60 Taitel, Y. and Barnea, D.: "Counter Current Gas-Liquid Vertical Flow, Model for Flow Pattern and Pressure Drop," *Int. J. Multiphase Flow* (1983) 9, 637-647.

61 Alves, I. N., Caetano, E. F., Minami, K. and Shoham, O.: "Modeling Annular Flow Behavior for Gas Wells," SPE Production Engineering, (November 1991), 435-440.

62 Henstock, W.H. and Hanratty, T.J.: "The Interfacial Drag and the Height of the Wall Layer in Annular Flow", *AIChE J.*, 22, No. 6, (Nov. 1976),990-1000.

63 Wallis, G.B.: One Dimensional Two phase Flow, McGraw-Hill (1969).

64 Gas Research Institute (GRI), Underbalanced Drilling Manual, published by Gas Research Institute, Chicago, Illinois, 1997.

65 Gray, K.E.: "The Cutting Carrying Capacity of Air at Pressures Above Atmospheric," *Trans AIME*, vol. 213, pp. 180, 1958.

66 Griffien, D.R., and Lyons, W.C.: "Case Studies of Design and Implementation of Underbalanced Wells" paper IADC/SPE 59166 presented at the 2000 IADC/SPE Drilling Conference held in New Orleans, Louisiana, 23–25 February 2000.

67 Span, R., Lemmon, E. W., Jacobsen, R. T., Wagner, W. and Yokozeki, A.: "A Reference Equation of State for the Thermodynamic Properties of Nitrogen for Temperatures from 63.151 to 1000 K and Pressures to 2200 Mpa." *J. Phys. Chem. Ref. Data*, Vol. 29, No. 6, 2000.

68 Lemmon, E.W. and Jacobsen, R.T.: "Viscosity and Thermal Conductivity Equations for Nitrogen, Oxygen, Argon, and Air." *Int. J. Thermophys.,* Vol. 25, No. 1, 2004.

69 Kolle, J.J. and Marvin, M.H.: "Jet-Assisted Drilling with Supercritical Carbon Dioxide," Company Report, Tempress Technology Inc, 2000.

70 Gupta, A.: Feasibility of Supercritical Carbon Dioxide as a Drilling Fluid for Deep Underbalanced Drilling Operations, thesis, Louisiana State University, May, 2006.

71 Hebach, A., Oberhof, A. and Dahmen, N.: "Density of Water + Carbon Dioxide at Elevated Pressures: Measurements and Correlation," J. Chem. Eng. Data, vol. 49, pp. 950-953, 2004.

APPENDIX A. MULTIPHASE FLOW PROPERTY CORRELATIONS

A.1 Mixture Density of Water and CO_2

The mixture density of water and CO_2 is taken from the correlation developed by Hebach, et. al.[71] based on the saturation pressure of CO_2. For liquid and supercritical CO_2 we have:

$$\rho_w = L_0 + L_1 P + L_2 T + L_3 P^2 + L_4 T^2 \qquad \text{A.1}$$

For vapor CO_2 the mixture density is calculated as:

$$\rho_W = G_0 + G_1 P + G_2 T + G_3 P^2 + G_4 T^2 + G_5 PT + G_6 P^3 + G_7 T^2 P + G_8 T P^2 \qquad \text{A.2}$$

Table A.1 shows the constant parameters used in the above expressions.

Table A.1 Parameters for Calculating Water-CO_2 Mixture Density

Parameter	Value
L_0	949.7109
L_1	0.559684
L_2	0.883148
L_3	-9.70E-04
L_4	-2.28E-03
G_0	805.1653
G_1	44.12685
G_2	1.573145
G_3	-1.45073
G_4	-3.13E-03
G_5	-0.19658
G_6	6.27E-05
G_7	2.09E-04
G_8	4.20E-03

APPENDIX B. SOLUTION OF HEAT TRANSFER MODEL

The solution of the second order differential equation is shown below taking into account both single flow of CO_2 inside the annulus and two phase flow of water and CO_2 inside the annulus.

Single Phase Flow Inside The Annulus

The solution of the second order linear differential equation (6.19) is shown below:

$$T_{DP}(L) = \Psi_1 - \Psi_2 + (L - \beta)Gg + T_{is} \quad \text{B.1}$$

The constants in the above solution are shown below as:

$$\psi_1 = T_{Inj} + \beta Gg - T_{is} \quad \text{B.2}$$

$$\psi_2 = 2\beta Gg + 2T_{Inj} - 2T_{is} \quad \text{B.3}$$

$$\Psi_1 = \frac{(2\alpha e^{\left(\frac{\zeta_1 L}{2\alpha\beta}\right)})(\psi_1 e^{\left(\frac{\zeta_2 WTD}{2\alpha\beta}\right)} - \frac{1}{2}Gg\zeta_1)}{2\alpha e^{\left(\frac{\zeta_2 WTD}{2\alpha\beta}\right)} + e^{\left(\frac{\zeta_1 WTD}{2\alpha\beta}\right)}(2\alpha + \zeta_1)} \quad \text{B.4}$$

$$\Psi_2 = \frac{2\alpha e^{\left(\frac{\zeta_2 L}{2\alpha\beta}\right)}(\psi_1 e^{\left(\frac{\zeta_1 WTD}{2\alpha\beta}\right)} - \frac{1}{2}Gg\zeta_1)}{(-\zeta_1 - 2\alpha)e^{\left(\frac{\zeta_2 WTD}{2\alpha\beta}\right)} - 2\alpha e^{\left(\frac{\zeta_1 WTD}{2\alpha\beta}\right)}} \quad \text{B.5}$$

$$\zeta_1 = \beta + \sqrt{\beta^2 + 4\alpha\beta} \quad \text{B.6}$$

$$\zeta_2 = \beta - \sqrt{\beta^2 + 4\alpha\beta} \quad \text{B.7}$$

Two Phase Flow Inside The Annulus

For the mixture of water and CO_2 inside the annulus the solution of the differential shown below is the same with the following parameters:

$$\Psi'_1 = \frac{1}{2\beta}\frac{(-\zeta_1 e^{\left(\frac{\zeta_2 L}{2\alpha\beta}\right)})(\psi_2 e^{\left(\frac{\zeta_1 WTD}{2\alpha\beta}\right)} - \zeta_2 Gg)}{\left(-2\alpha - \zeta_2\right)e^{\left(\frac{\zeta_2 WTD}{2\alpha\beta}\right)} - 2\alpha e^{\left(\frac{\zeta_1 WTD}{2\alpha\beta}\right)}} \quad \text{B.8}$$

$$\Psi'_2 = \frac{1}{2\beta}\frac{(\zeta_1 e^{\left(\frac{\zeta_1 L}{2\alpha\beta}\right)})(-\psi_2 e^{\left(\frac{\zeta_2 WTD}{2\alpha\beta}\right)} + \zeta_1 Gg)}{\left(2\alpha + \zeta_1\right)e^{\left(\frac{\zeta_1 WTD}{2\alpha\beta}\right)} + 2\alpha e^{\left(\frac{\zeta_2 WTD}{2\alpha\beta}\right)}} \quad \text{B.9}$$

$$\frac{dT_{DP}}{dL} = \Psi'_1 - \Psi'_2 + Gg \quad \text{B.10}$$

APPENDIX C. CORROSION RATE MODEL

The model developed by the NORSOK[41] to calculate corrosion rates in hydrocarbon production systems where the corrosive agent is CO_2. It takes into account temperature, pH, and fugacity of CO_2 in the system. The general form of the model is shown below

$$Corr\_Rate = K_t f_{CO2} f(pH)_t \qquad (T=5^{\circ}C) \qquad C.1$$

$$Corr\_Rate = K_t * 20.62 * f_{CO2} * F(\tau) \qquad (5<T<150) \qquad C.2$$

$$F(\tau) = (\tau/19) * 0.146 + 0.0324 * \log(f_{CO2}) * f(pH)_t \qquad C.3$$

In the above model:

f_{CO2} : Fugacity of CO_2 in bar

(K_t) is a constant and it has the values shown in Table C.1

Table C.1 K_t Values

Temperature °C	**Kt**
5	0,42
15	1,59
20	4,762
40	8,927
60	10,695
80	9,949
90	6,250
120	7,770
150	5,203

f(pH)t is the pH function and it is in terms of both temperature and pH and it is shown in Table C.2 at the given temperature range.

In addition (τ) is the wall shear stress and it is defined as

$$\tau = 0.5 \rho_m f_f v_m \qquad C.4$$

In the above expression

τ : Wall Shear Stress (Pa)

(ρ_m) : Mixture density (kg/m^3)

f_f : Friction factor

v_m : Mixture velocity (m/sec)

Table C.2 pH Function

Temperature °C	pH	f(pH)
5	3,5 ≤ pH < 4,6	f(pH) = 2,0676 - (0,2309 x pH)
5	4,6 ≤ pH ≤ 6,5	f(pH) = 4,342 - (1,051 x pH) + (0,0708 x pH^2)
15	3,5 ≤ pH < 4,6	f(pH) = 2,0676 - (0,2309 x pH)
15	4,6 ≤ pH ≤ 6,5	f(pH) = 4,986 - (1,191 x pH) + (0,0708 x pH^2)
20	3,5 ≤ pH < 4,6	f(pH) = 2,0676 - (0,2309 x pH)
20	4,6 ≤ pH ≤ 6,5	f(pH) = 5,1885 - (1,2353 x pH) + (0,0708 x pH^2)
40	3,5 ≤ pH < 4,6	f(pH) = 2,0676 - (0,2309 x pH)
40	4,6 ≤ pH ≤ 6,5	f(pH) = 5,1885 - (1,2353 x pH) + (0,0708 x pH^2)
60	3,5 ≤ pH < 4,6	f(pH) = 1,836 - (0,1818 x pH)
60	4,6 ≤ pH ≤ 6,5	f(pH) = 15,444 - (6,1291 x pH) + (0,8204 x pH^2) - (0,0371 x pH^3)
80	3,5 ≤ pH < 4,6	f(pH) = 2,6727 - (0,3636 x pH)
80	4,6 ≤ pH ≤ 6,5	f(pH) = 331,68 x $e^{(-1,2618 \times pH)}$
90	3,5≤ pH < 4,57	f(pH) = 3,1355 - (0,4673 x pH)
90	4,57≤ pH < 5,62	f(pH) = 21254 x $e^{(-2,1811 \times pH)}$
90	5,62 ≤ pH ≤ 6,5	f(pH) = 0,4014 - (0,0538 x pH)
120	3,5 ≤ pH < 4,3	f(pH) = 1,5375 - (0,125 x pH)
120	4,3 ≤ pH < 5	f(pH) = 5,9757 - (1,157 x pH)
120	5 ≤ pH ≤ 6,5	f(pH) = 0,546125 - (0,071225 x pH)
150	3,5 ≤ pH < 3,8	f(pH) = 1
150	3,8 ≤ pH < 5	f(pH) = 17,634 - (7,0945 x pH) + (0,715 x pH^2)
150	5 ≤ pH ≤ 6,5	f(pH) = 0,037

APPENDIX D. NOMENCLATURE

a	SW-EOS parameter
A	Area, (in2)
AAE	Average absolute error
BHP	Bottomhole pressure, (psi)
C1	Velocity profile coefficient for slug flow
CDC	Drill cuttings concentration in the gas
CO	Velocity profile coefficient for bubbly flow
Cp	Specific isobaric heat capacity, (BTU/lbm-°F)
CTR	Cutting transport ratio
c	heat capacity
d	SW-EOS parameter
Ek	Acceleration term
f	Friction factor term
G	Geothermal gradient, (°F/ft)
h	Specific enthalpy, (BTU/lbm)
H	Holdup
HE	Helmholtz energy
I	Cullender and Smith Integral Term
k	Conductivity, (BTU/ft-°F-hr), Specific heat ratio
K	Diameter ratio
L	Depth, (ft)
$\dot{m}$	Mass flow rate, (lbm/hr)

n SW-EOS parameter

NRE Reynolds number

P Pressure, (psi)

Q Heat flow, (BTU/hr)

QG Gas injection rate at standard conditions , (SCF/min)

R Universal gas constant, (ft^3/lbmole-R)

ROP Rate of penetration, (ft/hr)

T Temperature, (°F)

t SW-EOS parameter, time (hr)

U Heat transfer coefficient, (Btu/hr-F-ft^2)

v Velocity, (ft/sec)

WTD Well total depth, (ft)

z Compressibility factor

Z True vertical depth, (ft)

Greek Letter

α SW-EOS parameter, Heat transfer model parameter

α_{CS} Cullender-Smith specific gravity parameter

β SW-EOS parameter, Heat transfer model parameter

Δ SW-EOS function

δ Liquid film thickness, (ft)

Φ Dimensionless Helmholtz energy

λ No slip holdup

μ Viscosity, (cP)

ν_∞ Discrete gas bubble rise velocity, (ft/sec)

Θ Sphericity factor

ρ Density, (lbm/ft3)

σ Interfacial tension, (N/m)

τ_i Interfacial shear, (psi)

υ Specific volume, (ft3/lbm)

Ω Cullender-Smith friction factor parameter

ζ Heat transfer model parameter

ϑ Drag coefficient

Subscript

A Annulus

acc Acceleration

bh Bottomhole

crit Critical

D Dimensionless

DP Drill pipe

e Earth

ei Earth initial

el Elevation

ep Equi-periphery

f Fluid

F Formation

G Gas

H	Horizontal
h	Hydraulic
i	Summation index
IC	Inner casing
inj	Injection
is	Initial surface
L	Liquid
LS	Liquid slug
M	Mixture
mp	Middle point
n	nozzle
P	Pipe
r	Reduced
s	Surface
SG	Superficial gas
SL	Superficial liquid
sl	Slip
SU	Slug unit
TB	Taylor bubble
total	Total
V	Vertical
wb	Wellbore

Superscript

o Ideal

r Residual

n Swarm Effect

VITA

Faisal Abdullah ALAdwani Born in Kuwait City, Kuwait, in October 10, 1975. In January 1998, he received a Bachelor of Science degree in Petroleum Engineering from Kuwait University. In March 1998, he joined Kuwait Foreign Petroleum Exploration Company where he worked as a petroleum engineer and was assigned to field operations in the Southeast Asia Region. In May 2003, he received a Master of Science degree in petroleum engineering from the Craft & Hawkins Petroleum Engineering Department at Louisiana State University where he continues to pursue a doctoral degree in petroleum engineering. He is a member of the Society of Petroleum Engineers.